Ionene and Ionene Alkyl Sulfate Stoichiometric Complexes

temperature and humidity sensitive materials

Dissertation

Zur Erlangung des akademischen Grades

Doctor rerum naturalium

(Dr. rer. nat.)

vorgelegt

der Fakultät Mathematik und Naturwissenschaften

der Technischen Universität Dresden

von

Yu, Quanwei (Master of Science)

Geboren am 03.01.1971 in Shandong, VR. China

Gutachter: Prof. Dr. T. Wolff (TU-Dresden)

Prof. Dr. K. Arndt (TU-Dresden)

Prof. Dr. W. Goedel (TU-Chemnitz)

Eingereicht am: 2004-08-16

Tag der Verteidigung: 2004-10-28

Acknowledgement

I am very grateful to Prof. Dr. T. Wolff for supplying the interesting subject and position and looking after my research work.

I thank the Deutsche Forschungsgemeinschaft for the financial support of my work in the European Graduate College 720 „Advanced Polymeric Materials“.

I thank Dipl.-Chem. J. Frömmel for many encouraging and helpful discussions and numerous stimulations.

I thank Prof. K. Prochazka and Mr. M. Stepanek from the Department of Physical and Macromolecular Chemistry, Charles University in Prague for the friendly and helpful cooperation and for advice in the fluorescence and light scattering measurements.

I am very grateful to Mrs. A. Göpfert for friendly and good collaboration and for performing DSC.

Thanks are due to Mrs. Ch. Meißner, M. Rösler and H. Dallmann for performing light scattering, ATR-IR, and TG-MS measurements, respectively. I thank Mr. M. Söhnel and Mr. M. Gestrich for excellent mechanical work.

I thank Mrs. K. Scheider and Mrs. K. Körner for the friendly and helpful assistance in the purification of chemicals and solvents.

To all further persons, who performed a contribution to this research work or provided direct or indirect support of my work, I would like to express my thanks herewith.

Table of Contents

1. Introduction

1.1 Surfactants

Surfactant is an abbreviation for surface-active agent, which means active at the surface. A surfactant is characterized by its tendency to accumulate at interfaces.

All surfactant molecules consist of at least two parts, one which is soluble in a specific fluid (the lyophilic part) and one which is insoluble (the lyopholic part). When the fluid is water one usually talks about the hydrophilic and hydropholic parts, respectively. The hydrophilic part is referred to as the head group and the hydropholic part as the tail [1].

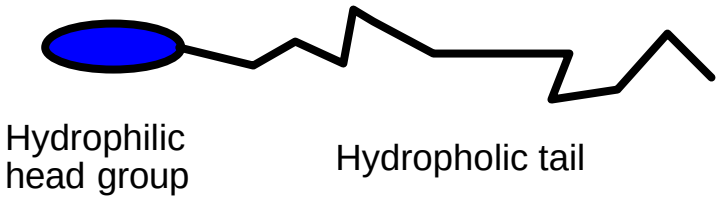

Figure 1.1 Schematic illustration of a surfactant

1.1.1 Classification of surfactants

The primary classification of surfactants is based on the charge of the polar head groups. It is common practice to divided surfactants into the classes anionics, cationics, non-ionics and zwitterionics. The latter class contains both an anionic and a cationic charge under normal conditions. Carboxylate, sulfate, sulfonate and phosphate are the polar groups found in anionic surfactants.

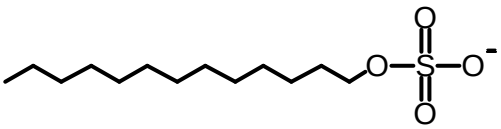

Alkyl sulfate

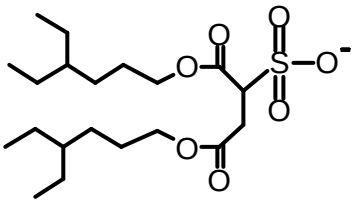

Dialkyl sulfosuccinate

Figure 1.2 Structures of the anionic surfactants

Non-ionics surfactants have either polyether or polyhydroxyl as the polar group.

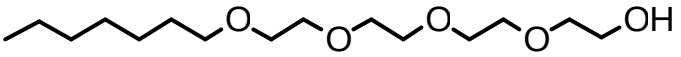

Fatty alcohol ethoxylate

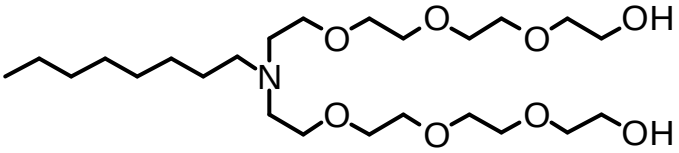

Fatty amine ethoxylate

Figure 1.3 Structures of the non-ionic surfactants

The vast majority of cationic surfactants are based on the nitrogen atom carrying the cationic charge. Both amine and quaternary ammonium-based products are common.

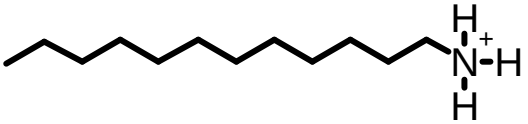

Fatty amine salt

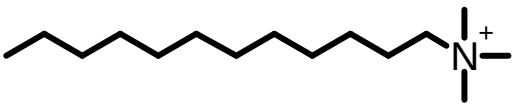

Alkyl 'quat'

Figure 1.4 Structures of the cationic surfactants

Zwitterionic surfactants contain two charged groups of different sign. Whereas the positive charge is mostly ammonium, the negative charge may vary, although carboxylate is by far the most common.

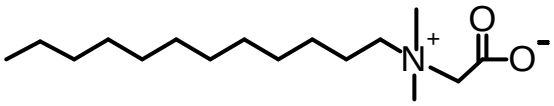

Betaine

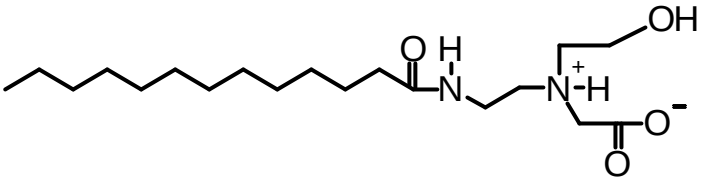

Imidazoline

Figure 1.5 Structures of the zwitterionic surfactants

1.1.2 Surfactant self-assembly property

Surfactants exhibit a number of ordered phases, which are the basis of the structure forming abilities of the polyelectrolyte surfactant complexes. Systems containing amphiphile are best classified into homogeneous or single phase systems and heterogeneous systems of two or more phases. The single phase systems can be divided into isotropic solutions, solid phases and liquid crystalline phases. The solid crystalline phases have both long distance range and short-range order, but the degree of short-range order varies between different phases. Isotropic solution phases are characterized by disorder over both short and long distances, while liquid crystalline phases or mesophases have a short-range disorder but some distinct order over longer distances. A single component system, neat surfactants, may have several different phases with increasing temperature [2].

They are mostly lamellae, the lateral extent of each layer varies so that they may exist as sheets, ribbon, or disks. A swallow-tailed structure such as AOT (di-2-ethylhexylsulfosuccinate) formed a stable crystalline hexagonal phase at 20 °C.

When a second component such as water is added to the surfactant, the volume ratio of the ionic and hydrocarbon components is changed and more complex liquid crystalline behavior is observed. Phases with different types of organization including lamellar, hexagonal, and cubic phases are known for a wide range of surfactants types. These phases are the most common and follow a general progression of phases with decreasing water content from

reversed micelles ↔ reversed hexagonal ↔ cubic ↔ lamellar ↔hexagonal ↔ micelles. The most important amphiphile systems can be arranged as following.

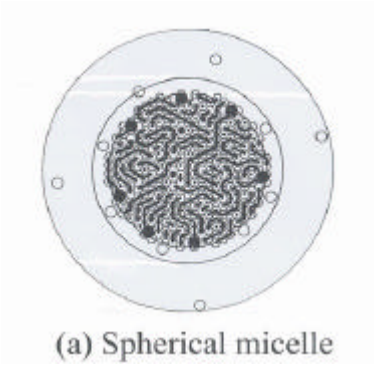

(a) Spherical micelles with an interior composed of the hydrocarbon chains and a surface of the polar head groups facing water. There is, however, intensive contact between the hydrocarbon moieties and water, since there can be only 5 to 7 head groups on an equatorial cut. Spherical micelles are characterized by a low surfactant aggregation number (between 60 and 120, depending on size and shape of the surfactant molecule) and a strongly positive spontaneous curvature. The hydrocarbon core has a radius close to the length of the extended alkyl chain.

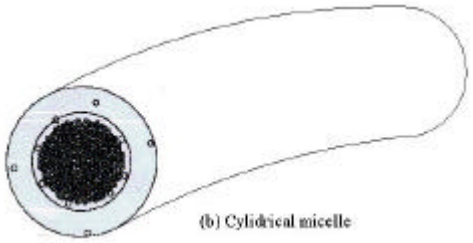

(b) Cylindrical micelles with an interior composed of the hydrocarbon chains and a surface of the polar head groups facing water. They form from spherical systems upon increasing the surfactant concentration or upon the addition of salt. As compared to spherical micelles the head groups are closer. The cross section of the hydrocarbon core is similar to that of spherical micelles. The micellar length is highly variable so these micelles are polydisperse.

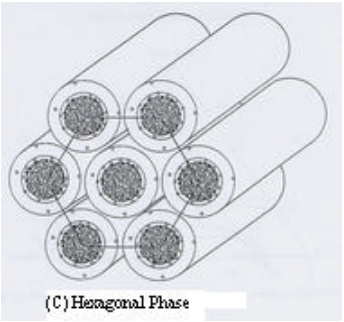

(c) In hexagonal phases the long axes of rod-like micelles are hexagonally arranged, the hexagonal phases are continuous in one dimension, and each micelle is surrounded by six others. It is divided into normal hexagonal and reversed hexagonal [3].

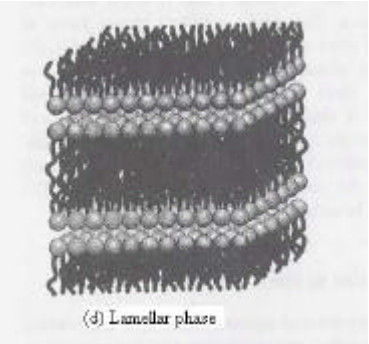
(d) Lamellar phase

(d) Surfactant bilayers build up lamellar liquid crystals. For surfactant-water systems a hydrocarbon layer has a thickness of ca. 80 % of the length of two extended alkyl chains.

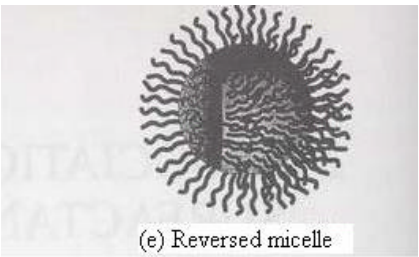
(e) Reversed micelle

(e) Reversed or inverted micelles have a water core (droplet) surrounded by the surfactant polar head groups. The alkyl chains together with a non-polar solvent make up the continuous medium.

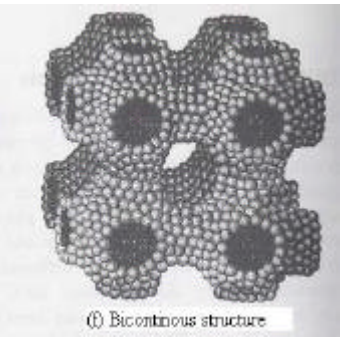
(f) Bicontinous structure

(f) A bicontinuous structure with the surfactant molecules aggregated into connected films is characterized by two curvatures of opposite sign.

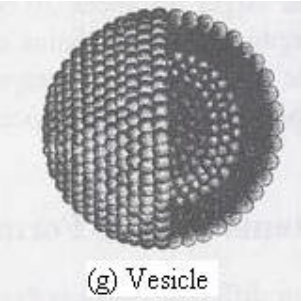

(g) Vesicles are built from bilayers similar to those of the lamellar phase and are characterized by two distinct water compartments, one forming the core and the other one the external medium. Vesicles may have different shapes and there are also reversed type vesicles [4]. Vesicles do not form spontaneously; usually sonication is needed to prepare them.

1.2 Polyelectrolytes

The term polyelectrolyte will be used to denote any polymeric material which contains ionic groups attached to the polymer chains. The chain may be linear, branched, or cross-linked. The ions may correspond to the ions of strong electrolytes, for example quaternary ammonium groups (chain), or to the ions of weak electrolytes, such as carboxyl ions (chain) [5]. Most of the polyelectrolytes examined so far have been polyanions (polyacrylate salts) and polycations (polyvinyl amine, polyethyleneimine). They are also divided into various synthetic and natural polyelectrolytes; the following figures display some polyanionic and polycationic examples.

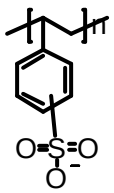

poly(stryrene sulfonate)

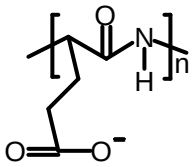

poly(glutamate)

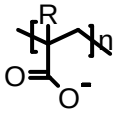

poly(methacrylate)

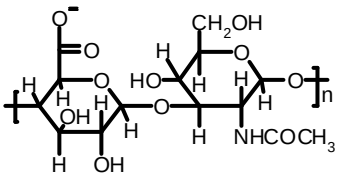

Hyaluronic acid anion

Synthetic poly(anion)

Natural poly(anion)

Figure 1.6 Structures of natural and synthetic anionic polyelectrolytes

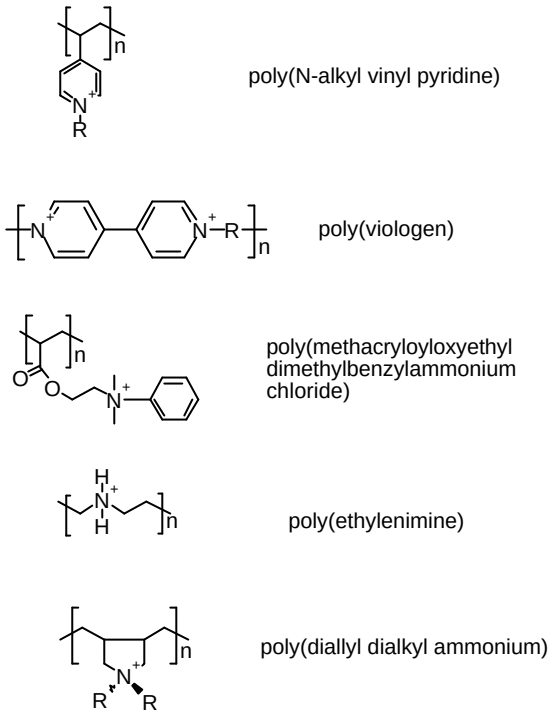

Figure 1.7 Structures of cationic polyelectrolytes

Polyelectrolytes possess a fascinating array of physical, chemical, and electrical properties, which are far different from those of conventional polymers, and which can be put to use in a variety of unusual and practical applications. Polyelectrolytes are used for defined applications such as the treatment of waste water [6] and of paper slurries [7] and furthermore for the flocculation of colloidal nanoparticles such as dyes [8]. A new field of application is the generation of selectively active or inert surfaces with respect to interaction with drugs and biopolymers [9]. Polyelectrolyte layers are under way to address novel application fields in nano- and bioscience, especially in sensor and biomaterial development [10].

1.3 Polyelectrolyte-surfactant complexes

Complex formation between polymer electrolytes and oppositely charged surfactants is a highly cooperative process in which the driving force is predominantly electrostatic in nature. The oppositely charged species strongly attract each other. In addition, the highly ionic environment around the polymer electrolyte screens the charges on the surfactant head groups

from each other, diminishing electrostatic repulsion. They are also stabilized by hydrophobic interactions of nonpolar moieties of the surfactant. An additional feature of these mixtures is that a phase separation can take place into two phases consisting of a concentrated phase of polyelectrolyte and surfactant in equilibrium with a dilute solution of the excess component. It is this process that can be used for the direct synthesis of polyelectrolyte-surfactant complexes [11].

1.3.1 Properties of polyelectrolyte-surfactant complexes in solution

Rjumtsev et al. have investigated the interaction of polyelectrolytes and surfactants in dilute solution. They found that the concentration at which polyelectrolyte-surfactant micelles form (known as the critical aggregation concentration (cac)) is typically several orders of magnitude lower than the critical micelle concentration (cmc) for the surfactant alone. This interaction can be considered here as a special kind of polymer ligand binding. As with surfactant micelles, hydrophobic effects of the nonpolar tails of the surfactant molecules also contribute to the formation of micelle-like structures in polyelectrolyte-surfactant complexes.

1.3.1.1 The regularities of formation and structure in aqueous solutions

The regularities of formation and structure of such complexes in aqueous solutions have been studied in detail. Depending on the polyelectrolyte to surfactant ratio, the formation of stoichiometric or equimolar complexes and nonstoichiometric complexes may occur. In the latter case, the composition of the complexes formed, expressed as the molar ratio of surfactant to polycation chain units, normally does not exceed 0.3-0.5. An increase of surfactant concentration in the mixture above 0.3-0.5 results in a disproportionation reaction. As a result of this disproportionation, phase separation occurs. The precipitate consists of stoichiometric or equimolar complexes, while nonstoichiometric complexes remain in solution. Further increase in surfactant concentration leads to an increase in the mass of the precipitate, stoichiometric or equimolar complexes, while still no change in the nonstoichiometric complexes composition is observed. Thus, a disproportionation reaction in polyelectrolyte-surfactant aqueous solutions precludes the synthesis of nonstoichiometric complexes with $f > 0.3$-0.5 via direct mixing of oppositely charged components [12, 13].
Ilekti et al. found that at sufficiently low water contents a single-phase mixture was stable, but on addition of water a dilute phase eventually separated. More added water caused a third, even more concentrated mesogenic hexagonal phase to form, and then the initial phase

disappeared, leaving only the hexagonal and the dilute aqueous phase. The concentration of the concentrated phases always increased with increasing amounts of water.

In a concentrated mixture a high concentration of simple salt is present that screens the attraction between oppositely charged surfactant aggregates and polyions. Hence, no phase separation occurs. On dilution with water, however, the simple salt is diluted, its screening effect becomes weaker, and the attraction between the highly charged aggregates increases. This increasing attraction leads first to a phase separation and then to a contraction of the phase containing the complex salt, on addition of more water [14, 15].

1.3.1.2 The structure of the polyelectrolyte-surfactant complexes

The structure of the polyelectrolyte-surfactant complexes depends greatly on the competition between the rate of complex formation and the rate by which a thermodynamically equilibrated complex phase is eventually formed. Some structures that are the same as in surfactant and water binary system should be observable in polyelectrolyte-surfactant complexes. In the meantime, threading polyelectrolyte chains through these mesophases may also create different geometrical constraints from surfactants, thus producing some new structures. The nature of the chain has a strong influence on the phase behaviour in polyelectrolyte-surfactant mixed systems. It is likely that this is reflected also in the precise structure of the polyelectrolyte-surfactant complex.

Carnali [16] found a hexagonal phase in the phase diagram of 50 % neutralized sodium poly (acrylate), (NaPA), tetradecyltrimethylammonium bromide, and water. Likewise, Ilekti et al. [14] found cubic, hexagonal, and lamellar phases in a phase diagram of complexes between NaPA and cetyltrimethylammonium bromide. Ordered structures have been observed also in systems of covalently cross-linked polyelectrolyte gels, either in a lamellar, cubic, or hexagonal arrangement [17].

The structures of the complexes formed by cationic gels of poly (diallyldimethylammonium chloride) (PDADMACl) interacting with anionic surfactants of sodium alkyl-sulfate (SCnS) exhibited hexagonal packing of cylinders for complexes of PDADMACl-SCnS at n = 12 and cubic structures for complexes of PDADMACl-SCnS at n = 10, respectively. Novel phase structures were observed in Poly(MAA/NIPAM) gel-TTA and -DTA complexes: structures of Pm3n space group cubic, face-centered cubic close packing of spheres, and hexagonal close packing of spheres were observed in polyelectrolyte-surfactant complexes [18].

Kabanov et al. [19] reported a lamellar structure for complexes of poly (sodium acrylate) gel-alkyltrimethylammonium bromide. Okuzaki and Osada proposed a simple cubic structure for the complexes formed by poly (2-(acrylamido)-2-methylpropanesulfonic acid) (PAMPS) and alkylpyridinium chloride (APCl). It could be seen that most of the polyelectrolyte-surfactant complexes studied so far showed lamellar, cylindrical, and undulating layered structures.

1.3.1.3 Application of polyelectrolyte surfactant complexes

The study of polyelectrolyte-surfactant complexes has attracted a great deal of attention because of fundamental interest in their mesoscale properties and their potential applications in wastewater purification, biomimetic materials, and electroluminescent displays. Substantial interest in these systems arises in part from their propensity to self-assemble into mesostructured or nanostructured materials. Importantly, a wide variety of materials with different properties can be readily assembled from such ionic building blocks without the use of difficult synthetic procedures [20]. The materials produced can be modified by simply changing either the surfactant or the polyelectrolyte employed..

Complexes made from polyelectrolyte gels or by hydrogen bonding instead of charge coupling are regarded as potentially interesting hosts for guest polymerization reactions. Polyallyldimethylammonium chloride (pDADMAC) and sodium dodecyl sulfate (SDS) as hosts for the structure-directed polymerization of some vinyl monomers used as guests. It combines mesoscopic order, appropriate charge density and good binding properties with good solubility and swellability [21]. An ordered mesomorphous polyelectrolyte-surfactant complex of this surfactant di(undecenyl) phosphate (ωC11) and polydiallyldimethylammonium chloride (pDADMAC) can be used as a template for the polyaddition reaction of dithiols and the formation of nanostructured polyelectrolyte-polyelectrolyte complexes [22, 23].

1.3.2 General methods for the creation of complexes

Most researchers add aqueous solutions of polyelectrolyte to surfactant solutions to form the complex using metathesis (or ion exchange) as in the following equation.

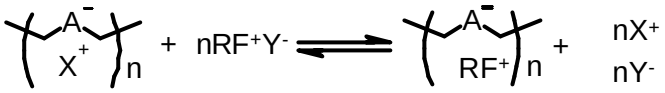

Metathesis

For example, if aqueous solutions of the salt of poly(acrylic acid) and a quaternary ammonium salt are mixed, a gel will form when the polyelectrolyte and surfactant are added in stoichiometric quantities. The gel is then extracted until no more soluble component can be removed. The resulting purified gel is dried to form a solid, whose properties vary from elastomeric to brittle and from crystalline to non-crystalline depending on the components of the complex [24].

In addition to metathesis, several other processes are conceivable. A selection of the most important of these are neutralization, chemical change, redox chemistry, quaternization, and miscellaneous reactions as shown in the figure below.

In this figure the polyanion or its source polymer is represented by - (A^-) - while the polycation is given by - (B^+) -. Counterions are shown as X^+ and Y and the surfactant is represented by RF*, where F is some functional group that determines the positive or negative charge on the surfactant fragment.

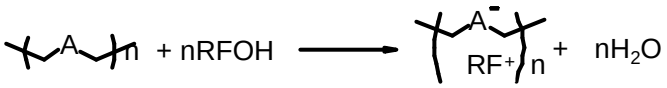

Neutralization

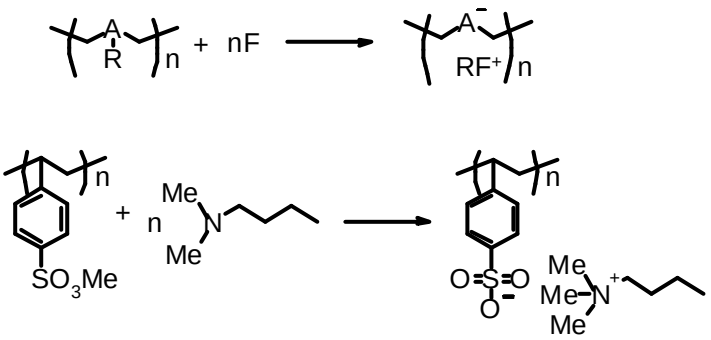

Chemical Change

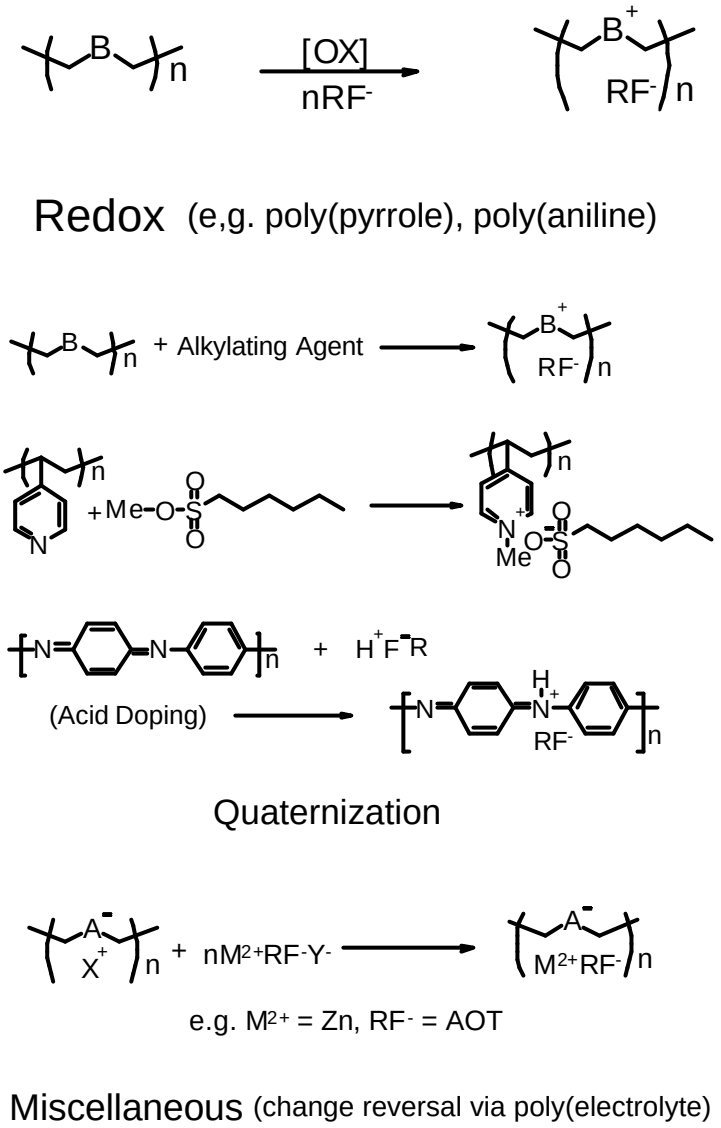

Figure 1.8 General techniques for and some example of the production of polyelectrolyte-surfactant complexes.

1.3.3 Solid state of polyelectrolyte-surfactant complex

Polyelectrolyte-surfactant complexes in the solid state are considered to be promising for the development of smart materials that are characterized by self-organized supramolecular structures [25]. The ready variability of the components provides opportunities for tailoring the microstructures of such complexes and for control of macroscopic properties. Assembly processes based on electrostatic interactions, formation of hydrogen bonds, or charge transfer has been shown to lead to the spontaneous formation of ordered structures in the solid state. The assembly through noncovalent interactions offers advantages over chemical synthesis in that it does not involve complicated preparative procedures, equilibrium structures can often

be realized, and adaptive rearrangement of the structure may be possible, if the external conditions (e.g., solvent or temperature) are changed. The mechanical properties of polyelectrolyte-surfactant complexes have been shown to depend on the chemical structure of the amphiphile. Complexes with double-chain surfactants in the amorphous state can exhibit mechanical properties similar to those of high-performance rubbery polymers, with elastic moduli in the range of 20-200 MPa [26].

1.3.3.1 The solid-state organization of polyelectrolyte surfactant complexes

The solid-state organization of complexes of flexible polyelectrolytes and oppositely charged surfactants is dominated by the tendency of the amphiphilic molecules to assemble in layered structures. Complexes formed by linear or cross-linked polyelectrolytes and oppositely charged single- or double-chain surfactants can spontaneously adopt lamellar structures, consisting of alternating layers of polymer chains separated by layers of surfactant. The long period of the lamellae depends on the organization of the surfactant molecules within the layers, which is governed by alkyl chain length and chemical structure of the amphiphile. Surfactants with shorter chains (fewer than 16 carbon atoms) are typically disordered in the complexes, while surfactants with longer chains (at least 16 carbon atoms) can crystallize in the complex [27,28].

Antonietti et al. have investigated the solid-state structures of various polyelectrolyte-surfactant complexes. Lamellar, modulated-lamellar, face-centered-cubic packing of undulated cylinders, hexagonal packing of cylinders, and bicontinuous sponge phase structures have been observed and analysed [29,30].

In complexes of cross-linked polymethacrylate anions and hexadecyltrimethylammonium cations, the surfactant chains crystallize on a hexagonal lattice in the solid state. Surfactant crystallites in the complex are considerably smaller than those of the uncomplexed surfactants, as indicated by their lower melting temperatures. For complexes of poly (styrenesulfonate) with alkyltrimethylammonium surfactants, no crystalline order was observed for chains with up to 18 carbon atoms. The strong mobility differences between the ionic and alkyl phase in the lamellar complex PSS-C18 are reflected: in the surfactant tails, a mobility gradient towards the terminal methyl group is observed. This fact as well as a high content of gauche conformations suggest a non-interdigitating morphology of the tails at room temperature. The behavior changes during cooling below an endothermic transition centered at 255 K where a high trans content and a homogenisation of the side chain dynamics is

observed. This is due to the formation of a highly transoid, interdigitated phase of the surfactant tails which is however not crystallized in a classical sense. The distance between mobile and immobile regions of the sample varies. For the complex PSS-C14, the length scale is essentially that of the primary lamellar structure. For PSS-C18, a characteristic length of the density fluctuations within the proposed undulated lamellar structure is estimated. This suggests that the polyelectrolyte chains impose restrictions on surfactant chain packing that decrease the tendency of the surfactant to form ordered structures.

Kabanov et al. [19] proposed a lamellar structure for poly (sodium acrylate) gel-CnTAB complexes. Okuzaki and Osada [31] proposed a simple cubic structure for complexes formed by poly (2-acrylamido-2-methylpropanesulfonic acid) with alkylpyridinium chloride. Antonietti et al. [28] have clearly shown poly (styrenesulfonate) (PSS) and alkyltrimethylammonium bromide (CnTAB) forms lamellar phases and exhibit a periodicity of 3-4 nm. Potassium poly (1, 4-phenyleneethynylene carboxylate) forms aggregates similar to cylinders. Complex of dihexadecyldimethylammonium-poly (1, 4-phenyleneethynylene carboxylate) forms an undisturbed lamellar mesophase in the solid state and can be used for a blue LED with a low turn-on point [32]. The nanostructures of Poly (MAA/NIPAM) gel complexes with C14TA and C12TA were observed to form structures of Pm3n cubic, face-centered cubic and hexagonal close packing of spheres [33]. Poly (diallyldimethylammonium chloride) (PDADMACl) and anionic surfactants of sodium alkyl sulfate (SCnS), the decrease in surfactant tail length could induce a structural transition from a two-dimensional (2D) hexagonal structure to Pm3n cubic structure, while in complexes between anionic hydrogels of poly (N-isopropylacrylamide-co-sodium methacrylate) [P(NIPAM-co-MAA)] and alkyltrimethylammonium bromide (CnTAB), the decrease in charge density of polyelectrolyte chains could induce a structural transition from Pm3n cubic to face-centered cubic and then to a 3D hexagonal close packing of spheres. For poly (vinylamine hydrochloride) (PVACl) and sodium alkyl sulfate (SCnS), A pH induced structural transition in the PVACl-SC10S complex from Ia3d cubic to bilayer lamellar and then to 2D hexagonal close packing of cylinders [34].

Another type of morphology was observed for the complexes formed between cationic copolymer poly (ethylene oxide)-g-polyethyleneimine and anionic surfactants. These systems self-assemble in micelle-like aggregates with a hydrophobic core from neutralized polyethyleneimine chains and surfactants and a corona from hydrated poly (ethylene oxide) chains [35].

In complexes based on poly (α-L-glutamate), the polypeptide chains are predominantly in the α-helical conformation at room temperature. As the temperature is increased, disruption of hydrogen bonds and a transition to a disordered conformation. The conformational changes are completely reversible on cooling. A reversible helix-to-coil transition is observed at elevated temperatures. Poly (L-lysine) complexes can adopt either β-sheet or α-helical conformations in the solid state. Poly (L-lysine) also adopts a β-sheet conformation in complexes with negatively charged lipids and in the protonated form in the solid state. Casting of films from chloroform-trifluoroacetic acid mixtures in which the poly (L-lysine) chains are disordered yields complexes in which the polypeptide chains are predominantly α-helical. The ordered conformations of the polypeptide chains in the complexes are considerably more susceptible to changes in environment (e.g., temperature, solvent) than those of the covalent analogues, suggesting that dipole-dipole interactions of the "side chains" destabilize the ordered arrangement of the polypeptide chains in the solid state and in organic media [36, 37].

1.3.3.2 Potential application of the solid-state polyelectrolyte-surfactant complexes

The potential use of poly(N-ethyl-4-vinylpyridinium bromide) and sodium dodecyl sulfate (SDS) can be used for the synthesis of new type of ionomers [38].

The amphiphilic properties of water-insoluble polyelectrolyte-surfactant complexes make these compounds promising as materials for molecular composites electronic devices such as light-emitting diodes as suggested by Neher et al [39].

The development of new thin-film surface coatings continues to be an important motivation behind many materials research programs. New materials are being sought for applications in optical and electrochemical sensors or in fuel-cell-based power systems [40].

The polyelectrolyte surfactant complexes also are used in the fabrication of biocompatible materials to immobilize or release drugs and proteins [41].

Owing to the amphiphilic nature of polyelectrolyte-surfactant complexes and the easy variability of their components, such compounds are promising as materials for separation membranes, solubilization, and compatibilization.

A number of polyelectrolyte-surfactant complexes form dirt repellent and low-friction coatings with low surface energies [42] and with interesting optical or biological properties. Solid comblike or "bottle brush" complexes raise interest due to their potential as facile

building blocks for self-organizing materials [43]. A fluorinated complex can be used as a coating material for smooth surfaces [44,45].

1.3.4 Stoichiometric polyelectrolyte-surfactant complexes

Stoichiometric polyelectrolyte-surfactant complexes represent a new type of comb-shaped polymers, in which every polymer chain unit has an electrostatically bound "side chain" [46]. One of the attractive features of the stoichiometric polyelectrolyte-surfactant complexes is the simplicity of their synthesis, which simplifies the "fine-tuning" of the resulting structures.

If equimolar amounts of charged polymer chain units and surfactant are used, the stoichiometric complexes precipitate from water. Stoichiometric complexes consisting of hydrophobically modified polyelectrolytes and double chain surfactants, as well as complexes formed by conventional polyelectrolytes and oppositely charged amphiphilic molecules can be redissolved in some common organic solvents of low polarity (ε = 2-10) without dissociation. Stoichiometric polyelectrolyte-surfactant complexes also dissolve in relatively polar solvents (N,N-dimethylformamide, dimethyl sulfoxide, aliphatic alcohols) [47]. The solubility and conformational state of the complex in solution is dependent on the structure of the surfactant and the polyelectrolyte as well as on the properties of the solvent. Complexes consisting of linear or slightly cross-linked polyelectrolytes and oppositely charged amphiphiles adopt lamellar structures in the solid state, in which the lamellae are believed to consist of alternating layers of polymer chains and surfactant molecules. Polyelectrolyte-surfactant complexes are anticipated to exhibit interesting properties in organic solvents and in the solid state owing to the combination of their polymeric nature with the amphiphilic nature of the surfactants [48].

Stoichiometric polyelectrolyte complexes can be processed easily by casting from organic solvents. Melt processability is limited. The high density of ionic groups results in a high glass transition temperature (Tg), which exceeds the temperature of decomposition. An interesting approach to decrease Tg has been reported, in which surfactants are complexed with copolymers of ionic and nonionic monomers. For practical applications, this is a harsh restriction, and melt processing is a desirable goal. To maintain a high lyotropic mesomorphous order as well as the stoichiometry of complex formation, a long alkyl chain should covalently be bonded to this polar repeat unit [30].

1.3.4.1 The structure of the stoichiometric polyelectrolyte-surfactant complexes

The stoichiometric 1:1 complexation of polyelectrolytes with oppositely charged surfactants typically results in the formation of water-insoluble soft-matter materials with numerous interesting liquid crystalline-like phases that have been reviewed by Zhou, Chu [49], Ober and Wegner [24] as well as Tirrell and Thunemann [50].

Harada et al. [51] have shown that the stoichiometric complex of poly (vinyl sulfate) (PVS) and cetyltrimethylammonium bromide (C16TAB) also possesses a lamellar structure, with a longer period of about 5-6 nm. When cast as thin films, such stoichiometric materials most likely form relatively chemically uniform coatings, at least in the film plane. Depending on the preparation methods employed, their surfaces may be terminated by either the hydrophobic alkane chains of the surfactant or the hydrophilic ionic regions of the complex [52]. The stoichiometric complex of polystyrene-block-polyacrylate anions (PS-b-PAA-) and N-cetylpyridinium cations (C16Py+) showed in the solid state the nonionic and surfactant-neutralized polyion segments segregate. The resulting materials have a unique microheterogeneous structure combining sequences of ion pairs formed by surfactant and PAA units, crystalline domains formed by aliphatic surfactant radicals, and amorphous polystyrene [53]. The stoichiometric complexes of poly (ethylene oxide)-block-polymethacrylate anions and N-alkylpyridinium cations are soluble in water. It has been shown that these complexes spontaneously arrange in small vesicles with a wall from the surfactant-neutralized polyion surrounded by the hydrophilic ethylene oxide shell [54].

For the poly(L-lysine) - dodecyl sulfate complex, the ratios of the Bragg spacings are 1:1/2:1/3:1/5:1/6:1/7, indicating a lamellar structure. The long period of the lamellar does not depend on the conformation of the polypeptide chains, but the lamellar orientation is different for different conformations. For films cast from chloroform containing 1 vol % trifluoroacetic acid the reflections corresponding to the lamellar spacings are equatorial, indicating anisotropic orientation of stacks of the lamellae within the film. At high trifluoroacetic acid content, the films are characterized by an isotropic orientation of stacks of lamellae [37].

All poly (α-L-glutamate) complexes studied possess similar lamellar structures. This is shown by the dependence of the lamellar spacing on the surfactant chain length. The slope of the dependence is equal to the projection of the C-C bond along the molecular axis in the fully extended alkane chain (1.3 Å per CH_2 group), suggesting that the surfactant chains in the complexes are nearly fully extended, interdigitated, and perpendicular to the lamellar surface [27].

The minimum number of carbon atoms in the side chain required for crystallization is 10 in the case of the poly (α-L-glutamic acid) and 16 for the known complexes of conventional

synthetic polyelectrolytes and oppositely charged surfactants. It is likely that, in the polypeptide-surfactant complexes the α-helical polymer backbone combined with the bulky headgroups of the surfactants imposes additional restrictions on alkyl chain packing and increases the minimum crystallization chain length [27].

The polypeptide chains in the complexes were shown to be predominantly in the α-helical conformation at room temperature. At higher temperatures, weakening or disruption of intramolecular hydrogen bonds stabilizing the α-helical conformation was observed. The polypeptide-surfactant complexes were shown to adopt lamellar structures in the temperature range 20-150 °C [36]. The polypeptide chains complexed with the surfactants adopt α-helical conformations. The shorter surfactant alkyl chains, consisting of twelve and sixteen carbon atoms, are disordered in the complexes, while the longer surfactant chains of eighteen carbon atoms crystallize in a hexagonal lattice [37].

1.3.4.2 The application of the stoichiometric polyelectrolyte surfactant complexes

The stiff, helical polyglutamate backbone promotes formation of ordered structures in solution and in the solid state, while the flexible side chains promote solubility in a wide range of organic solvents. Owing to their unique combinations of physical properties, such as high solubility and the ability to form liquid crystal phases, rod-like polypeptides with flexible side chains show promise as materials for optoelectronics, separation membranes and molecular composites [48].

A combination of an anionic polyelectrolyte (sodium polystyrenesulfonate, Na-PSS) and polymerizable cationic surfactants of the 2-(methacryloyloxy) ethyl (dimethyl) (n-alkyl) ammonium bromide type (CnBr) was used for the complex formation. The introduction of monomeric surfactants into the self-assembly process leads to the possibility to create a stoichiometric polyelectrolyte-polyelectrolyte complex from a polyelectrolyte surfactant complex by internal polymerization. It also reveals a novel example to conduct polymerization reactions in organized media [55].

The complexation of poly (styrenesulfonate) with viologen-containing dialkyl sulfates capable of reversible structural rearrangement has been used to prepare membranes with controlled permeability, in which the temperatures of the liquid-solid transitions of the alkyl chains can be controlled by redox reactions of the headgroups [56].

1.4 Polyelectrolytes investigated here: Ionenes

A class of polyelectrolytes having ammonium groups (mostly quarternary ammonium groups) in the main chains is called ionenes [57]. These [x,y]-ionenes are polyelectrolytic molecules consisting of dimethylammonium charge centers interconnected by alternating alkyl chain segments containing x and y methylene groups as shown below.

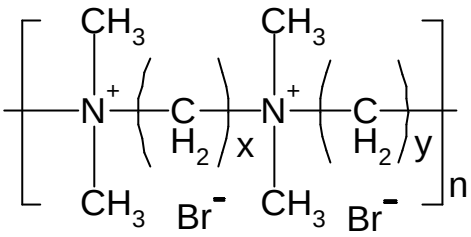

[X,Y] -ionene Bromide Polymer

1.4.1 Properties of ionenes

The properties of ionenes depend strictly on the charge density. Ionenes with high charge density demonstrate strong ionic interactions in aqueous solutions. Whereas ionenes derived from dihalides with long alkyl chains have lower charge density and show many similarities to non-charged organic polymers [58].

Ionenes containing short segments, that is, the [3,6]-, [6,6]-ionenes, and the [3,y]-ionenes in which $y < 14$, exhibit behavior typical of polyelectrolytes with rodlike or extended conformations. In contrast, the [3,y]-ionenes in which y is increased beyond 14 progressively form more compact (globular or micelle-like) aggregate structures and exhibit many of the properties (substrate solubilization, catalytic rate enhancements, counterion binding, etc.) reminiscent of those observed for aqueous cationic micellar solutions. As a consequence, such ionenes have been dubbed micelle-mimetic agents.

Polyelectrolyte solutions display strongly nonideal behavior due to electrostatic interactions between the highly charged polyions and small ions in solution [59]. In the absence of added salts, the aqueous solution of the [3,m]-ionenes with $m \leq 14$, and [6,6]-ionene exhibit a behavior typical of polyelectrolytes with extended or rodlike conformations. In contrast, the [3,16]-ionene forms spherical micelles [60]. In the presence of salt solution, the viscosity behaviour is similar to that of uncharged polymers. The conformation of ionenes in aqueous solutions for three species, 2,10-Br, 6,10-Br, and 6,6-Br (Br stands for bromide counterions)

was affected by the hydrophobic interaction between the CH_3 groups governing their conformations when the polyelectrolyte effect was suppressed by added salts, in which case the distribution of CH_3 groups along the backbone of the polymer played an important role [61]. Counterion binding appears to increase in the order $F^- < C1^- < Br^- < NO_3^- < I^- < CNS^-$, similar to that observed for strongly basic anion exchange resins. A variation in the charge density of the polymer chain does not appear to affect the root-mean-square end-to-end distance in salt solution [62]. Viscometric investigations indicated that these compounds are more compact at higher polarity of the solvent, and that this compactness is more dependent on the length of the alkyl chain than on the charge density. In less polar solvents this compactness is independent of the length of the side alkyl group chain as long as $R \geq 12$ (R is the side alkyl group chain) [63].

1.4.2 Potential application of ionenes

Ionenes like other polyelectrolytes have found potential applications ranging from the use as solid polymer conductors and as flocculation agents of clays in solution to modifiers of polymer-coated packing materials for capillary electrochromatography, polysoaps and vesicles, and for the preparation of simplex membranes for pervaporization [64]. Ionene polyelectrolyte-silica gels were suggested as stationary phases for high-performance liquid chromatography [65]. New ionenes with allyl pendant groups by quarternization of N,N'-diallylpiperazine with organic dihalides such as 1,4-dichlorobutane, 1,6-dibromohexane and 1,4-dichloromethylbenzene serve as cross-linkers. In the presence of the ionenes, free radical initiated copolymerization of acrylic acid gives transparent hydrogels, which would be of interest in preparing of simplex membranes [66].

1.5 The ionene surfactant complexes

The systematic study of the binding of anionic surfactants displayed that sodium alkyl sulfates (n = 6, 12) and sodium alkanesulfonates (n = 8, 10) has been reported by Y. Osada [67], with the synthetic polycations carrying charges on the chain backbone: x,y-ionene bromides (x = 3, 6, 12; y = 3, 4, 6, 12). Ionone polymers, depending on their structure, undergo two-step binding: first, they form stoichiometric one-to-one insoluble complexes and then non-stoichiometric soluble complexes. The formation of soluble complex was closely associated with the chemical structure of the ionenes. There existed a critical charge density and alkyl

chain length to give the two-step binding, below which only the conventional one-to-one stoichiometric binding took place.

Zheng et al found that in aqueous solution there is a narrow molar ratio of SDS/ionene (~1.0-1.35 depending on different ionenes), at which the viscosity of ionene-SDS aqueous solution rises suddenly due to the formation of water soluble inter-polymer aggregates via the SDS attached on the polymer chains. The viscosity falls sharply with further addition of excessive SDS, which forms micelles in solution and causes the de-aggregation of the inter-polymer aggregates [68]. Frömmel and T. Wolff researched the influence of ionene polyelectrolytes on rheology and photorheology of aqueous micellar cetyltrimethylammonium bromide containing 9-anthracene carboxylic acid, and found that solubilization of 9-anthracene carboxylic acid (9-AC) in aqueous solutions of [3,12]-ionene and [3,16]-ionene (with bromide counterions) generates hydrobromic acid. Photodimerization of solubilized 9-AC reverts this effect. Newtonian flow is observed in solutions of ionenes and 9-AC throughout. In contrast, aqueous solutions of cetyltrimethylammonium bromide containing 9-AC exhibit viscoelasticity. The addition of [3,16]-ionenes, as well as the photodimerization of 9-anthracene carboxylic acid, reduced viscoelastic features. Rheological analysis revealed up to four relaxation processes in sheared viscoelastic systems [69].

1.6 Aims and scope of studying ionenes and ionene surfactant stoichiometric complexes

1. The charge density of ionenes is solely determined by the choice of starting materials for synthesis and thus can be changed at will in a wide range. Moreover, with these materials it is possible to vary one parameter while keeping the other constant. It is possible to obtain samples with the same degree of polymerization but different charge density, or to keep the intercharge spacing constant and alter the polymer chain length. Viscosity and flow behaviour of methanol ionene solution will be investigated with and without simple salt and the size of ionene dodecyl sulfate complexes in methanol will be determined.
2. 1-anilinonaphthalene-8-sulfate (ANS) in methanol was used as the spectroscopic probe to determine the complex formation between the ionene and alkyl sulfate sodium.
3. The usual method of preparing the polyelectrolyte-surfactant complex from aqueous solution from ionene halides and alkali-surfactant salts has the following shortcoming:

adherent low molecular weight salts are found in the crude complex, purification affords reprecipitation several times. A new approach to prepare ionene-surfactant complex will avoid the formation of low molecular weight salts; one gets pure complexes after evaporation of methanol immediately.

4. Until now there are only few studies on the ionene-surfactant stoichiometric complexes in the solid state. The properties of stoichiometric complexes of several ionenes and alkyl sulfate-surfactants in the solid state will be studied with respect to the stability of stoichiometric complexes at high temperatures and to lyotropic and thermotropic phase transitions from the optically isotropic phase to the optically anisotropic phase. IR, DSC, and TG methods will be applied as well as polarized optical microscopy and birefringence measurements. Special attention will be payed to understanding the influence of water (or humidity) on the formation of mesogenic phases. It will be shown that some stoichiometric ionene surfactant complexes are temperature *and* humidity sensitive materials with according potential applications.

2 Experimental Part

2.1 Apparatus

2.1.1 Determination of isotropy/anisotropy (phase transition)

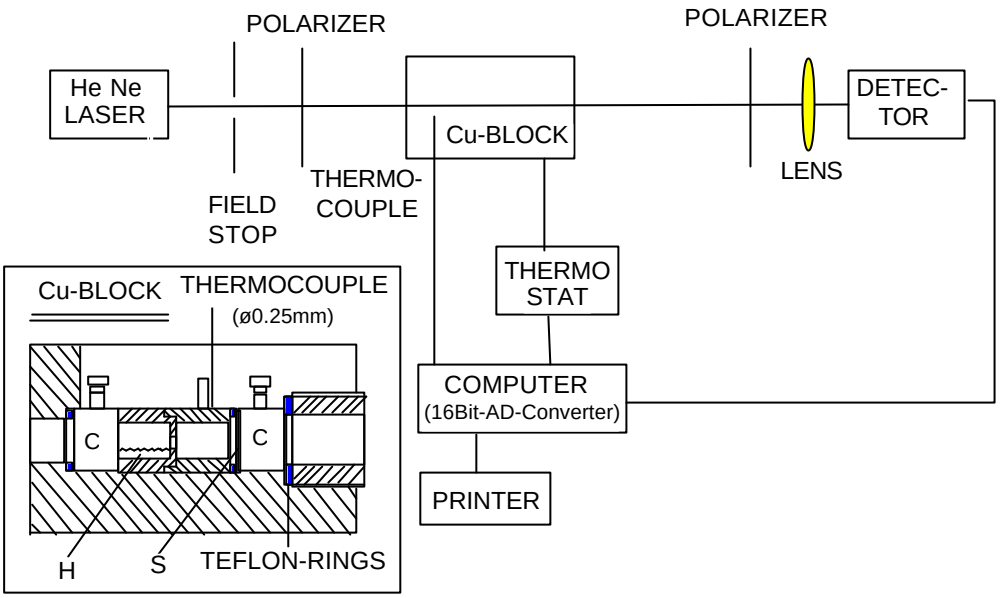

Figure 2.1 Schematic representation of the apparatus for the determination of phase transition temperatures ([70], modified by Jens frömmel). S = sample; C = cuvettes filled with water; H = salt solution for controlled humidity of the gas phase, which is in contact with the sample film S.

Figure 2.1 displays schematic representation of the apparatus for the determination of phase transition temperatures [70]. The method makes use of the fact that optically anisotropic phases are capable of converting linearly polarized light into circularly polarized light. Therefore, when the sample displays an anisotropic phase, the light of a He-Ne-laser can pass through a thermostatted sample placed between perpendicularly crossed filters for linearly polarized light. The transmitted light is recorded by the detector as photodiode voltage. The principle of the apparatus is shown in figure 2.2.

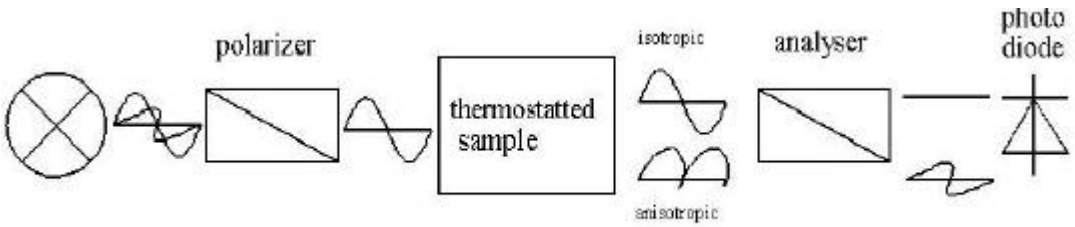

Figure 2.2 The principle of the apparatus for the determination of phase transition

Controlled relative humidity is achieved by placing an appropriate aqueous salt solution in the vicinity of the sample. This assures contact through the gas phase between the sample film and the salt solution. Constant relative humidity at 25 °C is provided by aqueous salt solutions with concentrations according to the desired water activity, which is shown in table 2.1 [71]. In the temperature range investigated in this study the relative humidities do not deviate significantly from the values at 25 °C.

aqueous salt solution	relative humidity (25 °C)
saturated $MgCl_2$	33 % [a]
saturated NaI	38 % [a]
5.75 mol/kg $CaCl_2$	41.9 % [b]
5.50 mol/kg $CaCl_2$	44.05 % [b]
5.25 mol/kg $CaCl_2$	46.8 % [b]
saturated $Ca(NO_3)_2$	51 % [a]
saturated $My(NO_3)_2$	53 % [a]
saturated NaBr	58 % [a]
saturated NH_4NO_3	62 % [a]
solutions of $CaCl_2$	64 % - 68 % [b]
saturated KI	69 % [a]
saturated $NaNO_3$	74 % [a]
saturated NaCl	75 % [a]
solution of NaCl	≥77 % [c]
pure water	100 %

[a] David R. Lide, CRC handbook of chemistry and physics 75 th Edition, 1994, CRC Press, p. 15-25.

[b] Gmelins (1957) Handbuch der anorganischen Chemie, vol. 28 (Ca), teil B lieferung 2. Verlag Chemie, Weinheim, p. 488 ff.

[c] Gmelins (1973) Handbuch der anorganischen Chemie, vol. 21 (Na), 7th supplement, 8th edn. Verlag Chemie, Weinheim, p. 10 ff.

Table 2.1 The relationship between aqueous salt solutions at various concentrations and the water activity in the gas phase

2.1.2 Thermogravimetry-mass spectrometry (TG-MS)

Thermogravimetric analyses were performed using a Netzsch TG/DTA STA 409 instrument, which is in conjunction with the mass spectrometer (MS). The low-molecular-weight gas products in pyrolysis and steam gasification were measured by a Balzers MID at the same time. During the experiment Argon gas was fed into the thermobalance reactor.

2.1.3 Differential scanning calorimetry (DSC)

Differential scanning calorimetry (DSC) curves were taken on a Setaram DSC 121 instrument. For low temperatures liquid nitrogen was used to control the temperature.

The sample preparation for differential scanning calorimetry (DSC): the predried stoichiometric complex was filled into a suitable crucible and was dried in a desiccator over phosphorous pentoxide for two days at normal pressure, then placed in a desiccator together with a cup of aqueous salt solution at the desired water activity for 24 h. The swollen sample was sealed in the crucible. This method can prevent water uptaken by the stoichiometric complex from escaping when the complex was heated during the DSC process.

2.1.4 Attenuated total reflection (ATR)-IR-spectra

For attenuated total reflection (ATR)-IR-spectra a Thermo-Nicolet AVATR instrument, fitted with a model 360 FT-IR detector, was available.

2.1.5 Polarized microscopy

Textures of mesogenic samples were obtained via polarizing microscopy using a Jenapol polarizing microscope with a Mettler FP80Ht central processor. The sample is held in the Mettler FP80Ht hot stage. In the process of experiment, the sample could be heated or cooled by the control of the Mettler FP80Ht central processor, which also allowed to adjust and control the heating and cooling rate of sample.

Mesogenic samples for polarized microscopy were prepared as follows: a film of the complex was casted from methanol solution on a glass plate; the film was dried in a desiccator over phosphorous pentoxide for two days at normal pressure. The dry complex was then placed in a desiccator together with a cup of aqueous salt solution at the desired water activity for 24 h. Grease (Glisseal) was casted on the four side edges on another glass plate, then the two glass plate were put together tightly to keep the sample and absorbed water between the two glass

plates. The method prevents water uptaken by the complex from escaping when the complex was heated on the hot stage.

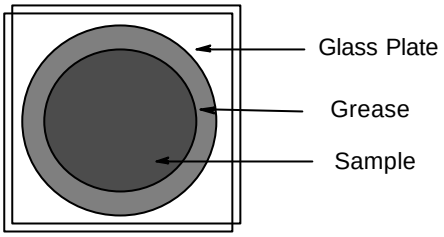

2.1.6 NMR spectra

NMR spectra were taken on Bruker models DRX-500 and Ac-200, respectively.

2.1.7 Quasielastic and Static Light Scattering

The light scattering set-up from ALV, which was used for both static and quasielastic light scattering (QELS), consists of a 632.8nm 22mW He-Ne laser light source and the detector optics coupled via a monomodal fiber to an ALV/CSG-8 goniometer. An ALV/High QE APD detector was connected to an ALV-5000/EPP multiple tau digital correlator. The Cuvettes were sealed after filtration through 0.22 µm Millipore filters and immersed in a large-diameter thermostated bath containing toluene placed at the axis of a goniometer. Apparent hydrodynamic radii of ionene and its complexes, R_H^{ap}, were measured at 90 ° at different sample concentrations [72].

Static light scattering was performed with the same apparatus by measuring the total scattering intensity and comparing it with that from toluene. The data were treated by the cumulant technique. Refractive index increments have been measured with a Brice-Phoenix differential refractometer.

A part of the ionene polyelectrolytes were reinvestigated on analogous apparatus set up at the Charles University at Prague in the group of Prof. Karel Procházka under the auspices of the Euorpean Graduate College “Advanced Polymeric Materials”. Results from both QLS apparatuses widely agreed.

2.1.8 Steady-State Fluorimetry

Steady-state fluorescence spectra (i.e., corrected excitation and emission spectra and steady-state anisotropy) were recorded with a SPEX Fluorolog 3 fluorometer in a 1 cm quartz cuvette

closed with a Teflon stopper. These experiments were performed at the Charles University at Prague in the group of Prof. Karel Procházka under the auspices of the Euorpean Graduate College “Advanced Polymeric Materials”.

ANS was purchased from Sigma, declared contents of EtOH and MeOH were 0.2% and less than 0.1%, respectively.

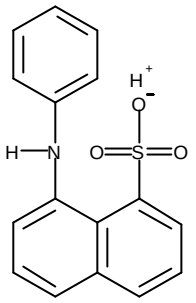

8-anilino-1-naphthalenesulfonic acid

Methanol was purchased from Fluka. It was "for luminescence" grade MeOH; the purity was more than 99.5%.

Excitation of fluorescence emission spectra was at 370 nm and the concentration of 8-anilino-1-naphthalenesulfonic acid (ANS) was 3 μmol l^{-1}; the concentration of ionene solution in methanol was 10 g l^{-1}.

2.1.9 Ubbelohde viscometer

Viscosities of ionenes were measured at 25±0.01 °C, using Ubbelohde viscometer. No correction for shear dependency was applied, since only low molecular-weight ionene was investigated.

2.2 Preparation of ionenes

2.2.1 Synthesis of [3,22]-ionene

2.2.1.1 Preparation of 1-morpholino-1-cyclohexene

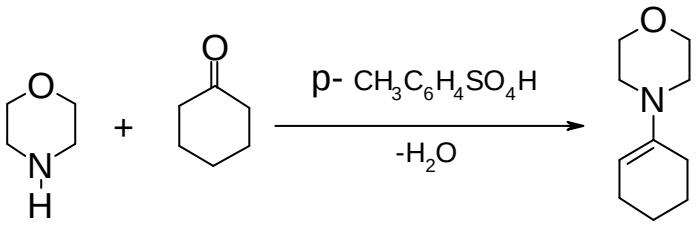

A solution of 147 g (1.50 mol) of cyclohexanone, 157 g (1.80 mol) of morpholine, and 1.5 g of p-toluenesulfonic acid in 300 ml of toluene is heated to boiling in a 1 liter round-bottomed flask fitted with a water separator under a reflux condenser. The separation of water begins at once and ceases after 4 ~ 5 hours. An indented Claisen distill head is attached to the flask, and the reaction mixture is distilled. Most of the toluene is removed at atmospheric pressure. 1-morpholino-1-cyclohexene is collected as a colorless liquid at boiling point 118-120 °C [73]. The yield is about 92 gram (37%).

Notes: an excess of morpholine is required because water which separates during the reaction always contains a considerable amount of it in solution; 1-morpholino-1-cyclohexene is very easily hydrolysed. Accordingly one must be careful to keep moisture out. On long standing in a refrigerator, the compound generally becomes somewhat yellowish, but this does not affect its usefulness in subsequent reactions.

^{1}H-NMR of 1-morpholino-1-cyclohexene (*d*/ppm at 500 MHz in $CDCl_3$): 1.53 (m, 2 H, δ-CH_2- in cyclohexene), 1.66 (m, 2 H, ε-CH_2- in cyclohexene), 2.01-2.07 (m, 4 H, (γ, ζ)-CH_2- in cyclohexene), 2.76 (t, 4 H, (γ, ε)-CH_2- in morpholin), 3.71 (t, 4 H, (β, ζ)-CH_2- in morpholin), 4.66 (t, 1H β-CH- in cyclohexene)

2.2.1.2 2,2'-Sebacoyldicyclohexanone

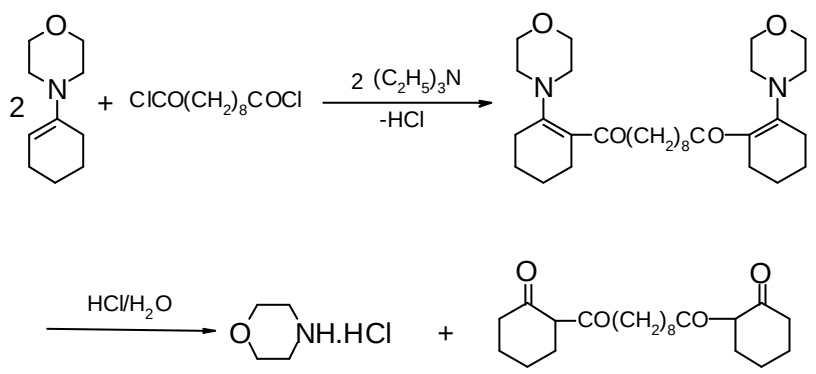

A solution of 33.4 g (0.2 moles) of 1-morpholino-1-cyclohexene and 20.2 g (27.8 ml 0.2 mole) of anhydrous triethylamine in 100 ml of dry chloroform is put into 1 liter, three necked, round-bottomed flask equipped with a mechanical stirrer, a dropping funnel, and a reflux condenser. Tubes with calcium chloride are inserted in the open ends of the dropping funnel and reflux condenser. The reaction flask is immersed in an oil bath at 35 °C, and a solution of

24 g (0.1 moles) of sebacoyl chloride in 40 ml of dry chloroform is added to the well-stirred reaction mixture over a period of about 1.5 hours. The reaction mixture gradually assumes an orange to red color, and a solid precipitates. The reaction mixture stirred for additional 3 hours at 35 °C, 100 ml of 20 % hydrochloride acid is added, and the mixture is boiled under reflux for 5 hours with vigorous stirring. The reaction mixture is cooled to room temperature, and the chloroform layer is separated and extracted with six 30-ml portions of water. The washing and the aqueous phase are combined, adjusted to pH 5-6 with 25% sodium hydroxide solution, and extracted with five 20-ml portions of chloroform. The chloroform extracts are combined with the chloroform layer, and the chloroform is removed by distillation. The residue gradually congeals to an oily solid on standing at room temperature under a pressure of 10-15 mm Hg. The yield is about 38.8 gram (53.7%).

Notes: sebacoyl chloride can be prepared as follows. A mixture of 150 g (0.74 moles) of sebacic acid (Acros) and 150 ml of thionyl chloride are heated in an oil bath at 60 °C. The acid gradually dissolves with evolution of HCl. After ceasing of the evolution, the mixture is distilled as rapidly as possible under reduced pressure.

2.2.1.3 Disodium 7,16-diketodocosanedioate

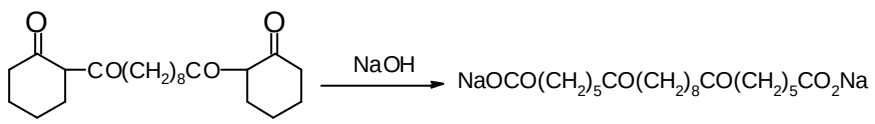

A mixture of 24 g (0.6 moles) of sodium hydroxide and 280 ml of commercial absolute ethanol are refluxed with stirring in a 1 liter round-bottomed flask until all the sodium hydroxide is dissolved (about 2 hours). The solution is cooled to room temperature, and a warm solution of 2, 2'-sebacoyldicyclohexanone in 60 ml of absolute ethanol is added. Within 15 min the mixture is heated by means of an oil bath and then refluxed for 1 hour. Colorless disodium 7,16-diketodocosanedioate separates during the heating. The reaction mixture is cooled to room temperature and the salt is collected on a Büchner funnel and pressed to become as dry as possible. The moist salt is suspended in 200 ml of absolute ethanol with stirring and is then collected on the Büchner funnel as before. The yield is about 47.4 gram (95%) [74].

2.2.1.4 1,22-Docosane diacid

$$NaOCO(CH_2)_5CO(CH_2)_8CO(CH_2)_5CO_2Na \xrightarrow{H_2NNH_2} HOCO(CH_2)_{20}COOH$$

Disodium 7,16-diketodocosanedioate of 47.4 g, 13.14 g (0.24 moles) potassium hydroxide, 110.6 ml diethylenglycol and 158 ml (82%) hydrazine hydrate are added and mixed in a 1 liter round-bottomed flask equipped with a reflux condenser, a thermometer, a stirrer, and a deep oil bath. The mixture is heated under reflux about 8 hours.

Potassium hydroxide (67.15 g, 1.23 moles) is dissolved in 395 ml diethylenglycol by heating the mixture. This solution is added to the reaction mixture. Reflux condenser is stopped, the reaction mixture was allowed to boil in order to remove the excess hydrazine hydrate, when the inside temperature of reaction mixture reaches 195 °C, the removing hydrazine hydrate process is stopped. Then the reflux condenser is opened, the residual mixture is refluxed for additional 14 hours. The reaction mixture is cooled to about 100 °C, washed out of the flask with hot water, and acidified to a pH between 2 and 3 with 12 N hydrochloric acid. The aqueous solution is centrifuged. The collected moist paste is heated to about 100 °C, and then cooled down to room temperature. The collected moist paste is filtered through a folded paper; the filter cake is pressed as dry as possible.

Under reflux the filter cake is dissolved in butanone (as little as possible), the solution is cooled to 0 °C very slowly. The 1,22-docosane diacid that crystallizes thereby is separated on a funnel and then dried completely in vacuum.

The crude 1,22-docosane diacid and 150 ml of nitric acid (65%) mixed in a 500 ml round-bottomed flask equipped with a reflux condenser, a stirrer, was heated for about 15 hours under reflux (producing much violet smoke). The solution was filtered, and the filter cake was washed until the pH of the filtrate reaches about 4. The filter cake was pressed as dry as possible and then dried completely in vacuum. The crude product was purified three times by recrystallizations from butanone [75]. Colorless 1,22-docosanedioic acid is obtained; mp 121-122 °C. (lit. mp 125-127 °C). The yield is about 13 gram (33%).

^{1}H-NMR of 1,22-docosane diacid (d/ppm at 500 MHz in $CDCl_3$): 1.24-1.30 (m, 32 H, (γ, δ, ε, ζ, η, θ, ι, κ,)-CH_2), 1.63 (m, 4 H, β-CH_2), 2.35 (t, 4 H, α-CH_2)

2.2.1.5 N,N,N′,N′-tetramethy-1,22-docosanediamine

$$HOCO(CH_2)_{20}COOH \xrightarrow[aq(CH_3)_2NH]{SOCl_2} (CH_3)_2NCO(CH_2)_{20}CON(CH_3)_2$$

1,22-docosane diacid (5.03 g, 13.6 mmol) was refluxed with about 30 ml of thionyl chloride for 5 hours. After this reaction, excess thionyl chloride was completely removed by vacuum distillation and the chloride of the acid was obtained as brown crystals. An ethyl ether solution (30 ml) of the acid chloride was added with vigorous stirring to a well-chilled aqueous solution of dimethylamine (40 %, 10 ml) containing 3 g of sodium hydroxide. After 1 hour reaction time, chloroform was added to this reaction mixture and the organic layer separated. This organic phase was dried over magnesium sulfate, and the solvent was removed by evaporation. The crude diamine thus obtained was recrystallized from ethyl acetate to get pure diamine [76]. Mp 97-98 °C (lit. mp 99-100 °C). The yield is about 4.09 gram (71%).

$$(CH_3)_2NCO(CH_2)_{20}CON(CH_3)_2 \xrightarrow{LiAlH_4} (CH_3)_2N(CH_2)_{22}N(CH_3)_2$$

Next, a portion of the diamine (total 4.09 g, 11.5 mmol) was added stepwise to a mixture containing $LiAlH_4$ (2.12 g, 55.9 mmoles) and 150 ml anhydrous THF, and the total mixture was refluxed for 18 hours. The excess $LiAlH_4$ was destroyed by adding several milliliters of ethyl acetate and then 300 ml of ethyl ether to the reaction mixture. A few milliliters of water were added until the white precipitate settled down to the bottom of the flask when the stirring was stopped. The precipitate was filtered and the filtrate solution dried over magnesium sulfate. The solvents were removed from the filtrate by evaporation, and N,N,N′,N′-tetramethy-1,22-docosanediamine was obtained as white crystals. The crystals were dissolved in 100 ml of aqueous hydrochloride acid, and the solution was neutralized by addition aqueous ammonium hydroxide solution. The precipitated diamine was filtered and dried under vacuum to obtain N,N,N′,N′-tetramethy-1,22-docosanediamine [77], GC-MS purity 93.45 %, mp 47 °C (lit. mp 48 °C). The yield is about 2.11 gram (62.6%).

^{1}H-NMR of N,N,N′,N′-tetramethy-1,22-docosanediamine (*d*/ppm at 500 MHz in $CDCl_3$):
1.23-1.26 (m, 36 H, (γ, δ, ε, ζ, η, θ, ι, κ, λ)-CH_2-docosano-), 1.43 (m, 4 H, β-CH_2-docosano-), 2.20-2.25 (m, 16H including 12 H in $(CH_3)_2N^+$ and 4 H, α-CH_2-docosano-)

2.2.1.6 [3,22]-ionene

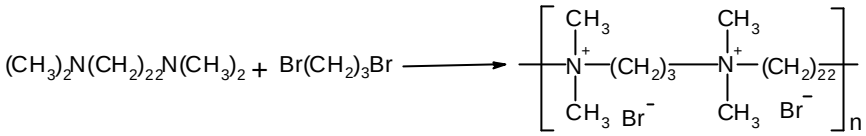

Equimolar quantities of the reactants, N,N,N′,N′-tetramethy-1,22-docosanediamine (purity 93.45% 4.765 g, 11.22 mmoles) and 1,3-dibromopropane (2.266 g 11.22 mmoles) were dissolved in 50 ml dry THF, and the solution was stirred for 96 hours at 40±1 °C. The resulting solution was added stepwise to dry ethyl ether (100 ml) from which the [3, 22]-ionene separated as a white powder. The mixture was cooled in an ice bath and stirred 1 hour to crystallize the ionene, which was filtered and dried over phosphorous pentoxide for two days at normal pressure and for another three days in vacuum. The yield is about 8.87 gram (79.2%).

The molecular weights for [3,22]-ionene was 8370 g/mol as revealed by light scattering experiments (QLS) in methanol.

^{1}H-NMR of [3,22]-ionene bromide (*d*/ppm at 500 MHz in CD_3OD): 1.35-1.49 (m, 36 H, (γ, δ, ε, ζ, η, θ, ι, κ, λ)-CH_2), 1.88 (m, 4 H, β-CH_2-docosano-), 2.41 (m, 2 H, β-CH_2-propano-), 3.26 (s, 12 H, $(CH_3)_2N^+$), 3.38 (m, 8H, α-CH_2).

2.2.2 Preparation of [3,12]-ionene, [3,10]-ionene and [5,10]-ionene

2.2.2.1 N,N,N¢,N¢-tetramethy-dodecane-1, 12-diamine and N,N,N¢,N¢-tetramethy-decane-1,10-diamine

1,10-dodecane diacid (0.1 moles) or 1,8-decane diacid (0.1 moles) was refluxed with about 50 ml of thionyl chloride for 5 hours. After this reaction, excess thionyl chloride was removed by vacuum distillation. An ethyl ether solution (150 ml) of the acid chloride was added with vigorous stirring to a well-cooled (about 0 °C) aqueous solution of dimethylamine (40 %, 87 ml) containing 26 g of sodium hydroxide. After 1 hour reaction time, chloroform was added to this reaction mixture and the organic layer separated. This organic phase was dried over magnesium sulfate, filtered, and the solvent was removed by evaporation. The crude diamine thus obtained was recrystallized from ethyl acetate to get the pure diamine. The GC-MS purity of 1,10-dodecane diacid bis-dimethylamide and 1,8-decane diacid bis-dimethylamide was 100 % in both cases.

Next, the diamine (0.019 mmoles) was added in portions to a mixture containing $LiAlH_4$ (2.4 g) and 120 ml anhydrous THF, and the completed mixture was refluxed for 12 hours. The

excess $LiAlH_4$ was destroyed by the addition of ethyl acetate and 200 ml of ethyl ether to the reaction mixture. A few milliliters of water were added until the white precipitate settled to the bottom of the flask when the stirring was stopped. The precipitate was filtered off and the filtrate dried over magnesium sulfate. The solvents were removed from the filtrate by evaporation and N,N,N′,N′-tetramethy-dodecane-1, 12-diamine or N,N,N′,N′-tetramethy-decane-1,10-diamine was obtained as a colorless liquid. The materials were dried over phosphorous pentoxide for two days at normal pressure and for another three days in vacuum. The GC-MS purities of N,N,N′,N′-tetramethy-dodecane-1, 12-diamine and N,N,N′,N′-tetramethy-decane-1,10-diamine were 100 % and 99.57 %, respectively. The yield of N,N,N′,N′-tetramethy-dodecane-1, 12-diamine is about 12.5 gram (48.6%) and the yield of N,N,N′,N′-tetramethy-decane-1,10-diamine is about 16.8 gram (70%).

^{1}H-NMR of N,N,N′,N′-tetramethy-dodecane-1, 12-diamine (*d*/ppm at 500 MHz in $CDCl_3$): 1.23-1.25 (m, 16 H, (γ, δ, ε, ζ)-CH_2), 1.41 (m, 4 H, β-CH_2-dodecano-), 2.17-2.21 (m, 16 H, including 12 H $(CH_3)_2N$) and 4 H, α-CH_2-dodecano-)

N,N,N′,N′-tetramethy-1, 10-decandiamine (*d*/ppm at 500 MHz in $CDCl_3$): 1.25 (m, 14 H, (γ, δ, ε)-CH_2-decano-), 1.41 (m, 4 H, β-CH_2-decano-), 2.17-2.21 (m, 16 H including 12 H, $(CH_3)_2N$) and 4 H, α-CH_2-decano-)

2.2.2.2 [3,12]-ionene, [3,10]-ionene and [5,10]-ionene [78,79,80]

Equimolar quantities of the reactants N,N,N′,N′-tetramethyl-dodecane-1,12-diamine or N,N,N′,N′-tetramethy-decane-1,10-diamine (purity 100% and 99.57%. 10.67 mmoles) and 1,3-dibromopropane (10.67 mmoles) or 1,5-dibromopentane (10.67 mmoles) were dissolved in 10 ml methanol, and the solution was stirred for 48 hours at 40±1 °C. The methanol was removed by evaporation and the residue was dried over phosphorous pentoxide for two days at normal pressure and for another three days in vacuum. The yield of [3,12]-ionene is about 82%, the yield of [5,10]-ionene is about 85% and the yield of [3,10]-ionene is about 88%.

Molecular weights for [3,10]-ionene, [3,10]-ionene, and [5,10]-ionene were 2090 g/mol, 1300 g/mol, and 2170 g/mol, respectively, as determined by light scattering experiments (QLS) in methanol.

^{1}H-NMR of [3,12]-ionene bromide (*d*/ppm at 200 MHz in CD_3OD): 1.42-1.49 (m, 16 H, (γ, δ, ε, ζ)-CH_2), 1.89 (m, 4 H, β-CH_2-dodecano-), 2.43 (m, 2 H, β-CH_2-propano-), 3.29 (s, 12 H, $(CH_3)_2N^+$), 3.66 (s, 8H, α-CH_2).

(*d*/ppm at 500 MHz in DMSO): 1.27 (br, 16 H, (γ, δ, ε, ζ)-CH_2), 1.68 (br, 4H, β-CH_2-dodecano-), 2.20 (br, 2 H, β-CH_2-propano-), 3.10 (br, 12 H, $(CH_3)_2N^+$), 3.32 (br, α-CH_2 and H_2O).

^{1}H-NMR of [5,10]-ionene bromide (*d*/ppm at 500 MHz in CD_3OD): 1.46-1.56 (m, 14 H including 12 H, (γ, δ, ε)-CH_2-decano- and 2 H, γ-CH_2-pentano-), 1.86 (m, 4 H, β-CH_2-decano-), 1.97 (m, 4 H, β-CH_2-pentano-), 3.20 (s, 12 H, $(CH_3)_2N^+$), 3.38-3.50 (m, 8H, α-CH_2); (*d*/ppm at 500 MHz in DMSO): 1.29 (br, 14 H including 12 H, (γ, δ, ε)-CH_2 -decano-and 2 H, γ-CH_2-pentano-), 1.66 (br, 4H, β-CH_2 -decano-), 1.73 (br, 4 H, β-CH_2-pentano-), 3.03 (br, 12 H, $(CH_3)_2N^+$), 3.33 (br, α-CH_2 and H_2O).

^{1}H-NMR of [3,10]-ionene bromide (*d*/ppm at 500 MHz in DMSO): 1.30 (br, 12 H, (γ, δ, ε)-CH_2 -decano-), 1.68 (br, 4H, β-CH_2 -decano-), 2.2 (br, 2 H, β-CH_2-propano-), 3.09 (br, 12 H, $(CH_3)_2N^+$), 3.33 (br, α-CH_2 and H_2O).

2.3 Preparation of the silver salts of surfactant alkyl sulfates

2.3.1 Silver dodecyl sulfate

Silver dodecyl sulfate (AgDS) precipitated from an aqueous solution of sodium dodecyl sulfate (SDS, Merck, 0.9 mol/l) and silver nitrate (Merck, 5.6 mol/l) at room temperature. The white solid of silver dodecyl sulfate was filtered, and pressed as dry as possible. AgDS was recrystallized several times from water (< 50 °C) until all the sodium salt was removed. The content of sodium salt was tested by the flame coloration method. The pure material was dried in vacuum. The yield is about 33.3%.

$$SDS + AgNO_3 \xrightarrow{water} AgDS\downarrow + NaNO_3$$

^{1}H-NMR of silver dodecyl sulfate (*d*/ppm at 500 MHz in CD_3OD): 0.97 (t, 3 H, -CH_3), 1.36-1.48 (m, 18 H, (γ, δ, ε, ζ, η, θ, ι, κ, λ)-CH_2), 1.72 (m, 2 H, β-CH_2) and 4.06 (t, 2 H, α-CH_2)

2.3.2 Silver decyl sulfate and silver octyl sulfate

Because the aqueous solution of sodium decyl sulfate or sodium octyl sulfate and silver nitrate at room temperature can not form the precipitate, the method described above for silver

dodecyl sulfate does not work any more. Cation exchange resins were chosen to prepare silver decyl sulfate and silver octyl sulfate. The ion exchange resins are highly ionized in both acid ($R\text{-}SO_3H$) and salt ($R\text{-}SO_3Na$) form of the sulfonic acid group. They can convert a metal salt to the corresponding acid by the reaction. The hydrogen and sodium forms of strong acid resins are highly dissociated and the exchangeable Na^+ and H^+ are readily available for exchange over the entire pH range. Consequently, the exchange capability of strong acid resins is independent of solution pH.

The column was filled with 500 ml cation exchange resin (Lewatit S 100, Na^+ form), and rinsed subsequently with 2 N aqueous nitric acid solution until all the sodium ions were removed, which was tested by the flame coloration method. The column was rinsed again by distilled water until the pH of the rinsing solution reached about 6-7. By that the exchange resin was converted to the acidic form ($R\text{-}SO_3H$).

The column was rinsed by 5 N aqueous silver nitrate solution (Merck). When the pH of the rinsing solution was about 4-5, the rinsing process was stopped and the acidic form of the resin became the salt ($R\text{-}SO_3Ag$). Distilled water was used to wash the column until the pH of the rinsing solution reached about 6-7, indicating that all the free ion of silver in the column has been removed. The Ag^+ attached on salt ($R\text{-}SO_3Ag$) can not be rinsed off by distilled water.

Notes: the outside of the column was wrapped by aluminum foil to prevent silver ions from reduction upon exposure to light.

$$R\text{-}SO_3Na + HNO_3 \longrightarrow R\text{-}SO_3H + NaNO_3$$

$$R\text{-}SO_3H + AgNO_3 \longrightarrow R\text{-}SO_3Ag + HNO_3$$

Thereafter the column was rinsed with aqueous decyl sodium sulfate or octyl sodium sulfate (Acros, 0.8 mol/l) slowly. The elute was collected in portions which were tested for the presence of sodium. When sodium was detected the rinsing was stopped. Decyl silver sulfate formed white crystals in aqueous solution, which were separated. The materials were dried in vacuum to remove all water. The yield is about 92 %. Silver octyl sulfate does not precipitate. Therefore the solution of silver octyl sulfate was kept at a temperature below 40 °C until most of the water was slowly evaporated. Then the materials were dried in vacuum to remove all water. White pure crystals were obtained. The yield is about 86%.

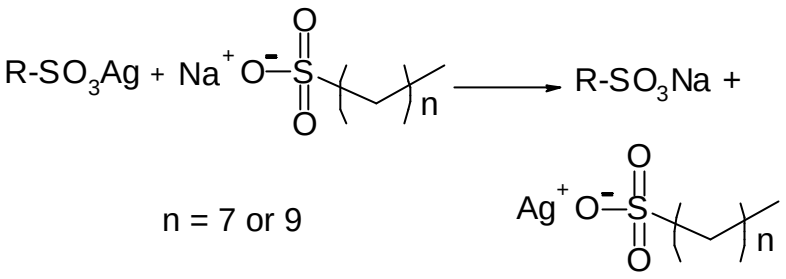

^{1}H-NMR of silver decyl sulfate (*d*/ppm at 500 MHz in CD_3OD): 0.97 (t, 3 H, -CH_3), 1.36-1.41 (m, 14 H, (γ, δ, ε, ζ, η, θ, ι)-CH_2), 1.73 (m, 2 H, β-CH_2) and 4.06 (t, 2 H, α-CH_2)

^{1}H-NMR of silver octyl sulfate (*d*/ppm at 500 MHz in CD_3OD): 0.97 (t, 3 H, -CH_3), 1.34-1.48 (m, 10 H, (γ, δ, ε, ζ, η)-CH_2), 1.73 (m, 2 H, β-CH_2) and 4.06 (t, 2 H, α-CH_2)

2.4 Preparation of the stoichiometric complexes of ionenes and alkyl sulfates

[3,22], [3,12], [5,10] or [3,10]-ionene bromide (about 1 g in 50 ml anhydrous methanol) was added drop-wise to dodecyl, decyl or octyl silver sulfate (50 mmol/l) dissolved in 50 ml dried methanol. The addition of ionene bromide was stopped, when the voltage of the electrochemical cell <Ag|Ag^+, DS^-, ionene, AgBr(s), methanol || K^+, Br^- (saturated), methanol, AgBr(s)|Ag> had passed its steepest slope as a function of added ionene bromide solution [81]. Silver bromide precipitated and was easily filtered off through a folded paper from the solution. After slow evaporation of the solvent at low pressure and low temperature (≤ 35 °C), the salt free stoichiometric complexes were obtained. Schematic representation of the preparation of the ionene alkyl sulfate stoichiometric complex is shown in Figure 2.3. The [3,12]-ionene dodecyl sulfate, [5,10]-ionene dodecyl sulfate, [5,10]-ionene decyl sulfate, [3,10]-ionene dodecyl sulfate, and [3,10]-ionene decyl sulfate stoichiometric complexes formed opaque films on a quartz plate, whereas the other stoichiometric complexes ([3,10]-ionene octyl sulfate, [5,10]-ionene octyl sulfate, [3,12]-ionene decyl sulfate, [3,12]-ionene octyl sulfate, [3,22]-ionene dodecyl sulfate, [3,22]-ionene decyl sulfate stoichiometric complexes) are all powders, they cannot form a clear and opaque film on a quartz plate.

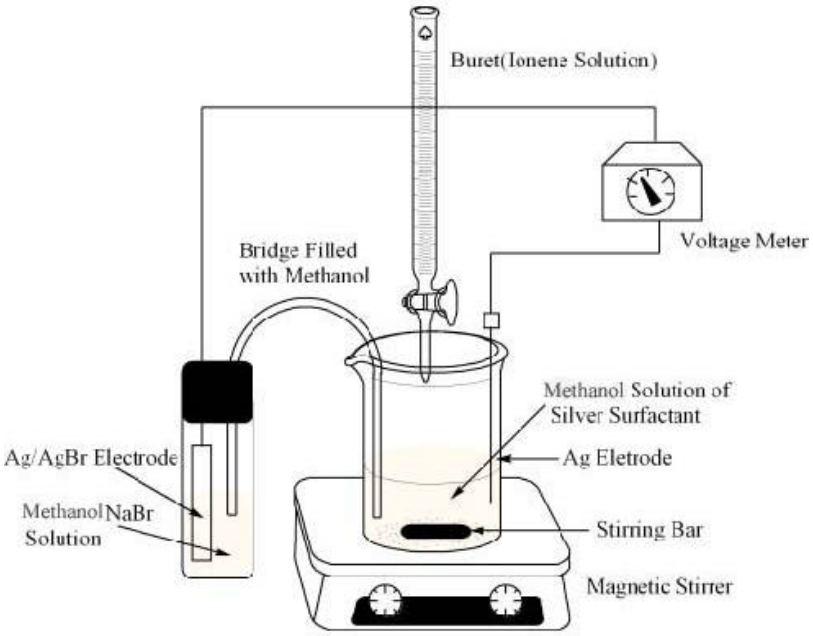

Figure 2.3 Schematic representation of the preparation of the ionene alkyl sulfate stoichiometric complex.

The [3,12]-ionene dodecyl sulfate, [5,10]-ionene dodecyl sulfate, [5,10]-ionene decyl sulfate [3,10]-ionene dodecyl sulfate, and [3,10]-ionene decyl sulfate stoichiometric complexes formed opaque films on a quartz plate placed at the bottom of the reaction beaker. Finally the films were dried in a desiccator over phosphorous pentoxide for two days at normal pressure and for another three days in vacuum.

The swelling of ionene-alkyl sulfate stoichiometric complexes due to uptake of water from the gas phase as a function of controlled relative humidity was investigated as follows: a film of the stoichiometric complex was casted from methanol on the inner wall of an open polyethylene screw cap bottle and dried over phosphorous pentoxide until constancy of weight. A high complex concentration in methanol insured a high viscosity of the solution so that the film at the wall remained stable during the drying process. Then the bottle with the dry film was weighed, placed in a desiccator together with a cup of aqueous salt solution at the desired water activity for 24 h, and weighed again. The bottle was tightly capped while weighing it in order to rule out the uptake of moisture from ambient air (or the loss of water).

3. Results

3.1 The solution properties of ionenes in methanol

3.1.1 Viscosity of ionenes in methanol in the absence of added electrolytes

The viscosity (η) of dilute solutions of uncharged polymers can usually be represented, over a reasonably large range of concentrations, as a linear function of concentration

$$(h - h_0)/h_0 c = [h] + k[h]^2 c \qquad (1)$$

Where h_0 is the viscosity of the solvent, $[h]$ the intrinsic viscosity, c the concentration in grams of solute per 100 ml of solution, and k is a dimensionless constant (Huggins constant), which is characteristic of the polymer and solvent but normally independent of the molecular weight. Fuoss [82] reported that the reduced viscosity, η_{sp}/c, of solutions containing a pure, highly charged, flexible, linear polyelectrolyte increased sharply and continuously with dilution at very low concentration (here $\eta_{sp}=(\eta-\eta_0)/\eta_0$). The observed concentration dependence of η_{sp}/c could be represented by the empirical relationship [82].

$$h_{sp}/c = \frac{A}{1 + B\sqrt{c}} + D \qquad (2)$$

where A, B, and D are characteristic constants of each sample.

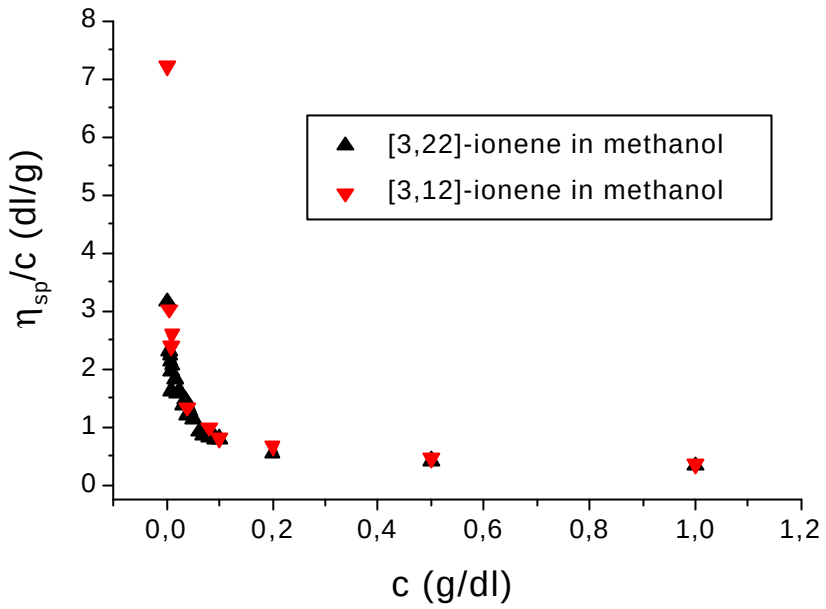

Figure 3.1 Reduced viscosities as a function of polyelectrolyte concentration.

From Figure 3.1 we can see the viscosity of [3, 22]-ionene and [3, 12]-ionene as a function of concentration. The behaviour is typical for polyelectrolytes in polar organic solvents (such as methanol) in the absence of added electrolyte [83]. The plot in Figure 3.1 could be very accurately represented by eq 2. The data were fitted to this relationship by plotting $(\eta_{sp}/c\text{-}D)^{-1}$ *us.* $c^{1/2}$. D was first obtained approximately from a plot of η_{sp}/c *us.* $c^{-1/2}$ and the values of D so obtained were found to produce perfectly linear plots of $(\eta_{sp}/c\text{-}D)^{-1}$ *us.* $c^{1/2}$. From eq 2, the value of η_{sp}/c is equal to (A + D) as *c* approaches zero. Since D is negligibly small, for all practical purpose, A is the value of the intrinsic viscosity i.e., the limit of the reduced viscosity as the concentration approaches zero A = [*h*]. [84]. The intercept of the plot of $(\eta_{sp}/c\text{-}D)^{-1}$ *us.* $c^{1/2}$ is equal to 1/A, and the slope is equal to B/A. It was not possible to determine the values of A very precisely, because of the small magnitude of 1/A. The results are listed in table 3.1.

ionene	A / dl g^{-1}	B / $(dl/g)^{1/2}$	D / dl g^{-1}
[3,22]-ionene	89.206	463.99	0.15255
[3,12]-ionene	29.710	128.49	0.21055

Table 3.1 Fuoss equation parameters of ionenes

A or [η] are related to the molecular weight of the polyelectrolyte. The data suggest that the molecular weight of [3,22]-ionene is ca. three times that of [3,12]-ionene.

3.1.2 Viscosity of ionenes in methanol in the presence of added electrolytes

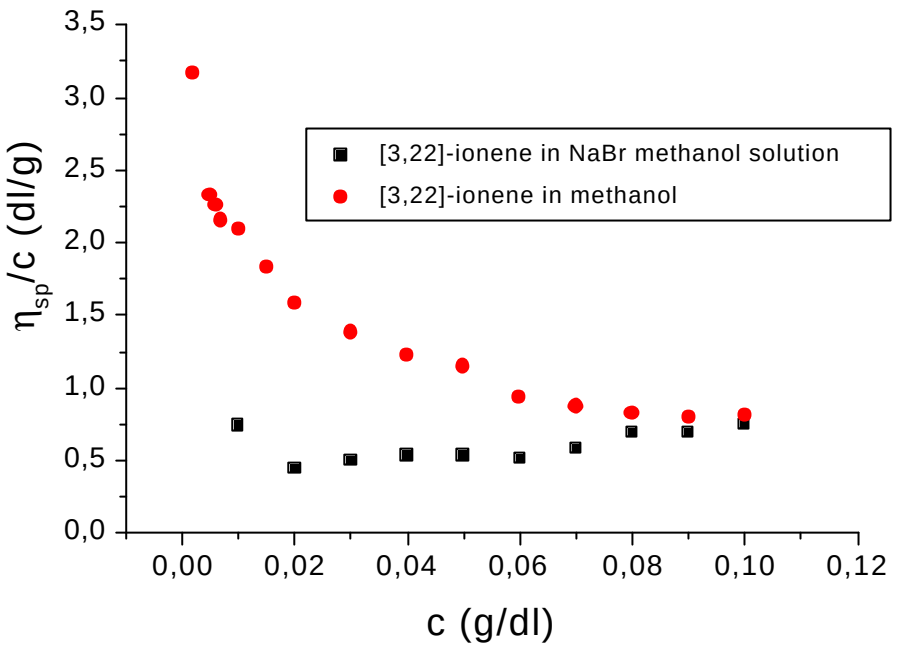

Figure 3.2 Concentration dependence of the reduced viscosity with and without salt.

In this solution the simple salt concentration is not constant, and its concentrations changed with the ionene concentration. The first ionene solution only contained ionene, no simple salt in it. When the ionene solution became dilute, and then the salt was added in a quantity that kept the total ion concentration unchanged. For example the first concentration of [3.22]-ionene solution was 0.1 g/dl, the ion concentration was calculated to be $3.34*10^{-4}$ mol/l. When the ionene concentration was diluted to 0.5 g/dl, the ion concentration was $1.67*10^{-4}$ mol/l, NaBr salt (0.835 mol/dl) was added to the solution so that the ion concentration was kept constant at $3.34*10^{-4}$ mol/l.

3.1.3 The size of ionenes and their dodecyl sulfate complexes

Sample	[b]A_2(10^{-3} mol ml g^{-2})	[a]M_w(10^3 g mol^{-1})
[3,10]-ionene	4.43	1.3
[3,12]-ionene	0.08	1.9
[3,12]-ionene dodecyl sulfate complex	0.88	6.0
[5,10]-ionene	1.05	2.1
[5,10]-ionene dodecyl sulfate complex	1.63	6.7
[3,22]-ionene	-5.0	8.4

[a] molecular weight, evaluated from SLS data by the standard Zimm technique

[b] the second virial coefficient, evaluated from SLS data by the standard Zimm technique

Table 3.2 The molecular weight of ionenes and ionene-dodecyl sulfate stoichiometric complexes

For ionene and its surfactant complexes the second virial coefficients (A2), evaluated from SLS data by the standard Zimm technique, are all positive except [3,22]-ionene, (i.e., [3,12]-ionene is 0.08 mol ml g^{-2}, [3,12]-ionene dodecyl sulfate complex 0.88 mol ml g^{-2}, [5,10]-ionene 1.05 mol ml g^{2} and [5,10]-ionene dodecyl sulfate complex 1.63 mol ml g^{2}), therefore methanol was a good solvent for [3,12], [5,10], [3,10]-ionenes and for the [3,12]- and [5,10]-ionene dodecyl sulfate stoichiometric complexes, but for [3,22]-ionene the second virial coefficients (A2) is negative, so the methanol is not good solvent. At ambient condition the methanol solutions of ionenes and the [3,12]- and [5,10]-ionene dodecyl sulfate stoichiometric complexes are clear and transparent, no precipitate was observed.

Table 3.2 displays the molar masses of both complexes are clearly higher than those expected from stoichiometric reaction between ionene and dodecyl sulfate. The unit molar mass of [3,12]-ionene is 229.18 g/mol, and the unit molar mass of [3,12]-ionene dodecyl sulfate complex is 414.68 g/mol, from these data the expected molar mass of [3,12]-ionene dodecyl sulfate stoichiometric complex is $3.43*10^3$ g/mol, which is much less that the measured molar mass ($6*10^3$ g/mol); The [5,10]-ionene and its complex shows a similar regularity.

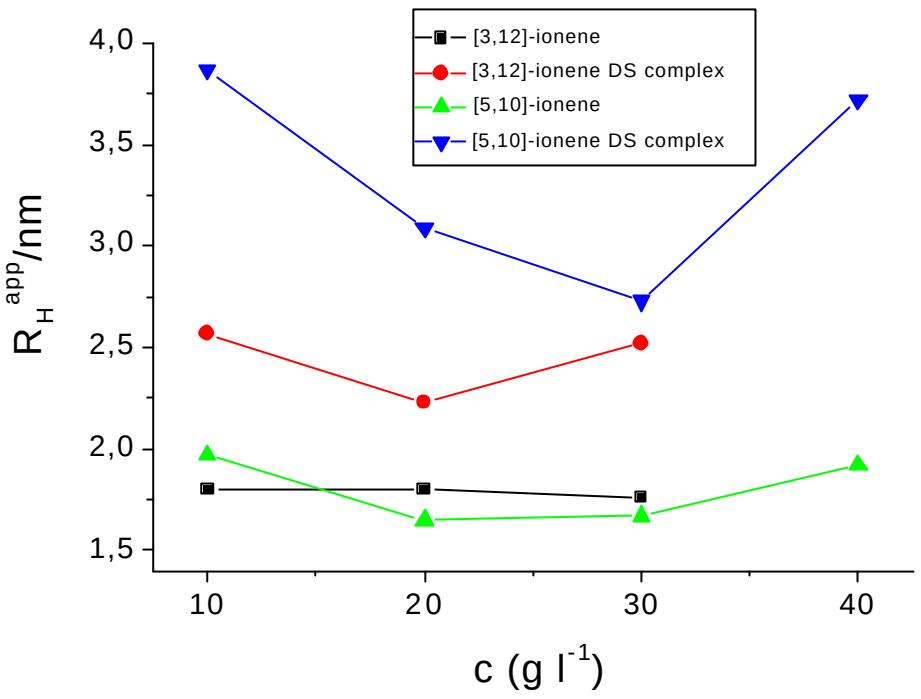

Figure 3.3 Apparent hydrodynamic radius, R_H^{app}, of ionenes and their stoichiometric complexes (no simple salt) in methanol (evaluated from DLS data by the cumulant method).

From figure 3.3 we can see that the apparent hydrodynamic radius; R_H^{app}, of all ionenes did not change significantly but for their stoichiometric complexes (no simple salt) the apparent hydrodynamic radius; R_H^{app} changed considerably within the concentration range 10-40 $g\,l^{-1}$. Light scattering data show that [3,12] and [5,10]-ionenes had almost the same molecular weight (M_w) ($1.9*10^3$ and $2.1*10^3$ g/mol, respectively) and the same apparent hydrodynamic radius, R_H^{app}, in methanol [86]. Of the complexes [5,10]-ionene dodecyl sulfate had a higher molar mass than [3,12]-ionenes dodecyl sulfate; also [5,10]-ionene dodecyl sulfate had a higher apparent hydrodynamic radius, R_H^{app}, than [3,12]-ionene dodecyl sulfate in methanol solution.

The complex was formed in solution by adding sodium dodecyl sulfate in methanol to [3,12]-ionene bromide which means in methanol NaBr was produced while forming the complex, so there is simple salt present while the hydrodynamic radius is being measured. In this process no precipitate was formed, and the complex solution is clear and transparent. The R_H vs. c (sodium dodecyl sulfate) dependence clearly showed a fast increase in R_H until c (sodium dodecyl sulfate) of about 20 mmol/l was reached; slower increase in R_H above this concentration was probably caused by increase in viscosity due to the sodium dodecyl sulfate

addition (methanol viscosity was about 0.5906 mPas at 20 °C, sodium dodecyl sulfate viscosity (0.1 M) in methanol about 0.6691 mPas at 20 °C) and had nothing to do with complex formation. Again, the transition from fast to slow increase occurred at a concentration which was approx. twice smaller than that corresponding to 1:1 stoichiometry between dodecyl sulfate and [3,12]-ionene. The apparent hydrodynamic radius, R_H, in methanol of stoichiometric [3,12]-ionene dodecyl sulfate complex which contained simple salt which was produced by Br^- in ionene and Na^+ in sodium dodecyl sulfate was about 3.7 nm, but R_H in methanol without simple salt was only 2.57 nm at the same concentration, which was much smaller than the above stoichiometric complex which contained simple salt.

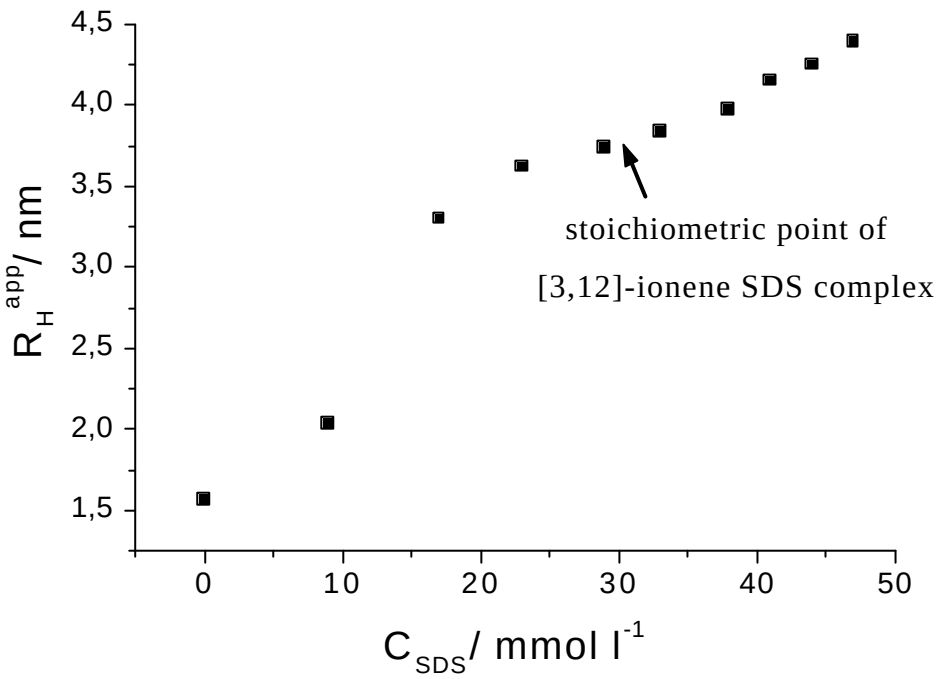

Figure 3.4 Apparent hydrodynamic radius, R_H^{app}, of [3,12]-ionene as a function of the concentration of sodium dodecyl sulfate (C_{SDS}). (concentration 10 g l^{-1})

3.1.4 Fluorescent probe investigation of ionene surfactant complexes

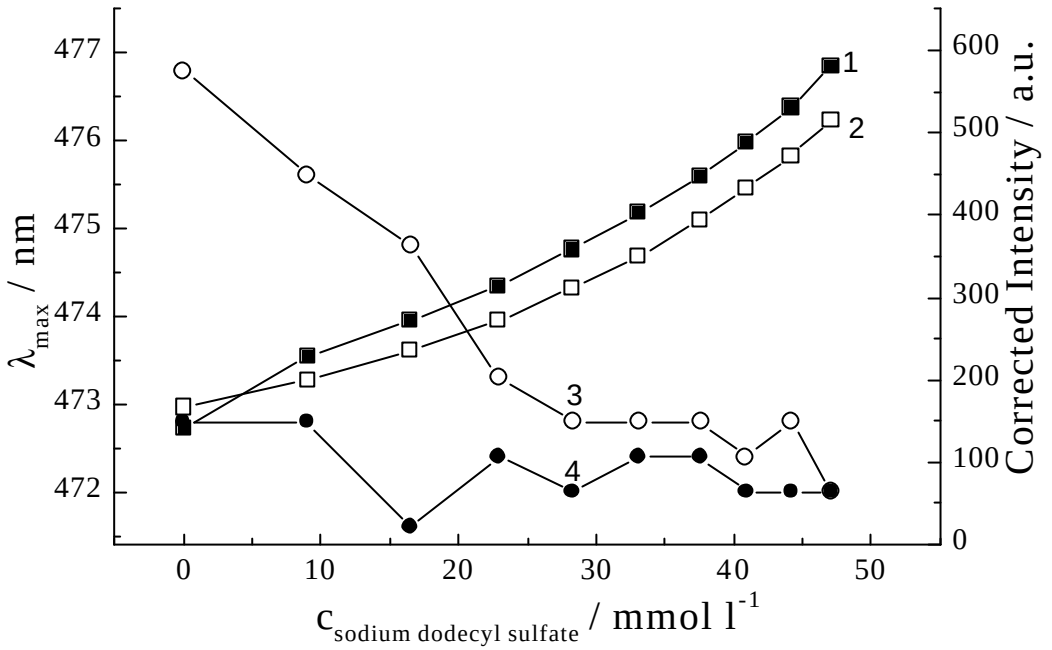

Figure 3.5 Emission maximum wavelengths (3,4) and maximum intensities (1,2) of the ANS fluorescence in methanol as a function of the sodium dodecyl sulfate concentration. Curves 2 and 3 in the presence, curves 1 and 4 in the absence of [3,12]-ionene.

The emission maximum wavelengths of the spectroscopic probe (with and without the [3,12]-ionene) decrease with the increase of the concentration of sodium dodecyl sulfate (SDS). While in the absence of [3,12]-ionene the emission maximum wavelengths decrease almost negligibly (Fig. 3.5, curve 4), in the presence of [3,12]-ionene the decrease is substantial below the stoichiometric point (SDS concentration at about 30.15 mmol l^{-1}) of [3,12]-ionene and SDS. Above this stoichiometric SDS concentration the decrease is poor, similar to the behavior in the absence of [3,12]-ionene (Fig. 3.5, curve 3). The intensities (with and without [3,12]-ionene) as a function of SDS concentration yields two parallel curves, both increase with increasing concentration of SDS (Fig. 3.5, curve 1 and 2).

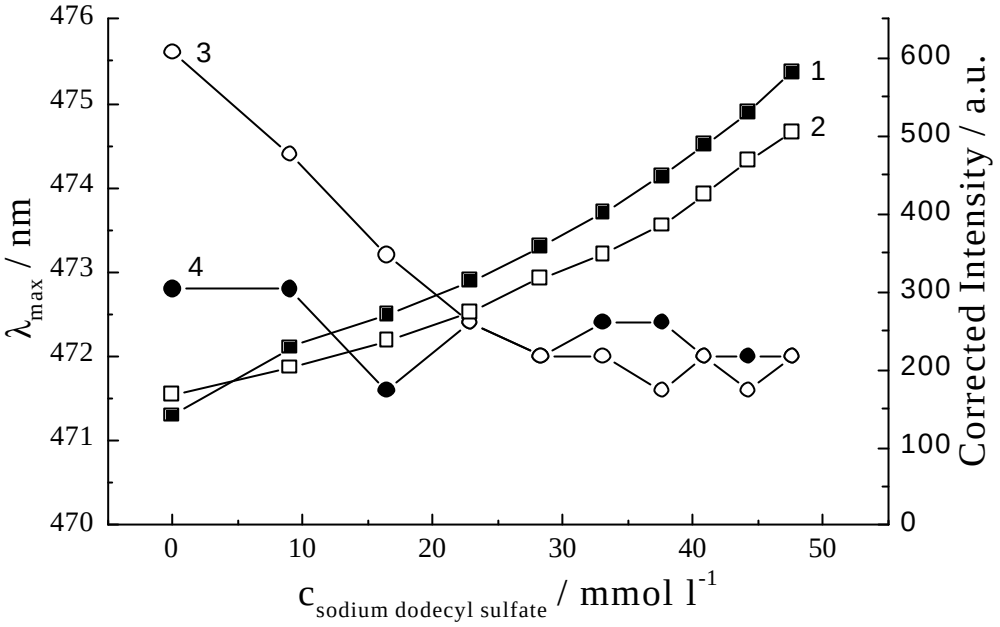

Figure 3.6 Emission maximum wavelengths (3,4) and maximum intensities (1,2) of the ANS fluorescence in methanol as a function of the sodium dodecyl sulfate concentration. Curves 2 and 3 in the presence, curves 1 and 4 in the absence of [5,10]-ionene.

When [3,12]-ionene was exchanged by [5,10]-ionene or by [3,10] ionene, respectively, the results qualitatively coincide and are quantitatively very similar (compare Fig. 3.5 with Fig. 3.6 and 3.7). A marked distinction, however, was found when SDS was exchanged by sodium decyl sulfate, see Fig. 3.8 and 3.9: in the absence of ionene the addition of sodium decyl sulfate leads to a more non-polar environment. In the presence of [3,10]- and [5,10]-ionene the levelling off at the stoichiometric point (at 30.53 mmol/l sodium dodecyl sulfate) is not observed.

In all cases the intensity of the maximum of the fluorescence emission increases monotonously with the surfactant concentration, a little less for the decyl sulfate. The stoichiometric point is not reflected. The reason for the increase of the intensity therefore probably has to do with changes in the refractive index of the solutions or differences in the reflectivity of cuvette walls in the presence of the surfactants.

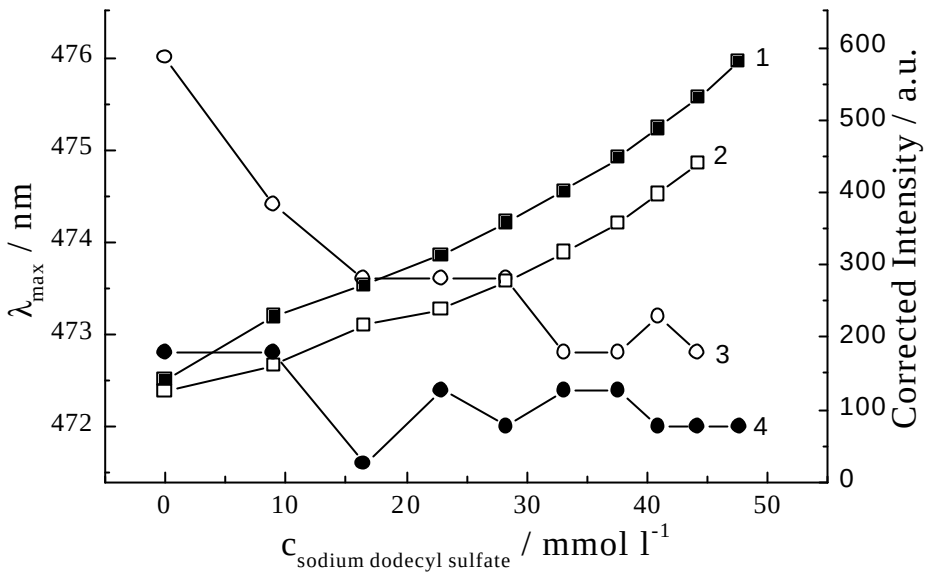

Figure 3.7 Emission maximum wavelengths (3,4) and maximum intensities (1,2) of the ANS fluorescence in methanol as a function of the sodium dodecyl sulfate concentration. Curves 2 and 3 in the presence, curves 1 and 4 in the absence of [3,10]-ionene.

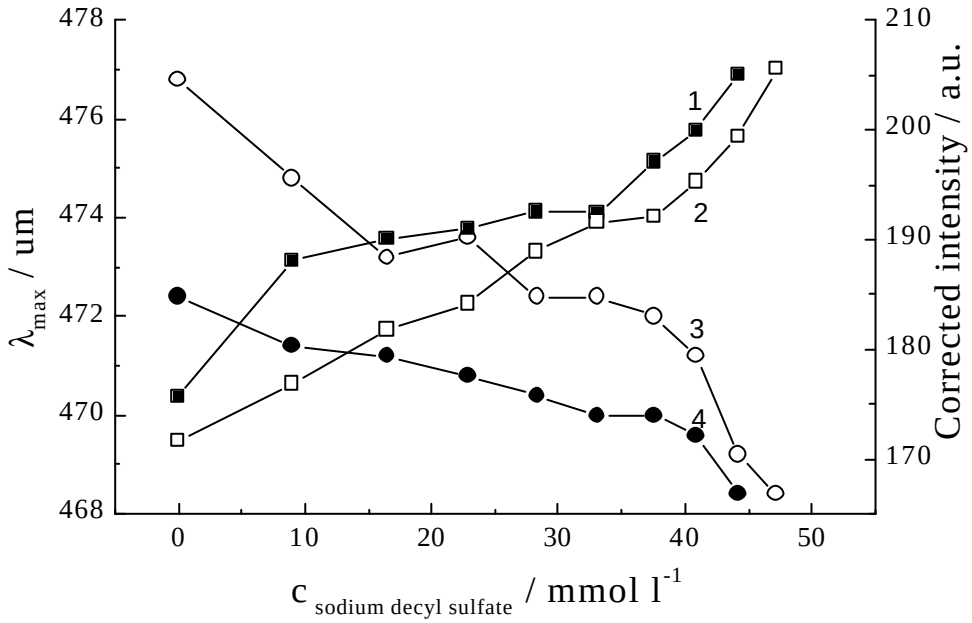

Figure 3.8 Emission maximum wavelengths (3,4) and maximum intensities (1,2) of the ANS fluorescence in methanol as a function of the sodium decyl sulfate concentration. Curves 2 and 3 in the presence, curves 1 and 4 in the absence of [5,10]-ionene

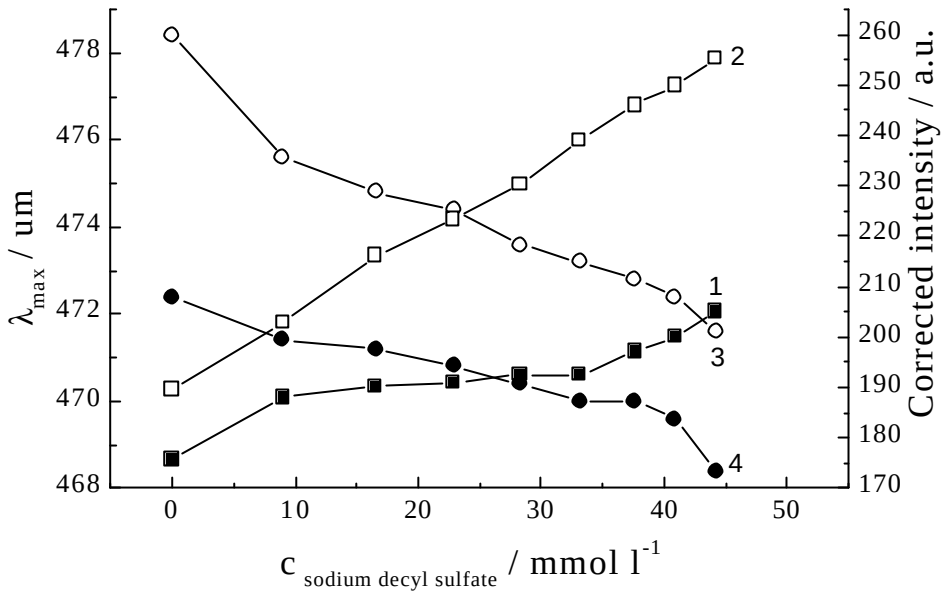

Figure 3.9 Emission maximum wavelengths (3,4) and maximum intensities (1,2) of the ANS fluorescence in methanol as a function of the sodium decyl sulfate concentration. Curves 2 and 3 in the presence, curves 1 and 4 in the absence of [3,10]-ionene.

3.2 The ionene and ionene alkyl sulfate stoichiometric complexes

3.2.1 Films formed from ionene alkyl sulfate stoichiometric complexes

To prepare water and salt free complexes according to reference [28], first the precipitate was formed in water between polyelectrolyte and surfactant, the resulting white precipitate usually coagulates, and the water is removed. The crude complex contains large amounts of excess surfactant, salt, and water. For purification, this mixture is redissolved in alcohol, and water is added until a phase separation of a complex rich gel phase and a salt and surfactant rich water phase takes place. After removal of the water phase, this phase separation is repeated until the water phase is practically free of halogenide ions. Ionene hydroxide as a necessary component would be unstable at room temperature. Therefore stoichiometric complexes of ionene and alkyl sulfate were prepared via the reaction of the bromide of the ionene and the silver salt of alkyl sulfate in methanol under precipitation of the silver halide. Films produced from [3,22]-ionene dodecyl sulfate, [3,22]-ionene decyl sulfate and [3,22]-ionene octyl sulfate, [3,12]-ionene decyl sulfate and octyl sulfate, [5,10]-ionene octyl sulfate, [3,10]-ionene octyl sulfate stoichiometric complexes turned out to be cloudy and to form undulated surfaces. These complexes were not investigated further. Films produced from [3,12]-ionene dodecyl sulfate,

[5,10]-ionene dodecyl sulfate, [5,10]-ionene decyl sulfate, [3,10]-ionene dodecyl sulfate, and [3,10]-ionene decyl sulfate, however, were clear, transparent, optically isotropic and flat; i.e. they showed the desired properties. Table 3.3 displays the film properties of stoichiometric complexes.

substance	Dodecyl sulfate	Decyl sulfate	Octyl sulfate
[3,22]-ionene	bad	bad	bad
[3,12]-ionene	good	bad	bad
[5,10]-ionene	good	good	bad
[3,10]-ionene	good	good	bad

Good film: clear, transparent, flat and optically isotropic

Bad film: cloudy and undulated surface

Table 3.3. Apparent properties of stoichiometric complex films

3.3 [3,12]-ionene and [3,12]-ionene dodecyl sulfate stoichiometric complexes

3.3.1 The silver dodecyl sulfate

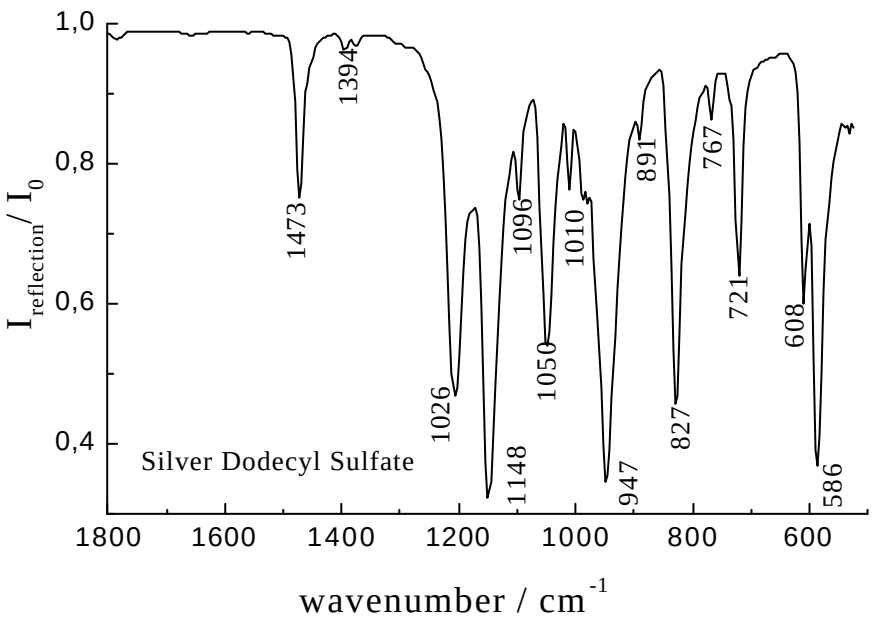

Figure 3.10 ATR-IR spectra of silver dodecyl sulfate

Similar to sodium dodecyl sulfate the silver dodecyl sulfate formed white crystals, and, but the solution of silver dodecyl sulfate was easily decomposed when it was exposed to light. So

it was kept in the dark (and at a dry place). Figure 3.10 shows the ATR-IR spectrum of silver dodecyl sulfate in the range from 1800 cm^{-1} to 500 cm^{-1}. The observed wavenumbers and band assignments for silver dodecyl sulfate are displayed in table 3.4 [87].

wavenumber(cm^{-1})	assignment
2955	asymmetric CH_3 stretching
2921	antisymmetric CH_2 stretching
2849	symmetric CH_2 stretching
1473	CH_2 scissoring
1394	CH_3 bending
1206	asymmetric (OSO_3^-) stretching
1148	asymmetric (OSO_3^-) stretching
1050	symmetric (OSO_3^-) stretching
947	asymmetric (C-O-S) stretching
827	symmetric (C-O-S) stretching
608	asymmetric (OSO_3^-) bending
586	symmetric (OSO_3^-) bending

Table 3.4 The wavenumber and band assignments of silver dodeyl sulfate after [87]

The ATR-IR spectrum is very similar to that of sodium dodecyl sulfate, see the literature [88]. The strong bands at 1206 cm^{-1} and 1148 cm^{-1} were caused by asymmetric (OSO_3^-) stretching and the strong band at 1050 cm^{-1} was symmetric (OSO_3^-) stretching. These bands were the characteristic ones in spectra of silver dodecyl sulfate.

3.3.2 [3,12]-ionene

[3,12]-ionene was a brittle material, and it was easy dissolved in methanol or water. The ATR-IR spectrum of [3,12]-ionene is displayed in Fig. 3.11. It exhibits a strong O-H band at 3411 cm^{-1}, but [3,12]-ionene has no O-H group, so [3,12]-ionene contained another compound, which probably was water or methanol. The strong band at 1466 cm^{-1} was caused by the C-H torsional vibration in the $–CH_2N^+$ moiety which is characteristic for [3,12]-ionene [89, 90].

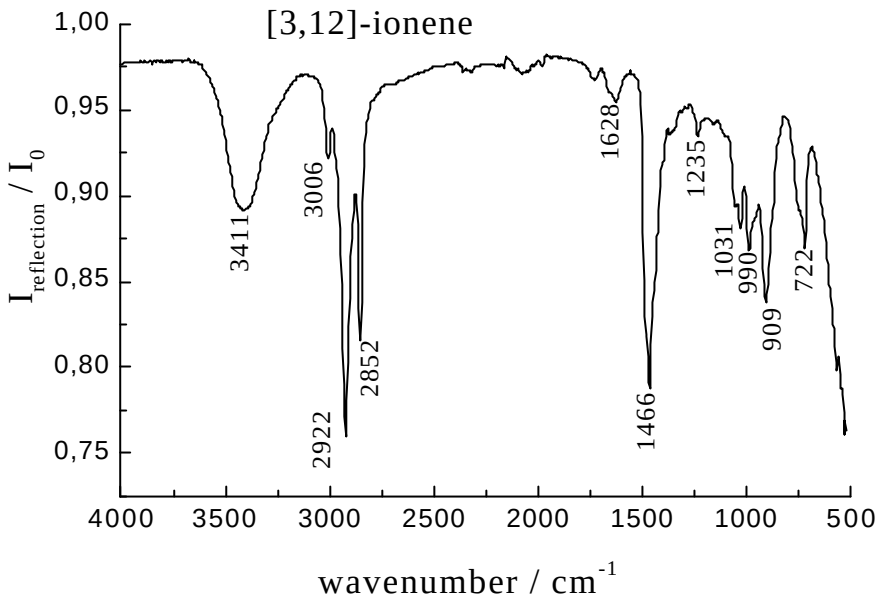

Figure 3.11 ATR-IR spectrum of [3,12]-ionene

The observed wavenumber and band assignments of [3,12]-ionene displayed in table 3.5.

wavenumber(cm^{-1})	assignment
3411	H-bridge, O-H stretching
3006	chelate H-bridge, O-H stretching
2922	antisymmetric CH_2 stretching
2852	symmetric CH_2 stretching
1466	C-H torsional vibration in the $–CH_2N^+$ moiety
1235	symmetric (C-C) stretching
1031	(C-O) stretching
990	symmetric (N-CH_3) stretching
909	symmetric (N-CH_2) stretching

Table 3.5 The wavenumber and band assignments of [3,12]-ionene, cf. [71,72]

3.3.2.1 The thermal stability of [3,12]-ionene

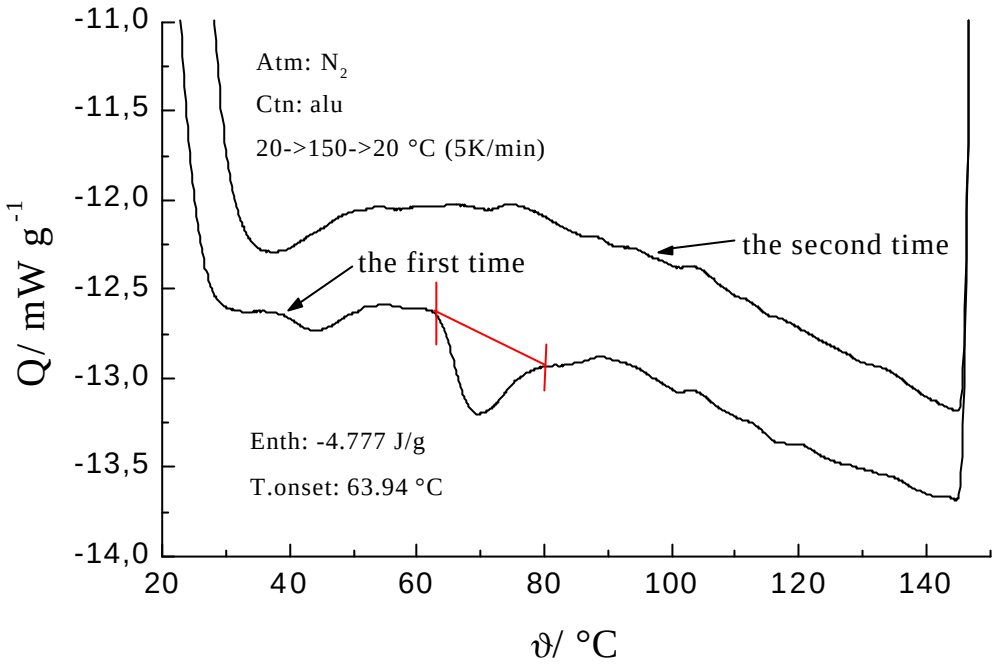

Figure 3.12 DSC of [3,12]-ionene

The differential scanning calorimetry (DSC) curve in Fig. 3.12 shows an absorption peak at about 70 °C when [3,12]-ionene was heated for the first time. The corresponding enthalpy was only about -4.8 J/g. After cooling the sample to room temperature and repetition of the above measurement from 20 °C to 140 °C there was no absorption peak any more, so this absorption peak indicates a volatile low-molecular-weight compound [91] (such as methanol left from the solvent) rather than the glass temperature of [3,12]-ionene. The boiling point of methanol is about 65 °C, so the O-H band (Fig. 3.11), which was displayed in ATR-IR spectrum, was probably methanol.

The assignment of the band to the loss of methanol was supported by a thermogravimetric analysis (TG). In the TG diagram (Fig. 3.13) and fragment diagram (Fig. 3.14) of [3,12]-ionene two fragment peaks at m/z = 32 and 18 were found at about 90-120 °C and 100-120 °C in pyrolysis and steam gasification of [3,12]-ionene, clearly indicating the m/z =32 as methanol as one of the fragments. The figure shows a peak at m/z =18, so [3,12]-ionene also contained water as the assigned band in the ATR-IR spectrum at 1628 cm^{-1} (Fig. 3.11 O-H bend band of water). But there is no DCS peak attributable the evaporation of water. According to Fig. 3.13 [3,12]-ionene contained about 6.8 % of methanol and water.

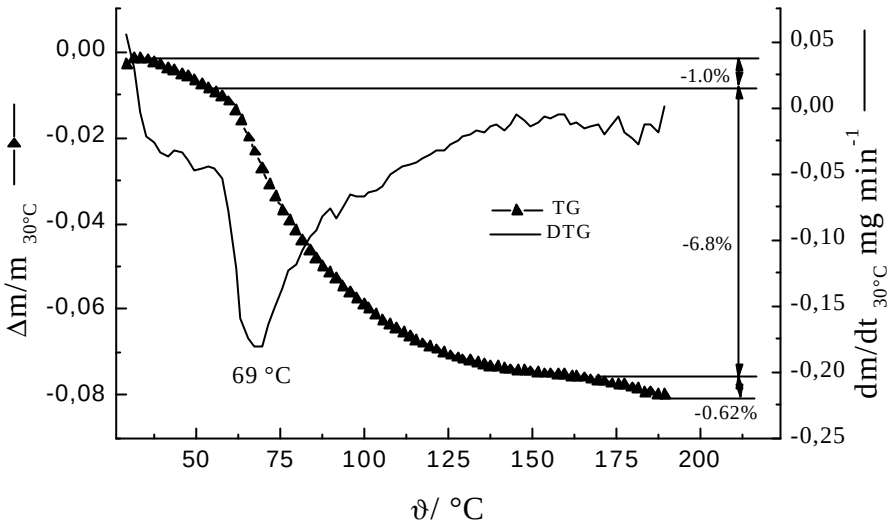

Figure 3.13 Thermogravimetric analysis of [3,12]-ionene; heating rate 5 K/min.

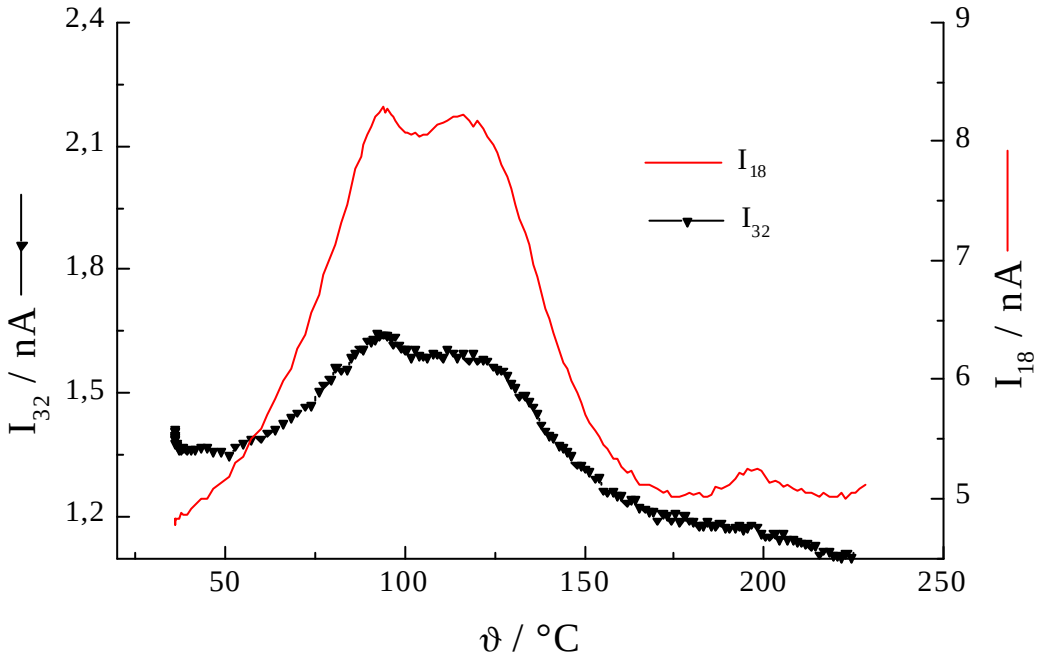

Figure 3.14 Fragments produced in thermogravimetric analysis of [3,12]-ionene; heating rate 5 K/min

The ATR-IR spectrum before and after heating the [3,12]-ionene to 150 °C was almost constant (Fig. 3.15). This shows that the functional groups of [3,12]-ionene did not change during heating, i.e. the complex is stable under these conditions.

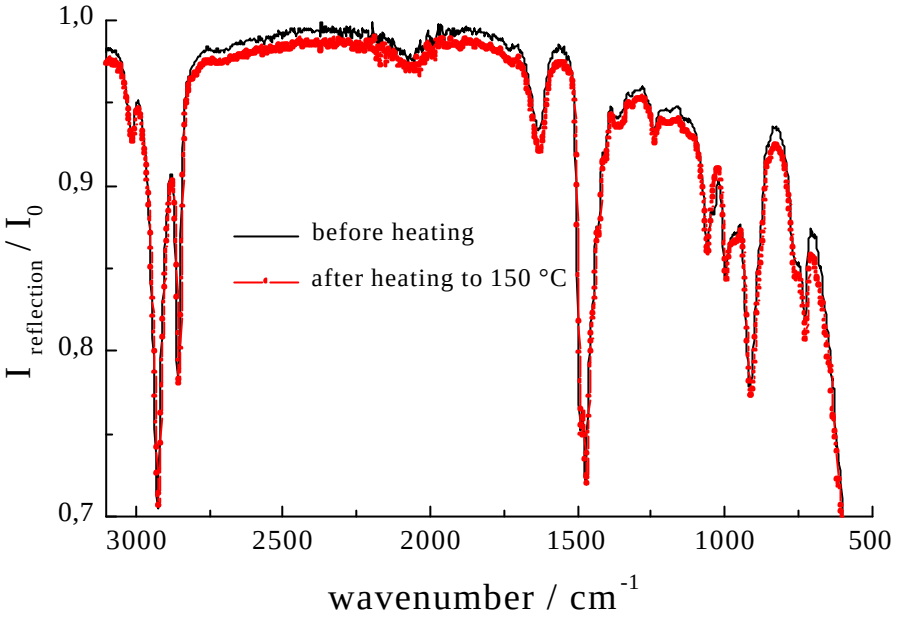

Figure 3.15 ATR-IR spectra of [3,12]-ionene before and after heating.

From DSC and ATR-IR spectra of [3,12]-ionene, [3,12]-ionene was stable between 20 °C and 150 °C. It was difficult to remove methanol completely, even over phosphorous pentoxide in vacuum, because [3,12]-ionene was prepared at room temperature.

3.3.3 [3,12]-ionene dodecyl sulfate stoichiometric complex

The stoichiometric complex structure of [3,12]-ionene dodecyl sulfate is displayed below.

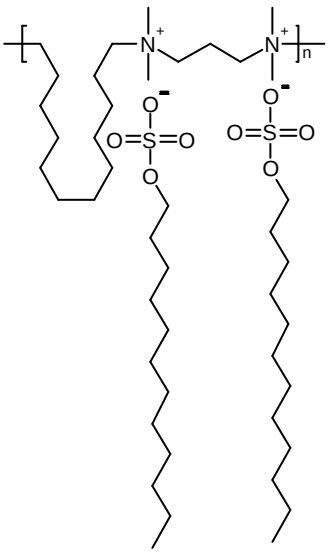

structure of [3,12]-ionene dodecyl sulfate complexes

The NMR spectra of [3,12]-ionene dodecyl sulfate stoichiometric complex in DMSO consisted of two parts, one was [3,12]-ionene, and the other was dodecyl sulfate.

^{1}H-NMR of [3,12]-ionene dodecyl sulfate stoichiometric complex (d/ppm at 500 MHz in DMSO): 0.97 (t, 3 H, -CH_3 in dodecyl sulfate), 1.24-1.27 (br, 34H including 18 H, ($\gamma, \delta, \varepsilon, \zeta, \eta, \theta, \iota, \kappa, \lambda$)-$CH_2$ in dodecyl sulfate and 16 H, ($\gamma, \delta, \varepsilon, \zeta$)-$CH_2$ in [3,12]-ionene), 1.47 (m, 2 H, β-CH_2 in dodecyl sulfate) 1.66 (br, 4H, β-CH_2 dodecano- in [3,12]-ionene), 2.14 (br, 2H, β-CH_2-propano- in [3,12]-ionene), 3.04 (br, 12 H, $(CH_3)_2N^+$), 3.32 (br, α-CH_2 and H_2O), 3.67 (t, 2 H, α-CH_2 in dodecyl sulfate).

wavenumber(cm^{-1})	assignment
3492	H-bridge, O-H stretching
3037	chelate H-bridge, O-H stretching
2921	antisymmetric CH_2 stretching
2852	symmetric CH_2 stretching
1639	H_2O
1466	C-H torsional vibration in the $-CH_2N^+$ moiety
1377	CH_3 bending of dodeyl sulfate
1212	asymmetric (OSO_3^-) stretching
1056	symmetric (OSO_3^-) stretching
990	symmetric (N-CH_3) stretching
914	symmetric (N-CH_2) stretching
622	asymmetric (OSO_3^-) bending
578	symmetric (OSO_3^-) bending

Table 3.6 The wavenumber and band assignments of [3,12]-ionene dodecyl sulfate stoichiometric complex

Fig. 3.16 displays ATR-IR spectra of both, the [3,12]-ionene dodecyl sulfate stoichiometric complex and the composite ATR-IR spectrum of [3,12]-ionene and silver dodecyl sulfate. It was found that the ATR-IR spectrum of the [3,12]-ionene dodecyl sulfate stoichiometric complex was not the simple addition of the IR spectra of the components. The two asymmetric (OSO_3^-) stretching bands at 1206 cm^{-1} and 1148 cm^{-1} of silver dodecyl sulfate

became a strong asymmetric (OSO_3^-) stretching band at 1212 cm^{-1} in the complex. The symmetric (C-O-S) stretching band at 947 cm^{-1} and the symmetric (C-O-S) stretching band at 827 cm^{-1} (which appeared in silver dodecyl sulfate) disappeared completely to give rise to a new strong band at 793 cm^{-1} in the [3,12]-ionene dodecyl sulfate stoichiometric complex (compare Table 3.6 with Table 3.5). This band is probably due to the symmetric ($N-CH_2$) stretching of the [3,12]-ionene dodecyl sulfate stoichiometric complex.

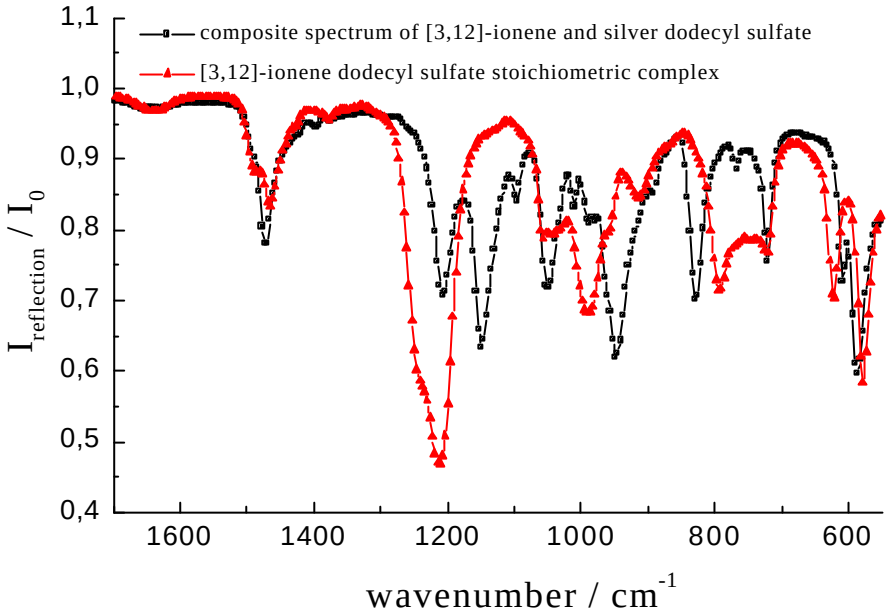

Figure 3.16 ATR-IR spectra of [3,12]-ionene dodecyl sulfate stoichiometric complex

3.3.3.1 The thermal stability of the [3,12]-ionene dodecyl sulfate stoichiometric complex

The ATR-IR spectrum before and after heating the [3,12]-ionene dodecyl sulfate stoichiometric complex to 200 °C was almost constant (Fig. 3.17). This shows that the functional groups of [3,12]-ionene dodecyl sulfate stoichiometric complexes did not change during heating, i.e. the complex is stable under these conditions. The spectra also reveal that the stoichiometric complexes contain some water (peak at 3470 cm^{-1}) [92], which the sample might have taken while it was exposed to air for recording the spectrum.

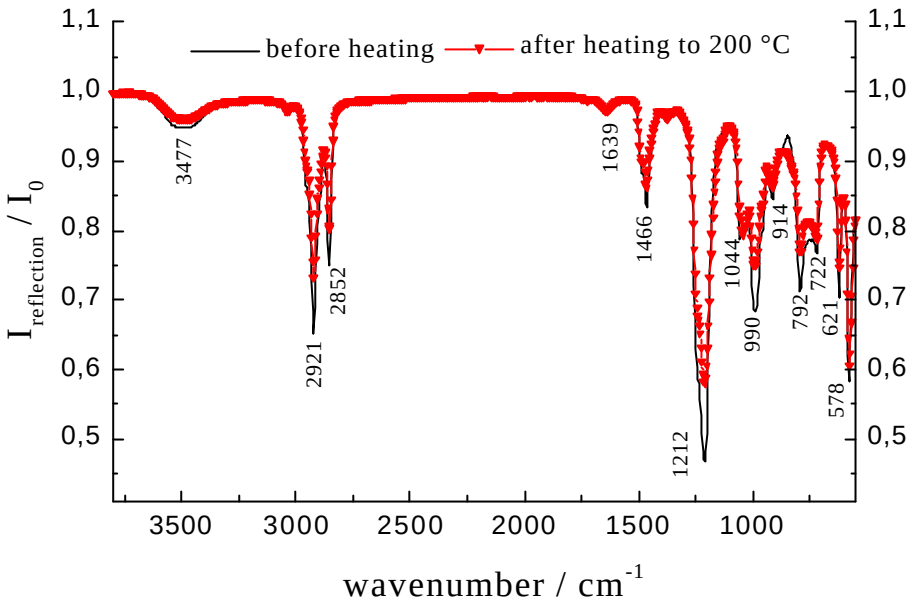

Figure 3.17 ATR-IR spectra of [3,12]-ionene dodecyl sulfate stoichiometric complex before and after heating.

In the DSC diagram (Fig. 3.18) there was also an absorption peak at about 100 °C, which was a weak peak and its enthalpy was only about 3 J g^{-1}. After cooling the sample to room temperature and repeating the DSC process (from 20 °C to 120 °C) there was no absorption peak any more (not shown in Fig. 3.18). Therefore after heating [3,12]-ionene dodecyl sulfate stoichiometric complex, water was removed from the stoichiometric complex, and the boiling point of water is 100 °C, so the O-H stretching band at 3470 cm^{-1}, which was displayed in Fig. 3.17, is attributed to water.

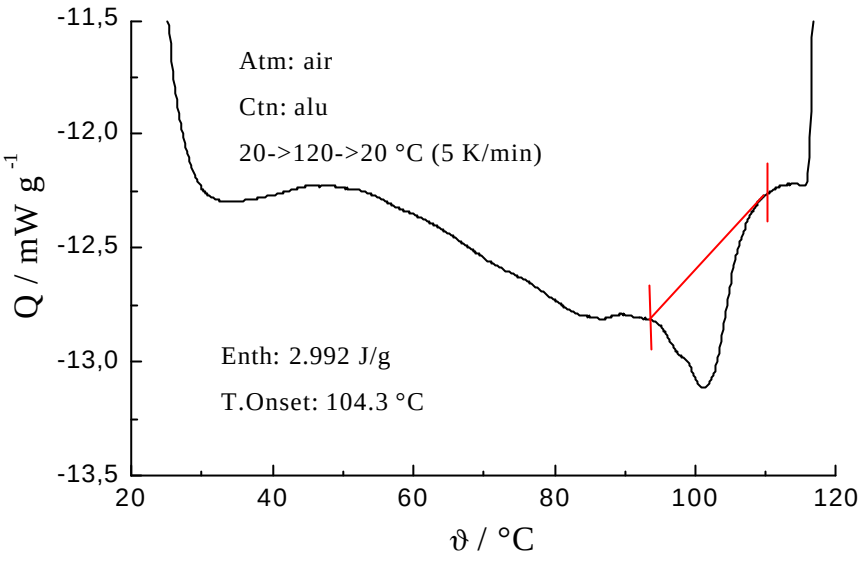

Figure 3.18 DSC of [3,12]-ionene dodecyl sulfate stoichiometric complex

The assignment of the absorption peak to the loss of water was also confirmed by a thermogravimetric analysis (TG). In the TG diagram (Fig. 3.19) in the first stage below 125 °C, water evaporation from [3,12]-ionene dodecyl sulfate stoichiometric complex was the main weight loss. Fragment peaks (Fig. 3.20) at m/z = 18 and m/z =17 were found at about 100 °C, clearly proving water as the evaporating species [93].

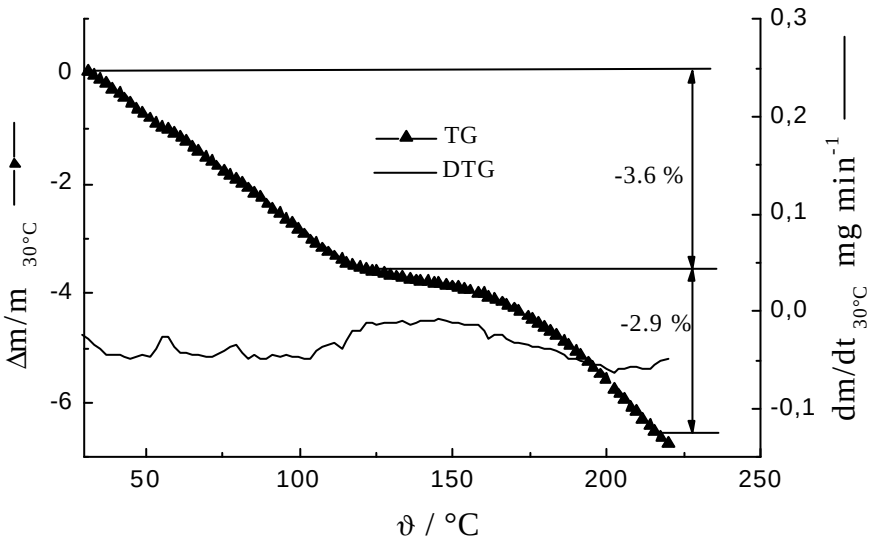

Figure 3.19 Thermogravimetric analysis of the [3,12]-ionene dodecyl sulfate stoichiometric complex; heating rate 5 K/min.

The according weight loss of the [3,12]-ionene dodecyl sulfate stoichiometric complex was about 3.6 %. From this value we calculate that every ion pair unit of the [3,12]-ionene dodecyl sulfate stoichiometric complex absorbs at least 0.9 water molecules, when the [3,12]-ionene dodecyl sulfate stoichiometric complex was in equilibrium with ambient air. The samples were optically isotropic when prepared at ambient conditions, the [3,12]-ionene dodecyl sulfate stoichiometric complex was stable below 120 °C, but it can easily absorb water in air.

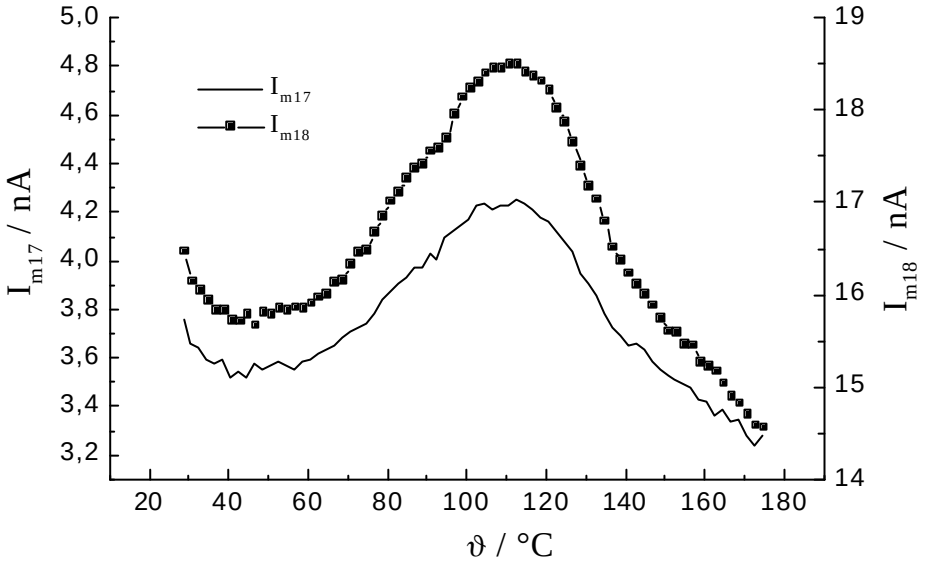

Figure 3.20 Fragments produced in thermogrametric analysis of [3,12]-ionene dodecyl sulfate stoichiometric complex; heating rate 5 K/min.

3.3.3.2 Isotropic-mesogenic transition of the [3,12]-ionene dodecyl sulfate stoichiometric complex

From the birefringence measurements at constant temperature (Fig. 3.21; performed using the apparatus sketched in Fig. 2.1; see experimental part) we learned that [3,12]-ionene dodecyl sulfate stoichiometric complexes easily absorbed more water when they were exposed to increased relative humidity. While the optical properties did not change at relative humidities up to 89.4 %, at 91.4 % the film changed from optically isotropic to optically anisotropic. We will show below that a mesogenic phase was formed thereby [94]. However, a quite long period needed for equilibration was noted.

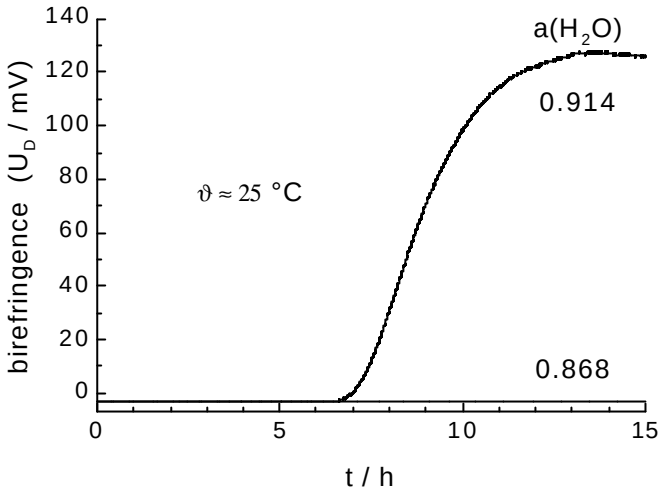

Figure. 3.21 Birefringence measured as detector voltage U_D in the apparatus sketched in Fig. 2.1 at 25 °C as a function of time at two activities $a(H_2O)$ of water in aqueous NaCl corresponding to 91.4 % and 86.8 % relative humidity.

Further evidence for the humidity induced transition from optically isotropic to optically anisotropic arose from DSC diagrams as in Fig. 3.22. When the diagram was measured at elevated relative humidity an exothermic peak appeared at 115 to 120 °C in addition to the endothermic peak attributed to water evaporation, cf. Fig. 3.18. The enthalpy as well temperature of the maximum of the emission peak exhibited a substantial change at the transition point (at a water activity of 0.91): as shown in Fig. 3.23 the enthalpy dropped from ca. 2.68 J/g to 1.4 J/g (after passing through a maximum). The temperature of the maximum of the emission peak displayed an analogous feature: At the transition point (a (H_2O) = 0.91) it decreased from 120 °C to 103 °C indicating that the evaporation of absorbed water is facilitated when the anisotropic phase is formed at room temperature.

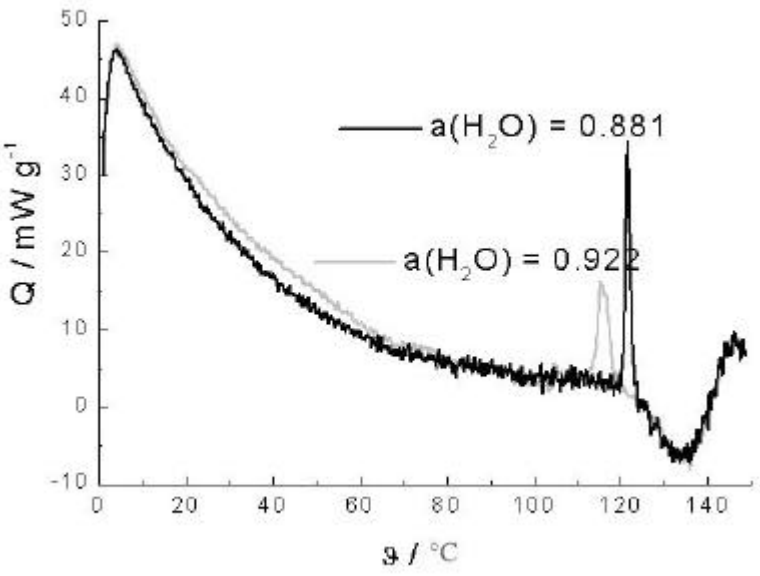

Figure 3.22 DSC-curves of [3,12]-ionene stoichometrically complexed with dodecyl sulfate for two samples equilibrated at constant relative humidities: 88.1 % and 92.2 %; heating rate 1 K/min.

This caloric effect is sensitive to the heating rate. In Fig. 3.24 it is shown that at a heating rate of 10 K / min both enthalpy and temperature of the maximum of the emission peak have moved to lower water activities (compare Fig. 3.22).

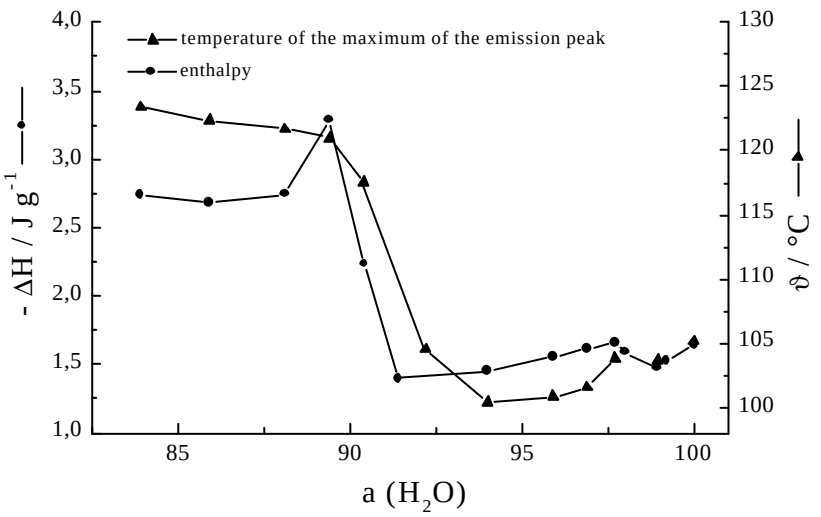

Figure 3.23 Enthalpy and temperature of the maximum of the DSC emission peak of [3,12]-ionene dodecyl sulfate stoichiometric complexes as a function of relative humidity, measured

by DSC after appropriate equilibration at the respective relative humidity; heating rate 1 K/min.

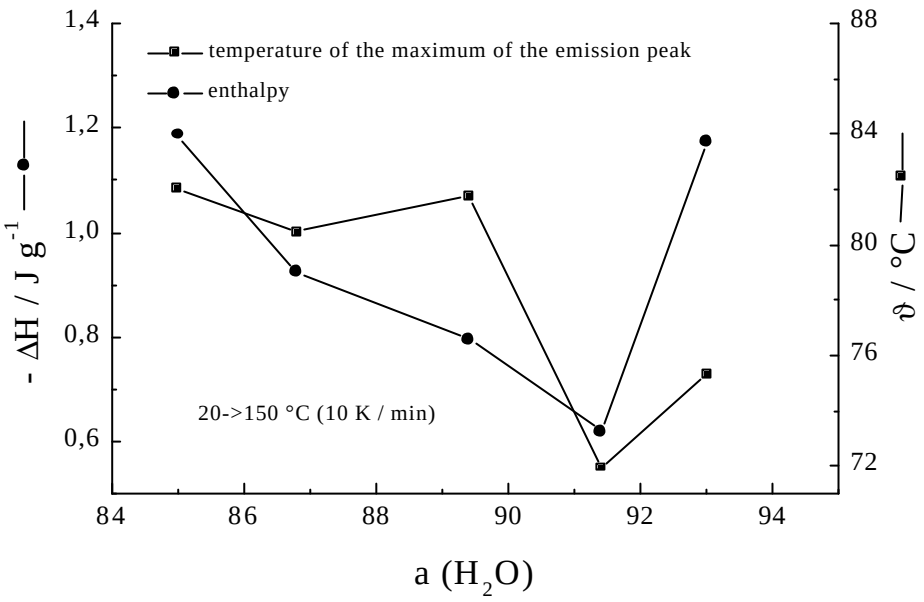

Figure 3.24 Enthalpy and temperature of the maximum of the emission peak of [3,12]-ionene dodecyl sulfate stoichiometric complexes measured by DSC; heating rate 10 K/min to be compared with 1 K/min in Fig. 3.22.

All these features indicate slightly different lyotropic structures of the various samples [95]. However, no caloric effect was found accompanying the transition isotropic-anisotropic between 45-55 °C described later.

From Figure 3.25 it follows that the take up of water was proportional to the fraction of water in the gas phase. At the transition point changing from optically isotropic to optically anisotropic every ion pair of [3,12]-ionene dodecyl sulfate stoichiometric complex absorbed about 4 water molecules.

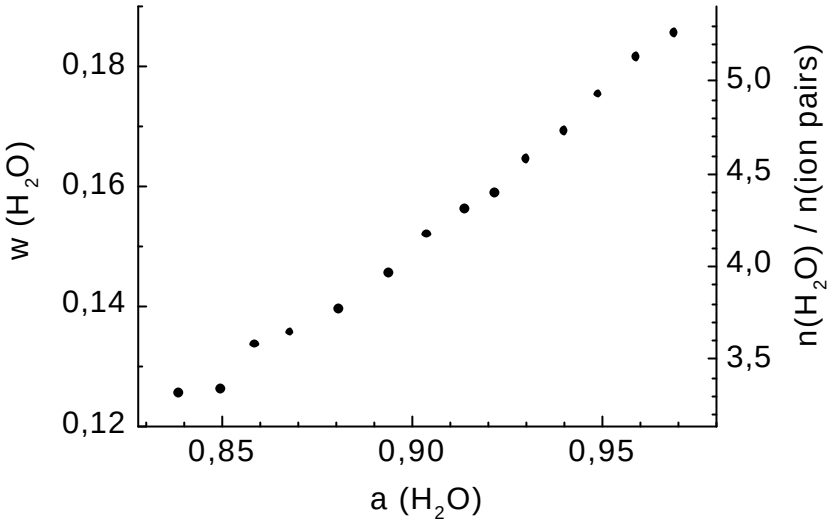

Figure 3.25 Swelling (mass fraction *w* of water) of [3,12]-ionene dodecyl sulfate stoichiometric complexes and number of water molecules per ion pair unit ($n(H_2O)$) as a function of the relative humidity ($a(H_2O)$) applied to the dry sample at room temperature.

For a sample at 91.4 % relative humidity, Fig. 3.26a depicts changes from the anisotropic to the isotropic phase and vice versa upon periodically sweeping the temperature (5 K/h) from 30 to 55 °C, i.e. across the transition point (using the apparatus sketched in Fig. 2.1). Taking the onset of the anisotropy-signal at decreasing temperature as the transition temperature, Fig. 3.26b revealed a transition isotropic-anisotropic (or isotropic-mesogenic) around 47 °C upon cooling the sample, and an anisotropic-isotropic transition around 51 °C upon heating the sample (under constant relative humidity), i.e. a hysteresis of ca. 4 K was found for the transition in the heating and cooling cycles. The material proved stable for the 7 cycles displayed. However, a drift of transition temperatures by 2-3 °C was noted within 70 h (Fig. 3.26c).

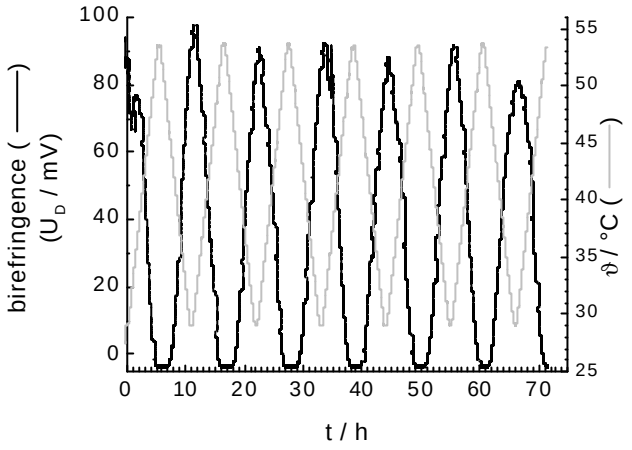
birefringence (———)
(U_D / mV)
ϑ / °C (———)
t / h

(a)

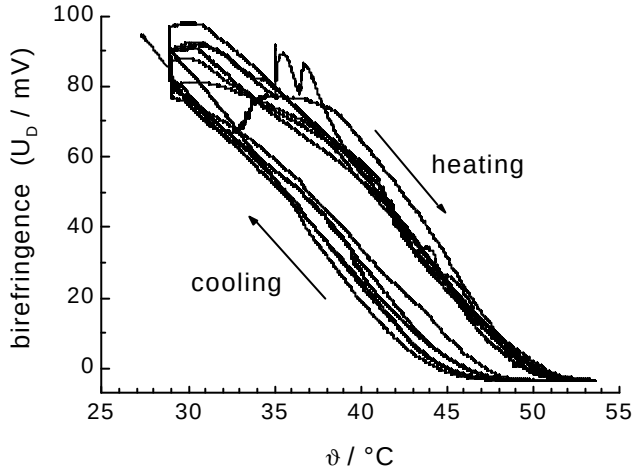
birefringence (U_D / mV)
heating
cooling
ϑ / °C

(b)

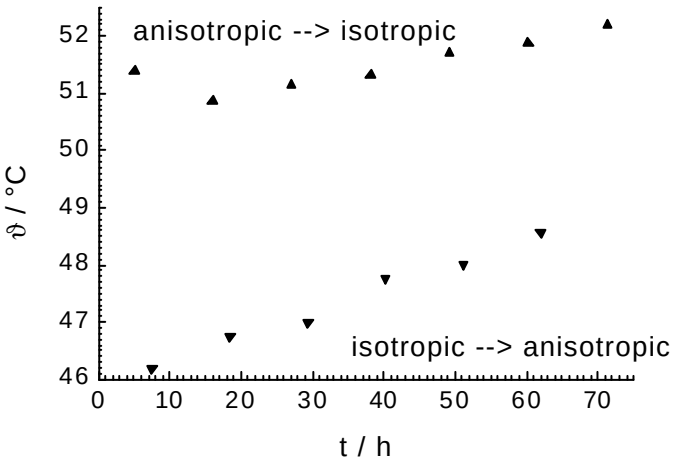
anisotropic --> isotropic
isotropic --> anisotropic
ϑ / °C
t / h

(c)

Figure 3.26 (a) Birefringence at varying temperature ϑ (5 K/h) as a function of time measured as detector voltage U_D with the apparatus sketched in Fig. 2.1; (b) birefringence as a function of temperature at 91.4 % relative humidity for the seven cycles anisotropic-isotropic-anisotropic shown in (a); (c) drift of transition temperatures within 70 h.

Figure 3.27 shows the texture of the anisotropic mesogenic phase of the stoichiometric complex after cooling at 103.5 ± 0.5 °C from the isotropic phase as it appeared on the polarizing microscope. The texture indicates a hexagonal mesogenic structure [96, 97].

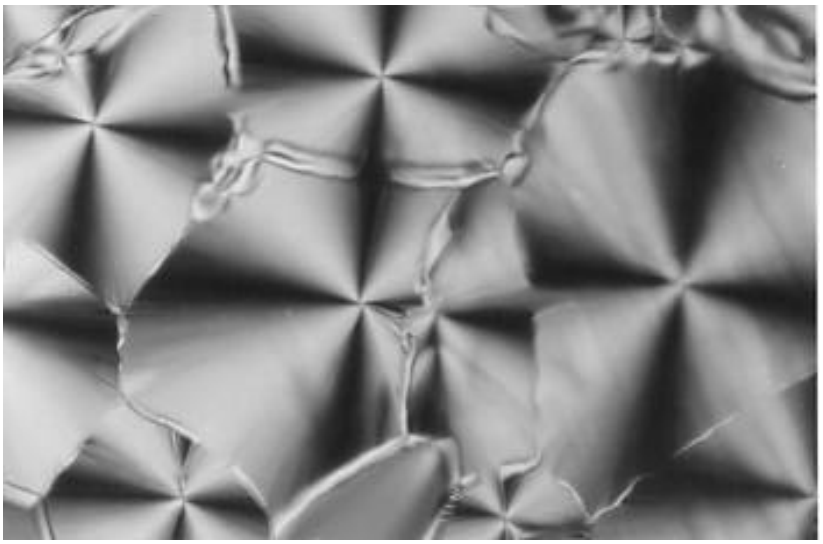

Figure 3.27 Texture of the anisotropic mesogenic phase in [3,12]-ionene dodecyl sulfate stoichiometric complexes obtained from a polarizing microscope. Magnification 100X, sample prepared at a(H_2O) = 0.95.

3.3.3.3 The mesogenic phase stability of the [3,12]-ionene dodecyl sulfate stoichiometric complex

When the relative humidity was raised from 91.4 to 93.0 %, the transition temperature increased to ca. 83 °C upon heating and to 68 °C upon subsequent cooling. During the next cycles both transition temperatures dropped. Upon further periodical heating and cooling the sample became liquid and eventually the anisotropy vanished completely. So the anisotropic [3,12]-ionene dodecyl sulfate stoichiometric complex was not stable at high relative humidity and high temperature. The NMR spectrum of a sample decomposed at 93 % relative humidity is shown in Fig. 3.28.

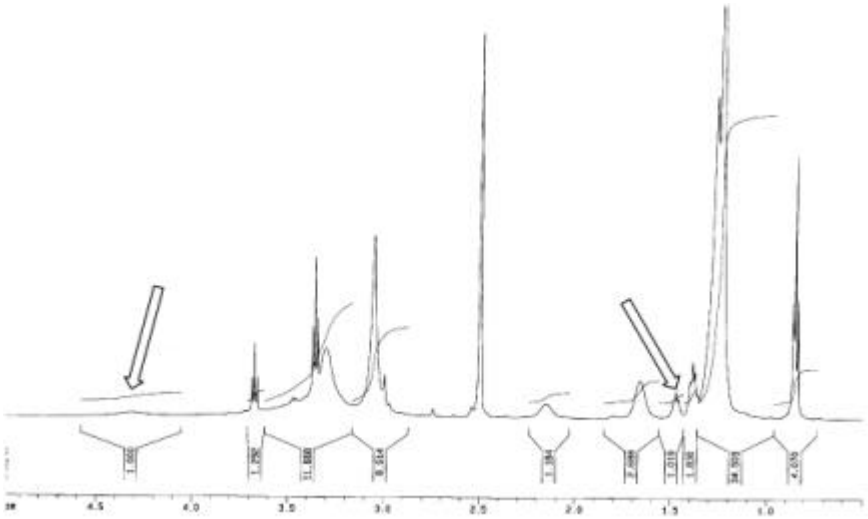

Figure 3.28 The NMR of [3,12]-ionene dodecyl sulfate stoichiometric complex decomposed at 93 % relative humidity

The arrows in Fig. 3.28 mark the two new peaks, which arise upon decomposition of the [3,12]-ionene dodecyl sulfate stoichiometric complex. The peaks at 4.31 ppm and 1.39 ppm (*d*/ppm at 500 MHz in DMSO) indicate that the dodecyl moiety of the complex was converted to the corresponding alcohol, i.e. 1-dodecanol[98]. This was also supported by the ATR-IR spectrum shown below.

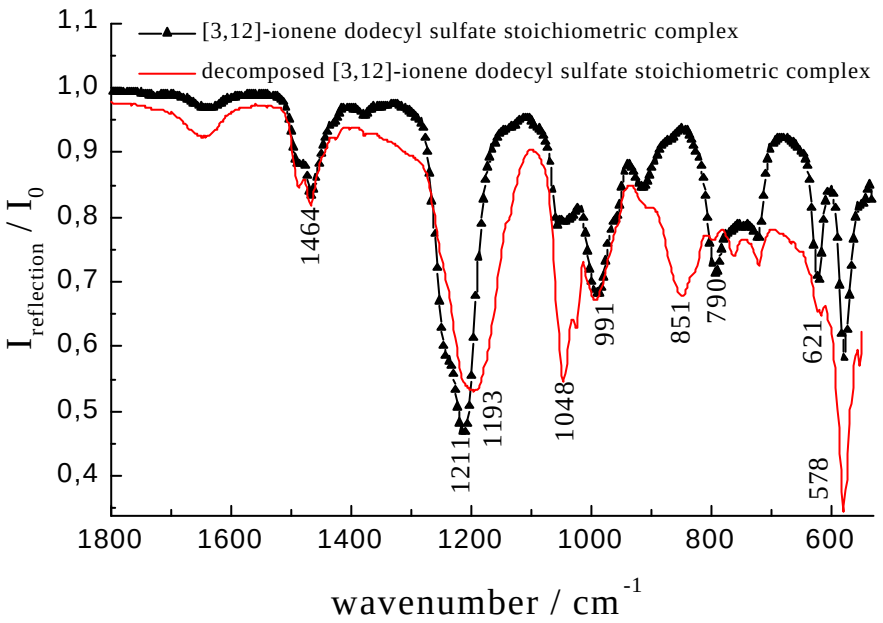

Figure 3.29 ATR-IR spectra of the decomposed [3,12]-ionene dodecyl sulfate stoichiometric complex.

Fig. 3.29 depicts the comparison between [3,12]-ionene dodecyl sulfate stoichiometric complex and the decomposed stoichiometric complex. After decomposition there was a strong absorption peak at 1048 cm^{-1}, which corresponds to the C-O stretching band in 1-dodecanol, in agreement with the spectrum of 1-dodecanol [99].

3.4 [5,10]-ionene and [5,10]-ionene alkyl sulfate stoichiometric complexes

3.4.1 [5,10]-ionene

[5,10]-ionene had an appearance similar to that of [3,12]-ionene, a brittle polyelectrolyte, which was easily dissolved in methanol or water. The ATR-IR spectrum of [5,10]-ionene is shown in Fig. 3.30. It widely agrees with the [3,12]-ionene, because both ionenes have the same functional groups. The only substantial difference is stronger symmetric ($N-CH_3$) stretching peaks at 963 cm^{-1} and 903 cm^{-1}. As in [5,10]-ionene a strong O-H band at 3422 cm^{-1} in both the ionenes indicates the presence of an impurity exhibiting an O-H functional group, probably from water or methanol. Table 3.7 displays the wavenumber and band assignments of [5,10]-ionene.

wavenumber(cm^{-1})	assignment
3422	H-bridge, O-H stretching
3005	chelate H-bridge, O-H stretching
2923	antisymmetric CH_2 stretching
2854	symmetric CH_2 stretching
1470	C-H torsional vibration in the $-CH_2N^+$ moiety
1235	symmetric (C-C) stretching
1030	(C-O) stretching
963	symmetric ($N-CH_3$) stretching
903	symmetric ($N-CH_2$) stretching

Table 3.7. The wavenumber and band assignments of [5,10]-ionene

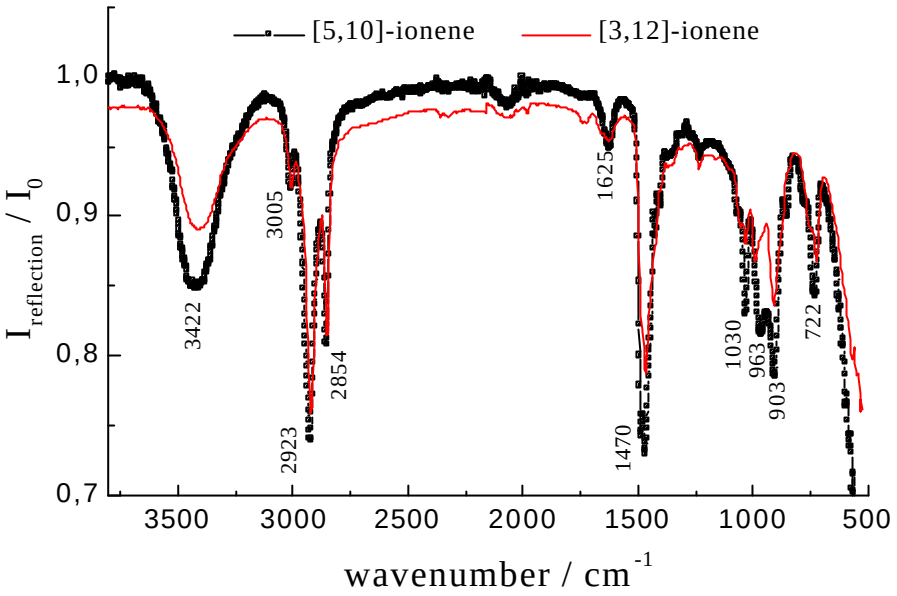

Figure 3.30 ATR-IR spectra of [5,10]-ionene compared to [3,12]-ionene

3.4.1.1 The stability of [5,10]-ionene

The differential scanning calorimetry (DSC) curve of [5,10]-ionene displays an absorption peak at about 140 °C with a corresponding enthalpy about -7.4 J/g. The boiling point of water is 100 °C, so the O-H band at 3422 cm^{-1} (Fig. 3.30), which was displayed in ATR-IR spectrum, was probably water, not methanol, because methanol has a lower boiling point of 65 °C. The assignment of the band to the loss of water was supported by a thermogravimetric analysis (TG).

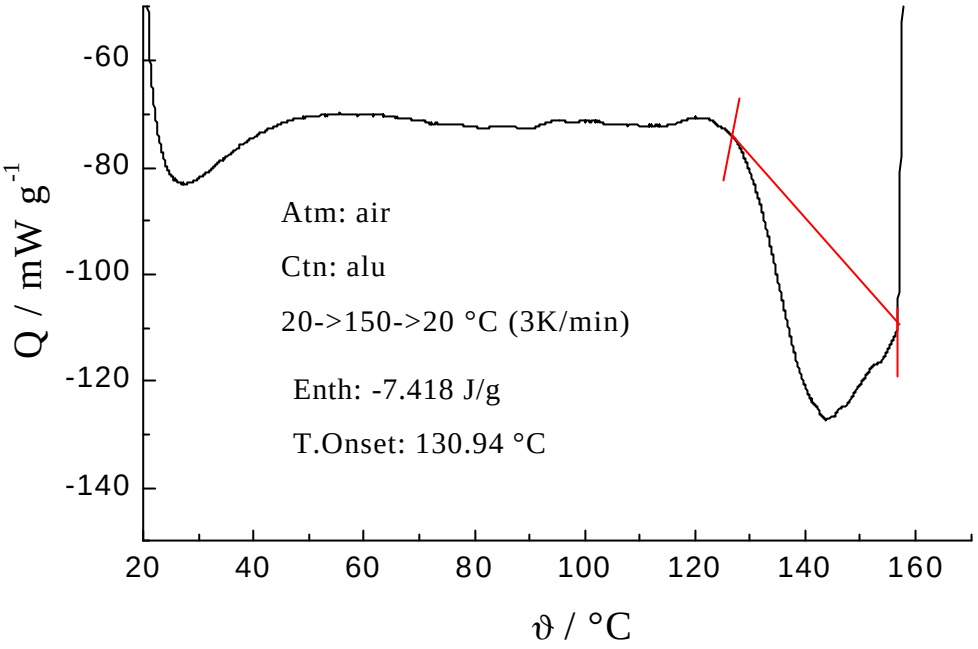

Figure 3.31 DSC of [5,10]-ionene

In the TG diagram (Fig. 3.32) there were four stages of the weight loss; the table 3.8 listed the minimal temperature, maximum temperature and weight loss in every stage. In the first stage before 170 °C the weight loss was 4.7 %, and this was mainly evaporation of water from [5,10]-ionene. The DTA in Fig. 3.32 showed that at about 144 °C the evaporation of water reached the maximum rate, which was consistent with the absorption peak in DSC (Fig. 3.31). At high temperatures above 170 °C [5,10]-ionene began to decompose, above 223 °C, [5,10]-ionene decomposed rapidly and completely. So [5,10]-ionene was not stable at high temperature.

stage	T_{min} / °C	T_{max} / °C	weight loss / %
1	35	170	4.71
2	170	223	1.61
3	223	249	5.7
4	249	274	22.2

Table 3.8 Weight loss and temperature range in every stage of [5,10]-ionene in TG

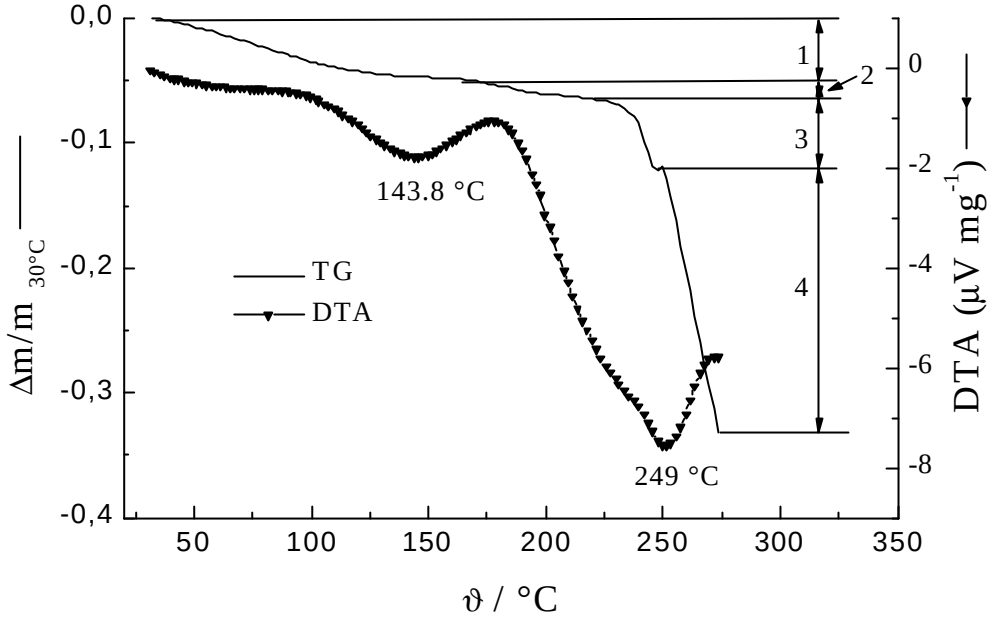

Figure 3.32 Thermogravimetric analysis of [5,10]-ionene; heating rate 5 K/min.

The sample from Fig. 3.31 was analysed by ATR-IR spectra. In Fig. 3.33 spectra [5,10]-ionene as prepared and after heating to 150 °C are compared. The absorption peak at 1031 cm^{-1} (pertaining to absorbed water) became weaker. It can be concluded that below 150 °C [5,10]-ionene was stable, in keeping with the TG diagram (Fig. 3.32).

At high temperatures above 170 °C [5,10]-ionone would become unstable due to thermal degradation, above 223 °C it decomposed completely as revealed by the TG analysis, cf. [100].

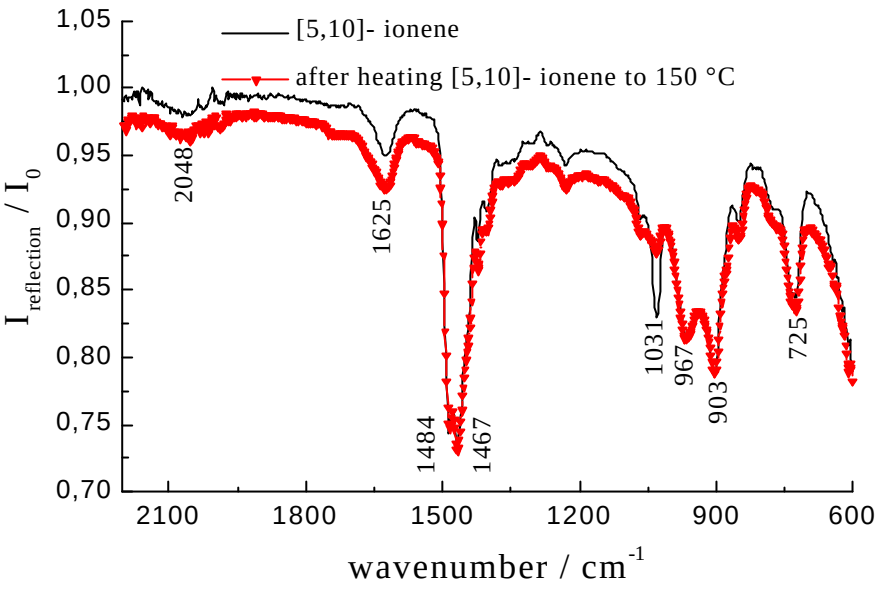

Figure 3.33 ATR-IR spectra of [5,10]-ionene before and after heating

3.4.2 [5,10]-ionene dodecyl sulfate stoichiometric complex

The structure of the stoichiometric complex of [5,10]-ionene and dodecyl sulfate displayed as follows.

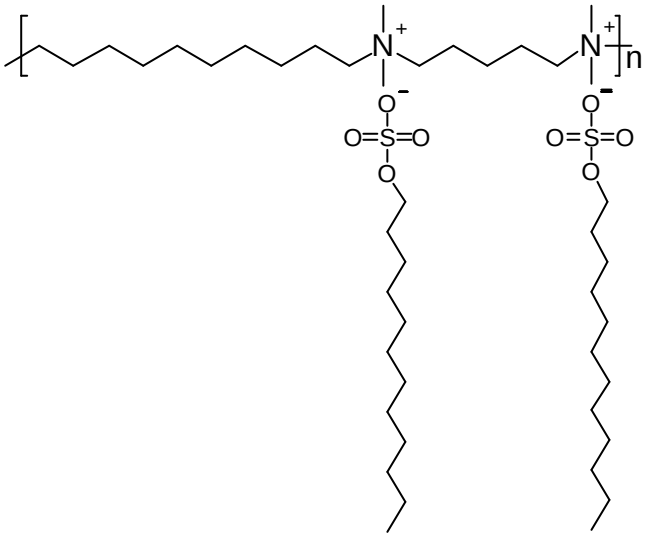

structure of [5,10]-ionene dodecyl sulfate complexes

The NMR spectra of the [5,10]-ionene dodecyl sulfate stoichiometric complex in DMSO agreed with a superposition of [5,10]-ionene and dodecyl sulfate moieties.

^{1}H-NMR of [5,10]-ionene dodecyl sulfate stoichiometric complex (*d*/ppm at 500 MHz in DMSO): 0.85 (t, 3 H, -CH_3 in dodecyl sulfate), 1.24-1.27 (br, 32 H including (18 H, (γ, δ, ε, ζ, η, θ, ι, κ, λ)-CH_2 in dodecyl sulfate) and (14 H including 12 H, (γ, δ, ε)-CH_2-decano- and 2 H, γ-CH_2-pentano-in [3,12]-ionene)), 1.47 (br, 2 H, β-CH_2 in dodecyl sulfate) 1.65 (br, 4 H, β-CH_2-decano- in [3,12]-ionene), 1.70 (br, 4 H, β-CH_2-pentano- in [3,12]-ionene), 2.49 (br, 12 H, $(CH_3)_2N^+$), 2.99-3.3 (br, α-CH_2 and H_2O), 3.67 (t, 2 H, α-CH_2 in dodecyl sulfate).

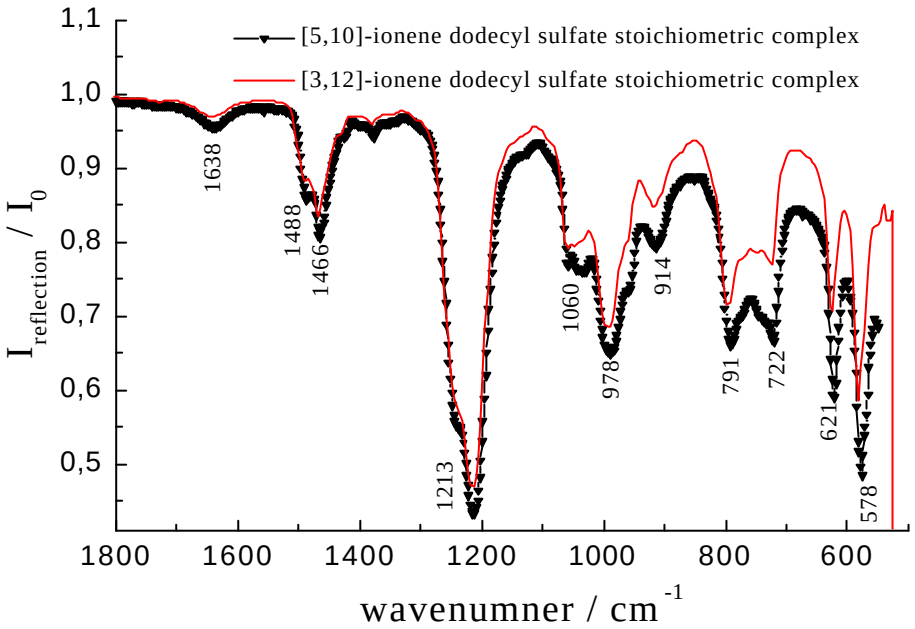

Figure 3.34 ATR-IR spectra of the [5,10]-ionene dodecyl sulfate stoichiometric complex compared with the [3,12]-ionene dodecyl sulfate complex

Fig. 3.34 displays the ATR-IR spectrum of the [5,10]-ionene dodecyl sulfate stoichiometric complex. Because [5,10]-ionene sulfate stoichiometric complex has functional groups very similar to the [3,12]-ionene sulfate stoichiometric complex, they had a similar ATR-IR spectrum. The strong asymmetric (OSO_3^-) stretching bands at 1213 cm^{-1} and the C-H torsional vibration in the $–CH_2N^+$ moiety at 1466 cm^{-1} are characteristic absorption peaks of the [5,10]-ionene dodecyl sulfate stoichiometric complex. In Table 3.9 the wavenumber and band assignments of the [5,10]-ionene dodecyl sulfate stoichiometric complex are listed.

wavenumber(cm^{-1})	assignment
3471	H-bridge, O-H stretching
3040	chelate H-bridge, O-H stretching
2922	antisymmetric CH_2 stretching
2852	symmetric CH_2 stretching
1638	H_2O
1466	C-H torsional vibration in the $–CH_2N^+$ moiety
1377	CH_3 bending of dodeyl sulfate
1213	asymmetric (OSO_3^-) stretching
1060	symmetric (OSO_3^-) stretching
987	symmetric (N-CH_3) stretching
914	symmetric (N-CH_2) stretching
622	asymmetric (OSO_3^-) bending
577	symmetric (OSO_3^-) bending

Table 3.9 The wavenumber and band assignments of [5,10]-ionene dodecyl sulfate stoichiometric complex

3.4.2.1 The stability of the [5,10]-ionene dodecyl sulfate stoichiometric complex

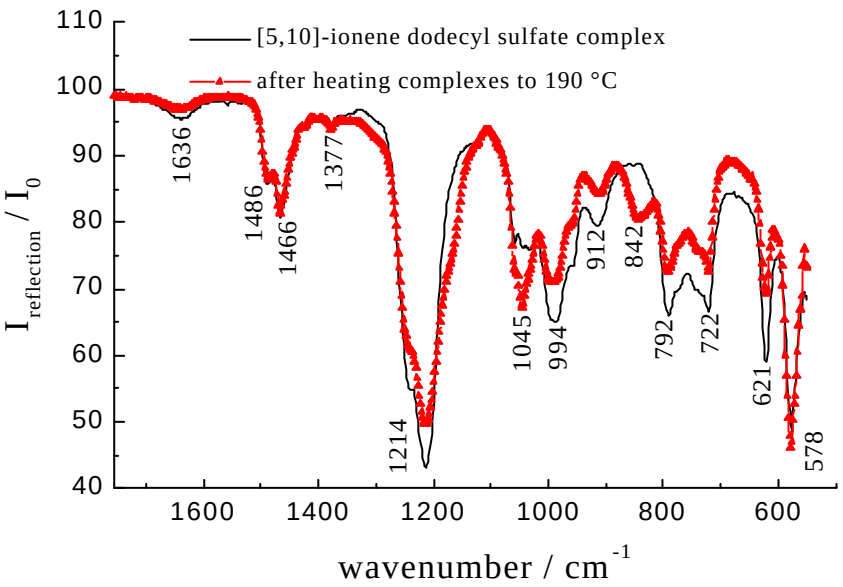

Figure 3.35 ATR-IR spectra of the [5,10]-ionene dodecyl sulfate stoichiometric complex before and after heating

In the ATR-IR spectra some difference before and after heating the [5,10]-ionene dodecyl sulfate stoichiometric complex to 190 °C (Fig. 3.35) were obtained. The absorption peak at 1045 cm^{-1} (which represents the symmetric (OSO_3^-) stretching band of dodecyl sulfate) became stronger and a new peak at 842 cm^{-1} appeared. This showed that some functional groups of [5,10]-ionene dodecyl sulfate stoichiometric complexes had changed during heating to 190 °C, i.e. the complex was somewhat unstable under these conditions. The spectra also reveal that the stoichiometric complexes contain some water (peak at 3470 cm^{-1}), which the sample might have taken up after exposure to air for taking the spectrum, and which reduces upon heating.

The assignment of the latter peak to water was supported by differential scanning calorimetry (DSC). In the DSC diagram (Fig. 3.36) there was an absorption peak at about 105 °C, which was a weak peak and its enthalpy was only about 2.8 J g^{-1}. After cooling the sample to room temperature and repeating the process, (from 20 °C to 140 °C) there was no absorption peak any more (Fig. 3.36). Therefore, after heating [5,10]-ionene dodecyl sulfate stoichiometric complex water was vaporized from complex. As the boiling point of water is 100 °C, the O-H stretching band at 3470 cm^{-1} was water.

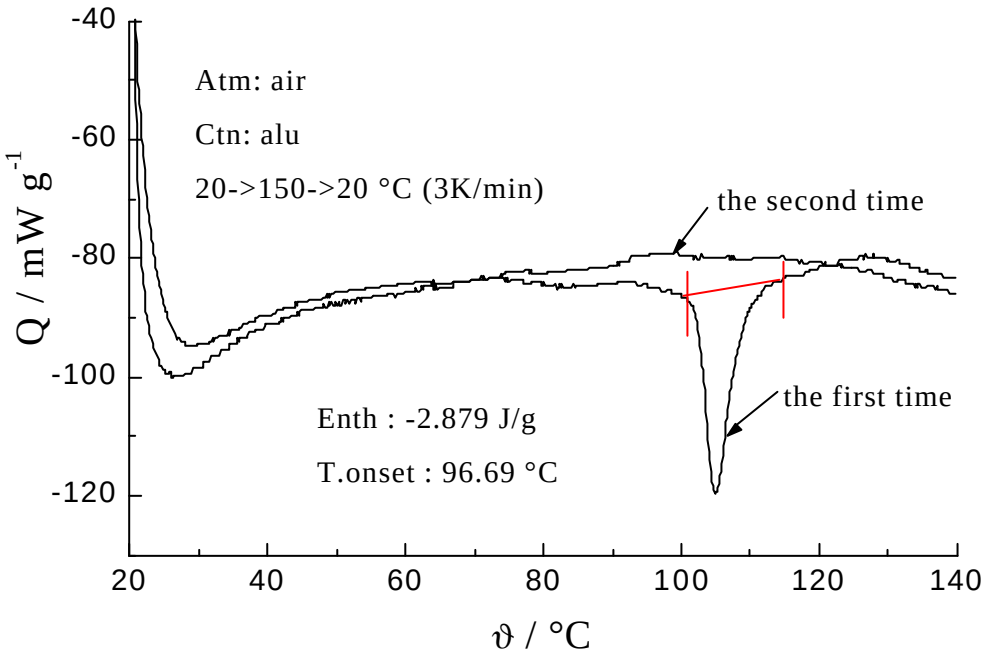

Figure 3.36 DSC of [5,10]-ionene dodecyl sulfate stoichiometric complex

The assignment of the absorption peak to water was also confirmed by a thermogravimetric analysis (TG). In the TG diagram (Fig. 3.37) in the first stage (below 130 °C) water evaporation caused the main weight loss of the [5,10]-ionene dodecyl sulfate stoichiometric complex, fragment peaks (Fig. 3.38) at m/z = 18 and m/z =17 were found at about 100 °C, clearly indicating water as the fragment evaporating from the complex.

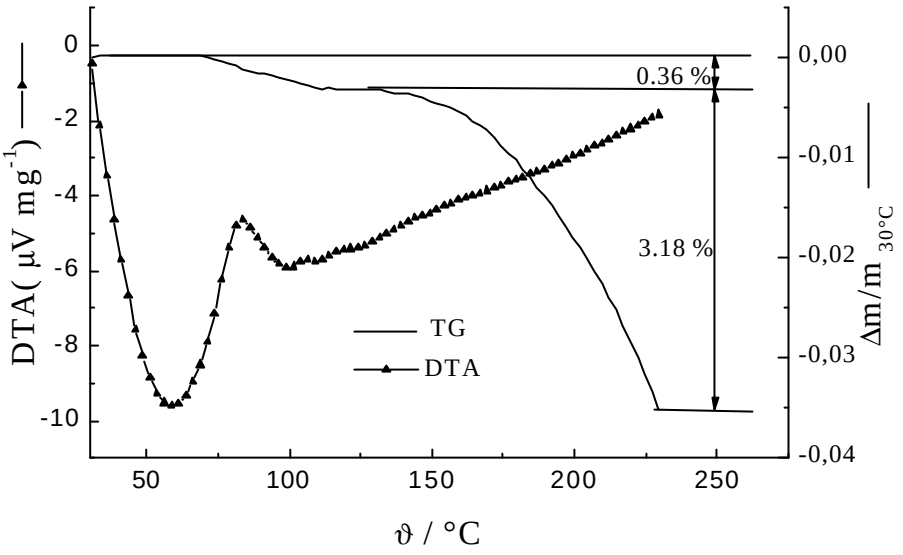

Figure 3.37 Thermogravimetric analysis of [5,10]-ionene dodecyl sulfate stoichiometric complexes; heating rate 5 K/min.

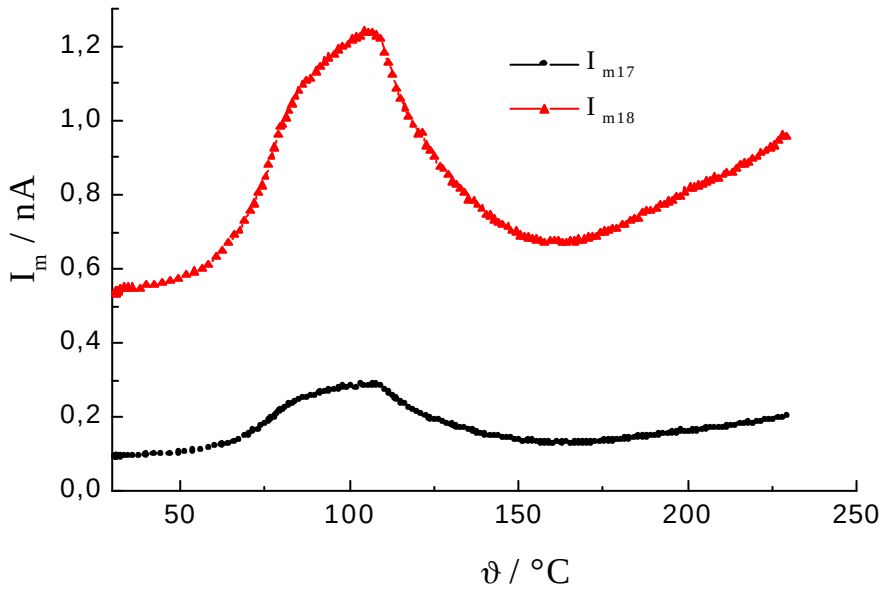

Figure 3.38 Fragments produced in thermogravimetric analysis of [5,10]-ionene dodecyl sulfate stoichiometric complexes; heating rate 5 K/min

The according weight loss of the [5,10]-ionene dodecyl sulfate stoichiometric complex was about 0.36 %, which corresponds to only 0.1 water molecules per ion pair unit absorbed in equilibrium with air. The samples were optically isotropic when prepared at ambient conditions. Thus the [5,10]-ionene dodecyl sulfate stoichiometric complex was stable below 130 °C, but it also absorbed some water in air, but much less as compared to the [3,12]-ionene dodecyl sulfate stoichiometric complex in which every ion pair unit absorbed at least 0.9 water molecules [101].

At high temperatures > 170 °C, the [5,10]-ionene dodecyl sulfate stoichiometric complex became unstable and began to decompose, similar to the non-complexed ionene (Fig. 3.32). This was supported by fragments produced in the thermogravimetric analysis of [5,10]-ionene dodecyl sulfate stoichiometric complexes (Fig. 3.39). Low-molecular-weight compounds were produced above 170 °C due to thermal degradation. Three fragments (Fig. 3.39) are shown at m/z = 2, 15 and 29. According to the mass fragments the [5,10]-ionene dodecyl sulfate stoichiometric complex decomposed into CH_3 (m/z =15) ion and CH_3N (m/z =29) ion [100].

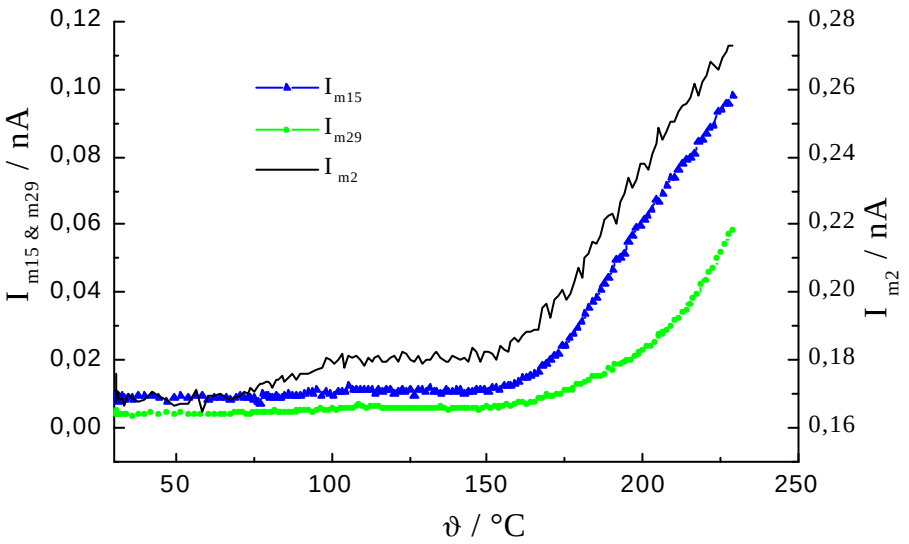

Figure 3.39 Fragments produced in thermogrametric analysis of [5,10]-ionene dodecyl sulfate stoichiometric complexes; heating rate 5 K/min

3.4.2.2 Isotropic-mesogenic behavior of the [5,10]-ionene dodecyl sulfate stoichiometric complex

The [5,10]-ionene dodecyl sulfate stoichiometric complexes easily absorbed more water when they were exposed to increased relative humidity. While the optical properties did not change at relative humidities up to 67.4 %. At 69 % the film changed from optically isotropic to optically anisotropic, i.e. at a lower humidity than in the case of the [3,12]-ionene dodecyl sulfate complex (cf. Fig. 3.21). A polarizing microscope confirmed the existence of optical anisotropy. It will be shown below that a mesogenic phase structure was formed thereby.
The DSC curve for samples equilibrated at 67.4 and 69 % relative humidity (Fig. 3.40) exhibited emission peaks at about 100 °C. These peaks were assigned to the chemical reaction of dodecyl sulfate as in the case of the [3,12]-ionene dodecyl sulfate complex. The dodecyl sulfate was hydrolyzed to form dodecanol, which is impossible in the absence of sufficient water (cf. Fig.3.36).

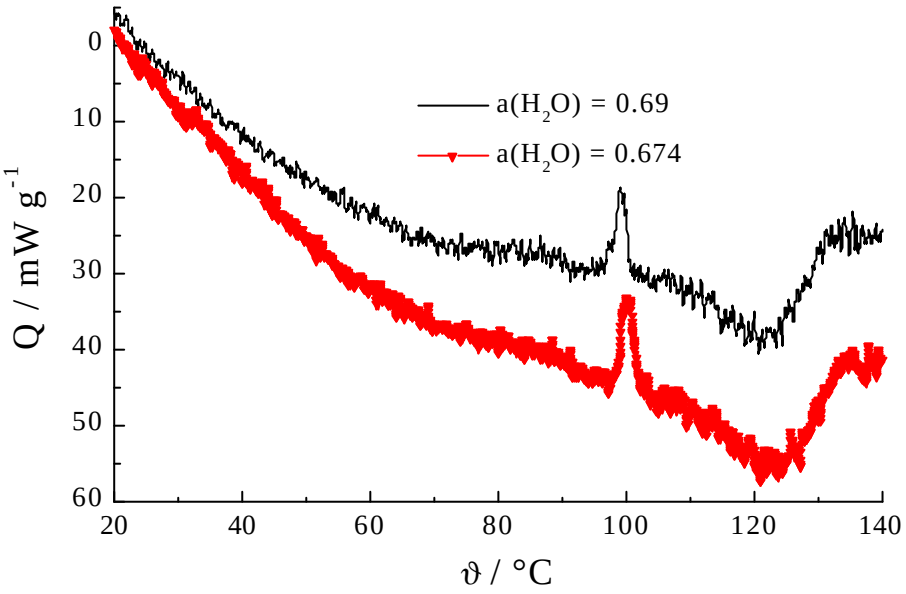

Figure 3.40 DSC-curve of [5,10]-ionene stoichiometrically complexed with dodecyl sulfate for two samples equilibrated at constant relative humidities: 67.4 % and 69 %; heating rate 1 K/min.

The transition point for the humidity induced transition from optically isotropic to optically anisotropic was also reflected by enthalpy and temperature of the maximum of the emission peaks measured by DSC (Fig. 3.41) as a function of relative humidity: The minima in the curves shown in Fig. 3.41 are between 65 and 69 % relative humidity, i.e. in the range of the transition.

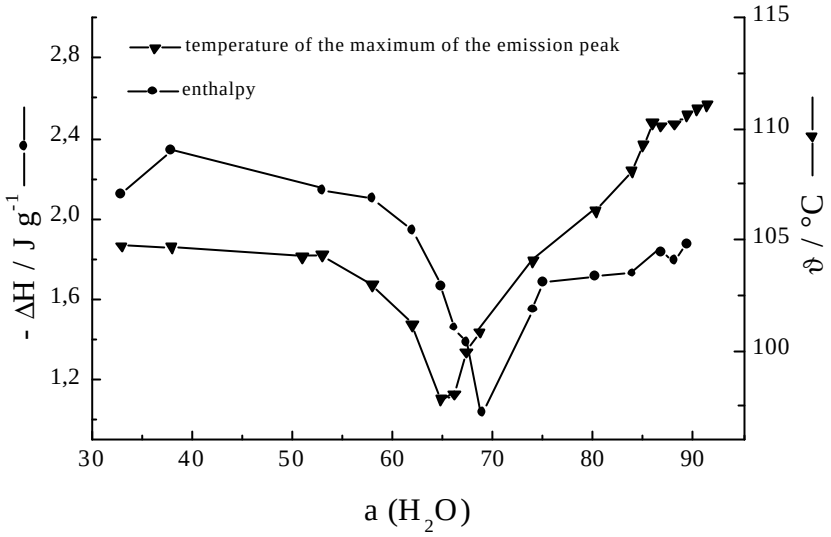

Figure 3.41 Enthalpy and temperature of the maximum of the exothermic peak of [5,10]-ionene dodecyl sulfate stoichiometric complexes measured by DSC; heating rate 1 K/min.

From Figure 3.42 it follows that the take-up of water was proportional to the fraction of water in the gas phase. At the transition point (isotropic to anisotropic) at 68 % relative humidity every ion pair of the [5,10]-ionene dodecyl sulfate stoichiometric complex had absorbed 2.38 water molecules.

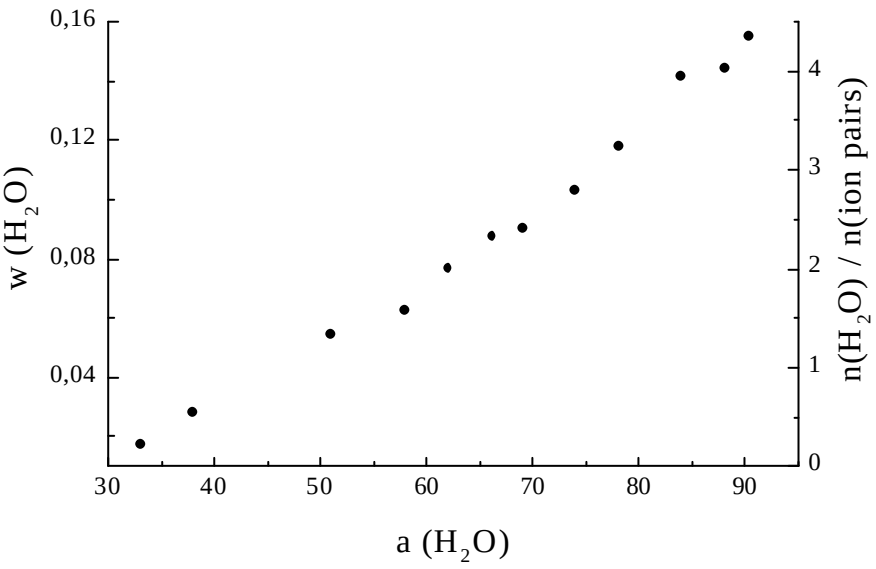

Figure 3.42 Swelling (mass fraction *w* of water) of [5,10]-ionene dodecyl sulfate stoichiometric complexes and number of water molecules per ion pair unit ($n(H_2O)$) as a function of the relative humidity ($a(H_2O)$) applied to the dry sample at room temperature.

Figure 3.43 shows the texture of the mesogenic phase of the stoichiometric complex after cooling (at 105 ± 1 °C) from the isotropic phase as it appeared on the polarizing microscope. The texture indicates a hexagonal mesogenic structure.

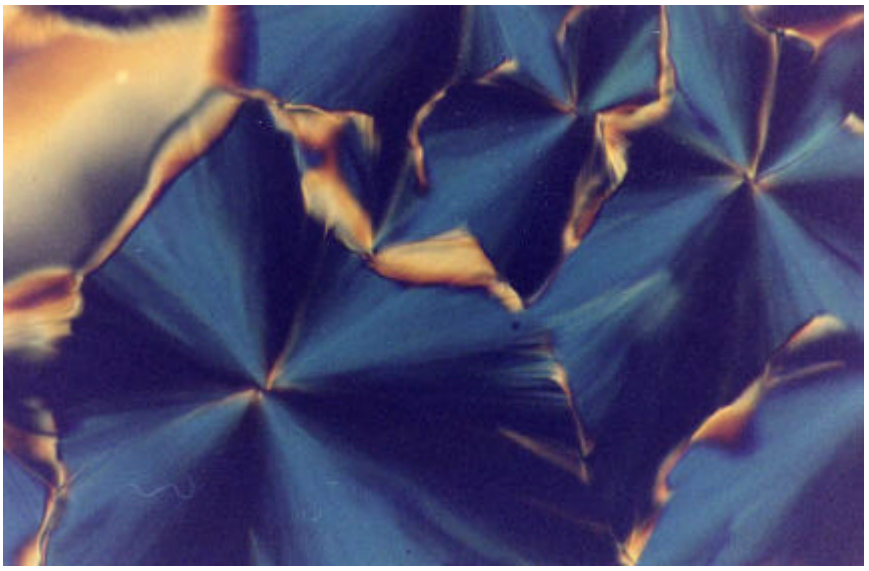

Figure 3.43 Texture of the mesogenic phase in [5,10]-ionene dodecyl sulfate stoichiometric complexes obtained from a polarizing microscope. Magnification 100X, sample prepared at a(H_2O) = 0.75.

3.4.3 [5,10]-ionene decyl sulfate stoichiometric complex

3.4.3.1 The silver decyl sulfate

The silver decyl sulfate was a white crystal, and similar to silver dodecyl sulfate, the solution of silver decyl sulfate was easily decomposed when it was exposed to light. So it should be kept in dark and dry place. The following figure depicts the ATR-IR spectrum of silver decyl sulfate. The observed wavenumbers and band assignments for silver decyl sulfate are comprised in Table 3.10 [102].

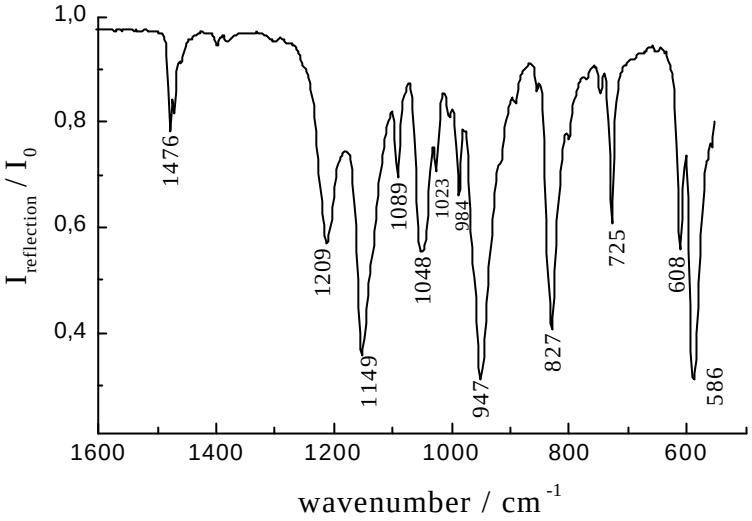

Figure 3.44 ATR-IR spectra of silver decyl sulfate

wavenumber(cm^{-1})	assignment
2957	asymmetric CH_3 stretching
2921	antisymmetric CH_2 stretching
2849	symmetric CH_2 stretching
1476	CH_2 scissoring
1209	asymmetric (OSO_3^-) stretching
1149	asymmetric (OSO_3^-) stretching
1048	symmetric (OSO_3^-) stretching
947	asymmetric (C-O-S) stretching
827	symmetric (C-O-S) stretching
608	asymmetric (OSO_3^-) bending
586	symmetric (OSO_3^-) bending

Table 3.10 The wavenumber and band assignments of silver decyl sulfate

The spectrum is similar to the ATR-IR spectrum of sodium decyl sulfate [103]. The strong bands at 1209 cm^{-1} and 1149 cm^{-1} were caused by asymmetric (OSO_3^-) stretching and the strong band at 1050 cm^{-1} was symmetric (OSO_3^-) stretching. These bands were the characteristic for silver decyl sulfate.

3.4.3.2 The [5,10]-ionene decyl sulfate stoichiometric complex

The stoichiometric complex structure of [5,10]-ionene decyl sulfate is displayed as follows.

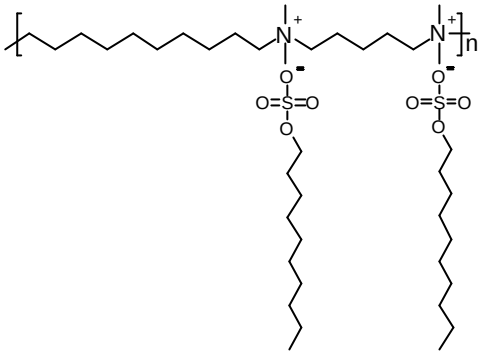

structure of [5,10]-ionene decyl sulfate complexes

The NMR diagrams of [5,10]-ionene decyl sulfate stoichiometric complex in DMSO were consisted of two parts, one was [5,10]-ionene, and another was decyl sulfate.

^{1}H-NMR of [5,10]-ionene decyl sulfate stoichiometric complex (*d*/ppm at 500 MHz in DMSO): 0.85 (t, 3 H, -CH_3 in decyl sulfate), 1.24-1.28 (br, 28 H including (14 H, (γ, δ, ε, ζ, η, θ, ι)-CH_2 in decyl sulfate) and (14 H including 12 H, (γ, δ, ε)-CH_2-decano- and 2 H, γ-CH_2-pentano- in [3,12]-ionene)), 1.47 (br, 2 H, β-CH_2 in decyl sulfate) 1.65 (br, 4 H, β-CH_2-decano- in [3,12]-ionene), 1.70 (br, 4 H, β-CH_2-pentano- in [3,12]-ionene), 2.49 (br, 12 H, $(CH_3)_2N^+$), 2.99-3.3 (br, α-CH_2 and H_2O), 3.67 (t, 2 H, α-CH_2 in decyl sulfate).

wavenumber(cm^{-1})	assignment
3493	H-bridge, O-H stretching
3036	chelate H-bridge, O-H stretching
2922	antisymmetric CH_2 stretching
2853	symmetric CH_2 stretching
1466	C-H torsional vibration in the $–CH_2N^+$ moiety
1373	CH_3 bending of dodeyl sulfate
1214	asymmetric (OSO_3^-) stretching
1058	symmetric (OSO_3^-) stretching
983	symmetric (N-CH_3) stretching
620	asymmetric (OSO_3^-) bending
577	symmetric (OSO_3^-) bending

Table 3.11 The wavenumber and band assignments of the [5,10]-ionene decyl sulfate stoichiometric complex

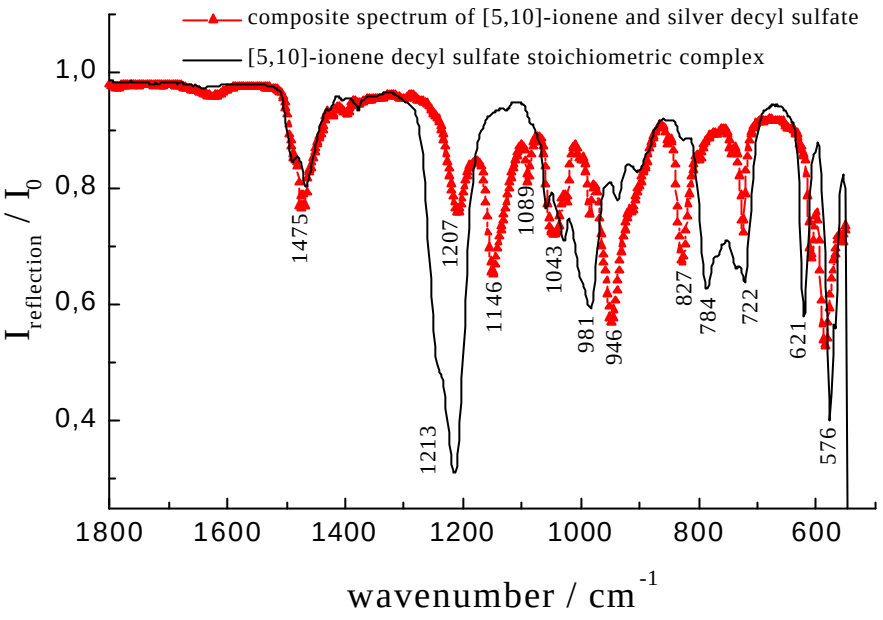

Figure 3.45 ATR-IR spectra of the [5,10]-ionene decyl sulfate stoichiometric complex and of the superposed components

Fig. 3.45 displays the ATR-IR spectrum of the [5,10]-ionene decyl sulfate stoichiometric complex and the composite ATR-IR spectrum of [5,10]-ionene and silver decyl sulfate. It was found that the two spectra did not coincide. The two asymmetric (OSO_3^-) stretching bands at 1207 cm^{-1} and 1147 cm^{-1} of silver decyl sulfate became a strong asymmetric (OSO_3^-) stretching band at 1213 cm^{-1} in the complex. The asymmetric (C-O-S) stretching band at 946 cm^{-1} and the symmetric (C-O-S) stretching band at 827 cm^{-1} which appeared in silver decyl sulfate almost disappeared in the complex. Instead a new strong band at 784 $cm^{-1}$was found. A comparison of Table 3.10 with Table 3.11 suggests that this band was probably the symmetric ($N-CH_2$) stretching of [5,10]-ionene decyl sulfate stoichiometric complex.

3.4.3.3 The stability of the [5,10]-ionene decyl sulfate stoichiometric complex

The ATR-IR spectrum before and after heating the [5,10]-ionene decyl sulfate stoichiometric complex to 160 °C was almost constant (Fig. 3.46). This shows that the functional groups of [5,10]-ionene decyl sulfate stoichiometric complexes didn't change during heating, i.e. the complex is stable under these conditions. The spectra also reveal that the stoichiometric complexes contain some water (peak at 3493 cm^{-1}, not shown), which the sample must have taken up after exposure to air for taking the spectrum. As compared to the [3,12]-ionene decyl

sulfate stoichiometric complex, the [5,10]-ionene decyl sulfate stoichiometric complex contained much less water.

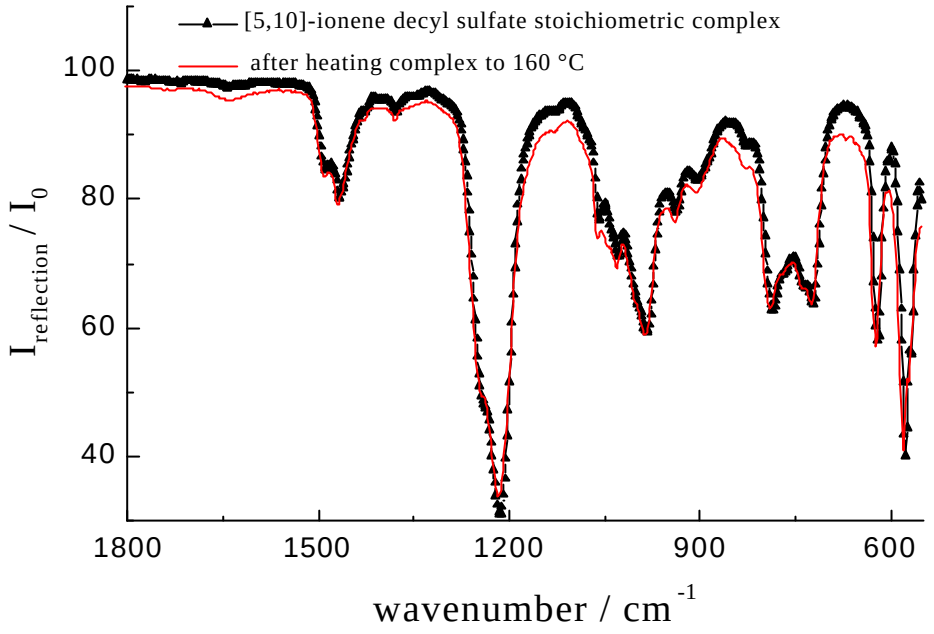

Figure 3.46 ATR-IR spectra of [5,10]-ionene decyl sulfate stoichiometric complex before and after heating

Consequently, differential scanning calorimetry (DSC) did not reveal the absorption peak attributable to the loss of water upon heating. In the DSC diagram (Fig. 3.47) there was no absorption peak at about 100 °C. There were, however, an absorption peak at 55 °C and an exothermal peak at about 132 °C, they were both weak peaks. After cooling the sample to room temperature and repeating the DSC experiment there was no peak any more (Fig. 3.47). The processes responsible for the small absorption and emission peaks in the first time curve could not be identified.

Accordingly, a loss of water was also not supported by a thermogravimetric analysis (TG) and mass spectra. In the TG diagram (Fig. 3.48) in the first stage before 130 °C, the weight loss was only about 0.13 % for [5,10]-ionene decyl sulfate stoichiometric complex.

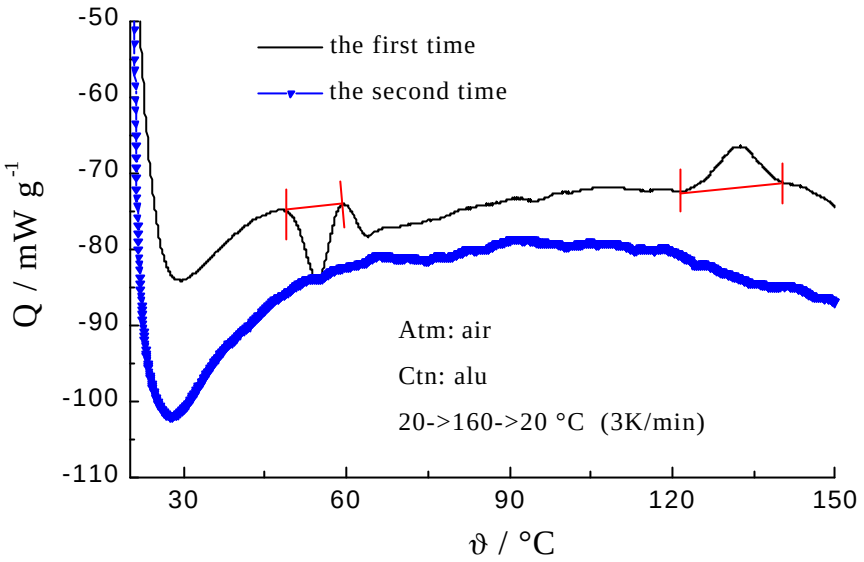

Figure 3.47 DSC of the [5,10]-ionene decyl sulfate stoichiometric complex

The missing intensity at m/z = 18 clearly indicated no peak from 80 °C to 130 °C for [5,10]-ionene decyl sulfate stoichiometric complex. The DTA displayed an absorption peak at 100 °C, which was a very weak peak. From above statement it can be concluded below 160 °C (Fig. 3.49) almost no water was vaporized from [5,10]-ionene decyl sulfate stoichiometric complex, and the stoichiometric complex was stable.

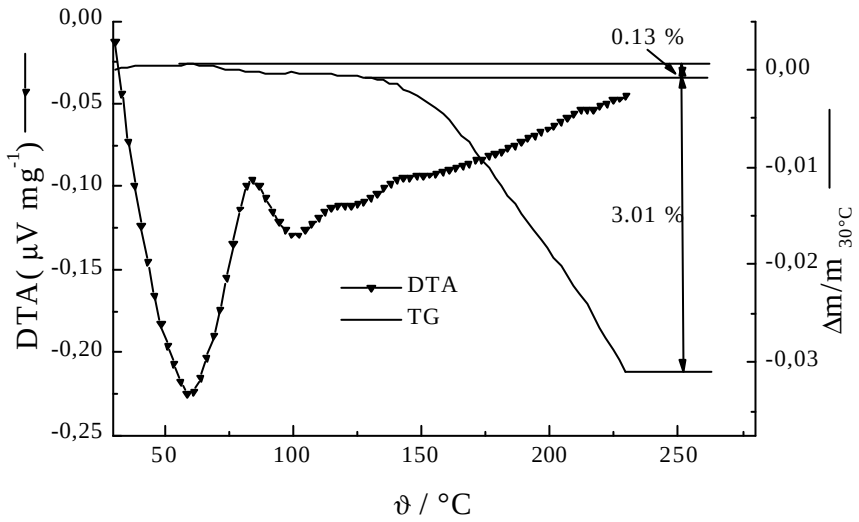

Figure 3.48 Thermogravimetric analysis of [5,10]-ionene decyl sulfate stoichiometric complexes; heating rate 5 K/min.

In the second stage above 160 °C, [5,10]-ionene decyl sulfate stoichiometric complex became unstable. The fragments at m/z = 2, 18 and 29 all increased with increasing temperature, indicating that [5,10]-ionene decyl sulfate stoichiometric complex had been decomposed, this was caused by thermal degradation of [5,10]-ionene (Fig. 3.49).

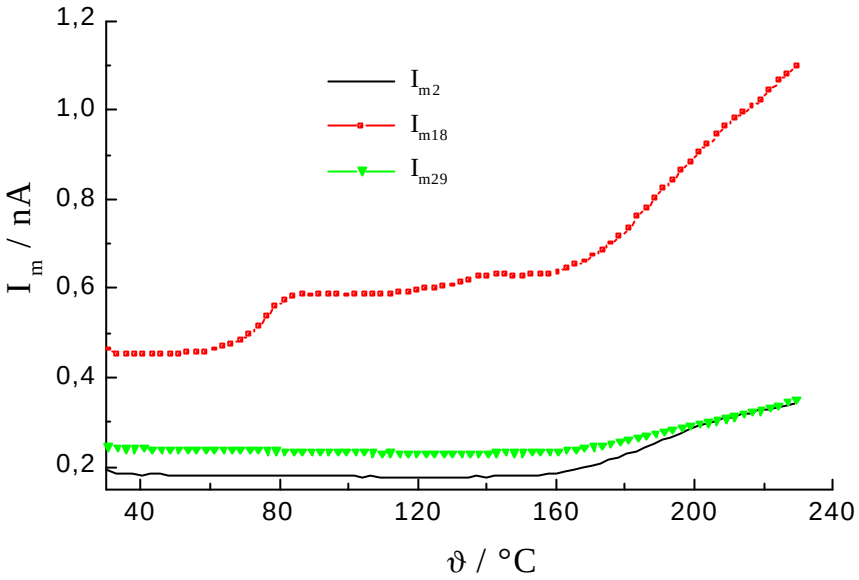

Figure 3.49 Fragments produced in thermogrametric analysis of [5,10]-ionene decyl sulfate stoichiometric complexes; heating rate 5 K/min

3.4.3.4 Isotropic-mesogenic property of [5,10]-ionene decyl sulfate stoichiometric complex

[5,10]-ionene decyl sulfate stoichiometric complexes absorbed more water when they were exposed to increased relative humidity. While the optical properties did not change at relative humidities up to 58 %, at 62 % the film changed from optically isotropic to optically anisotropic. A polarizing microscope confirmed the existence of optically anisotropic. We will show below that a mesogenic phase structure was formed thereby.

The DSC curve for a sample equilibrated at 58 % relative humidity (Fig. 3.50, curve for a(H_2O) = 0.58) exhibited an exothermic peak at about 62 °C. On further inspection of the figure we noted that the temperature of the maximum of the exothermic peak at transition point was lowest temperature (Fig. 3.51). This indicates slightly different lyotropic structures of the various samples.

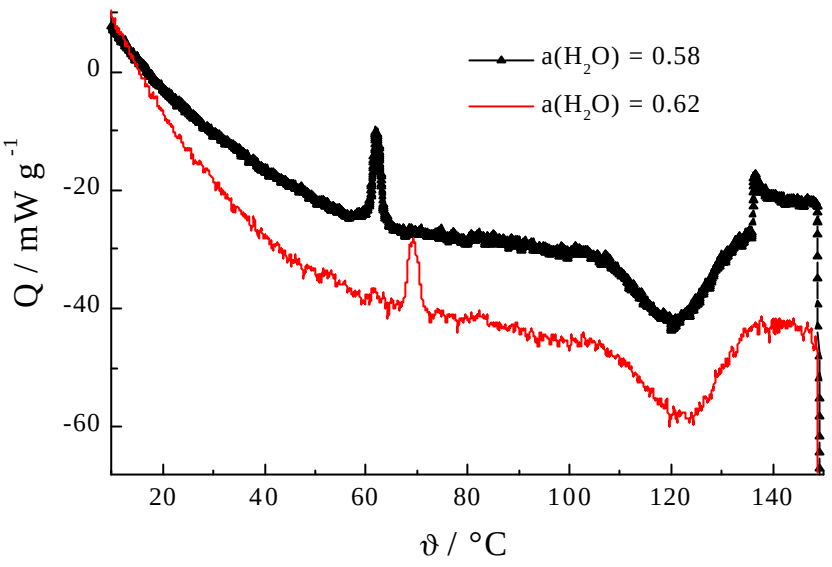

Figure 3.50 DSC-curve of [5,10]-ionene stoichometrically complexed with decyl sulfate for two samples equilibrated at constant relative humidities: 58 % and 62 %; heating rate 1 K/min.

In this system the humidity induced transition point from optically isotropic to optically anisotropic was less clearly revealed, when enthalpy and temperature of the maximum of the emission peak measured by DSC were plotted as a function of relative humidity (Fig. 3.51).

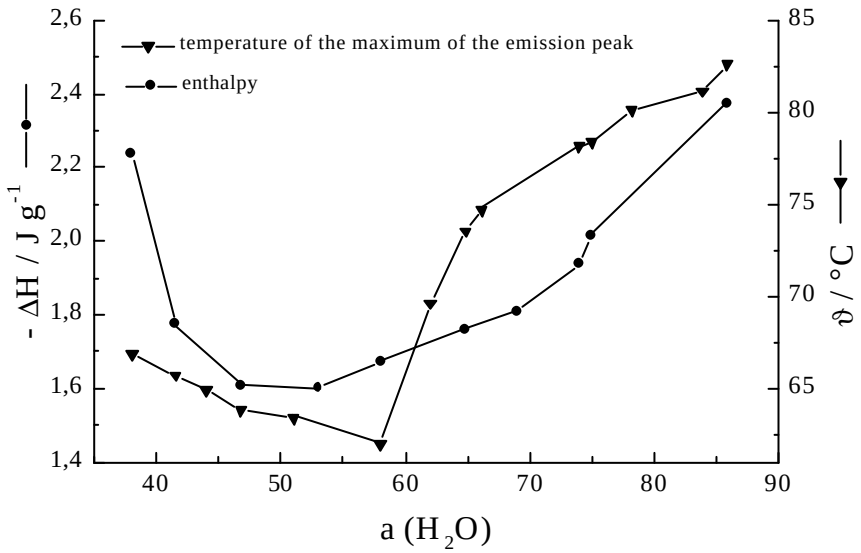

Figure 3.51 Enthalpy and temperature of the maximum of the exothermic peak of [5,10]-ionene decyl sulfate stoichiometric complexes measured by DSC; heating rate 1 K/min.

While the minimum of the temperature of the maximum of the emission peak exhibits a minimum at the transition point, the value of enthalpy passes through a broad minimum not indicating the transition.

From Figure 3.52 it follows that the take up of water was proportional to the fraction of water in the gas phase. At the transition point changing from optically isotropic to optically anisotropic every ion pair of [5,10]-ionene decyl sulfate stoichiometric complex absorbed about 2 water molecules.

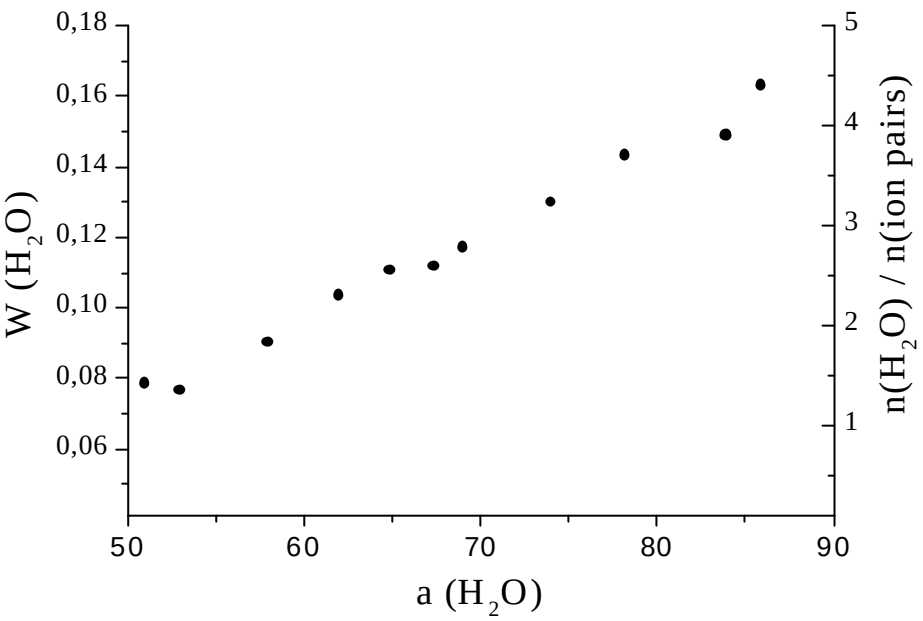

Figure 3.52 Swelling (mass fraction *w* of water) of [5,10]-ionene decyl sulfate stoichiometric complexes and number of water molecules per ion pair unit ($n(H_2O)$) as a function of the relative humidity ($a(H_2O)$) applied to the dry sample at room temperature.

Figure 3.53 showed the texture of the mesogenic phase of the stoichiometric complex after cooling (at about 76 ± 1 °C) from the isotropic phase as it appeared on the polarizing microscope. The texture indicates a hexagonal mesogenic structure.

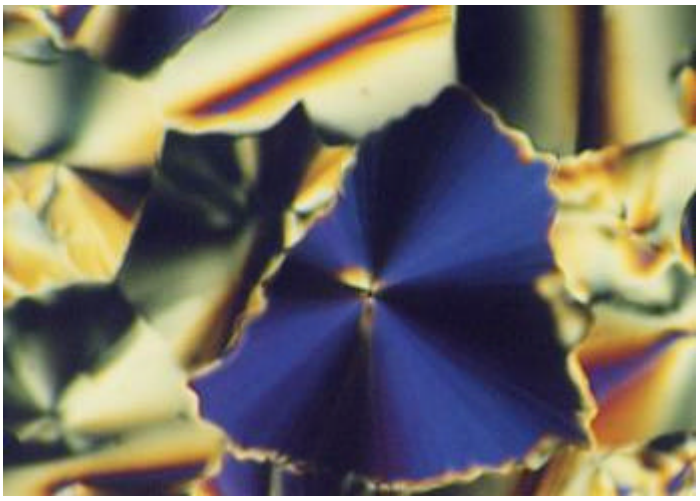

Figure 3.53 Texture of the mesogenic phase in [5,10]-ionene decyl sulfate stoichiometric complexes obtained from a polarizing microscope. Magnification 100X, sample prepared at a(H_2O) = 0.70.

3.5 [3,10]-ionene and its alkyl sulfate stoichiometric complexes

3.5.1 [3,10]-ionene

[3,10]-ionene had a structure similar to [3,12]-ionene and [5,10]-ionene and so similar properties can be expected. It was again a brittle polyelectrolyte, which easily dissolved in methanol and water. The following Fig. 3.54 depicts the ATR-IR spectrum of [3,10]-ionene, which is very similar to the spectra of [3,12]-ionene and [5,10]-ionene possessing the same functional groups. There was a strong O-H band at 3418 cm^{-1}, but there is no O-H functional group in [3,10]-ionene, so [3,10]-ionene contained another low-molecular-weight compound. It was probably water or methanol. The strong band at 1468 cm^{-1} was caused by C-H torsional vibration in the $–CH_2N^+$ moiety which was the characteristic spectrum of [3,10]-ionene. Table 3.12 displays the wavenumber and band assignments of [3,10]-ionene.

Wavenumber (cm^{-1})	assignment
3418	H-bridge, O-H stretching
3008	chelate H-bridge, O-H stretching
2924	antisymmetric CH_2 stretching
2854	symmetric CH_2 stretching
1468	C-H torsional vibration in the $–CH_2N^+$ moiety
1028	(C-O) stretching
991	symmetric (N-CH_3) stretching
901	symmetric (N-CH_2) stretching

Table 3.12 The wavenumbers and band assignments of [3,10]-ionene

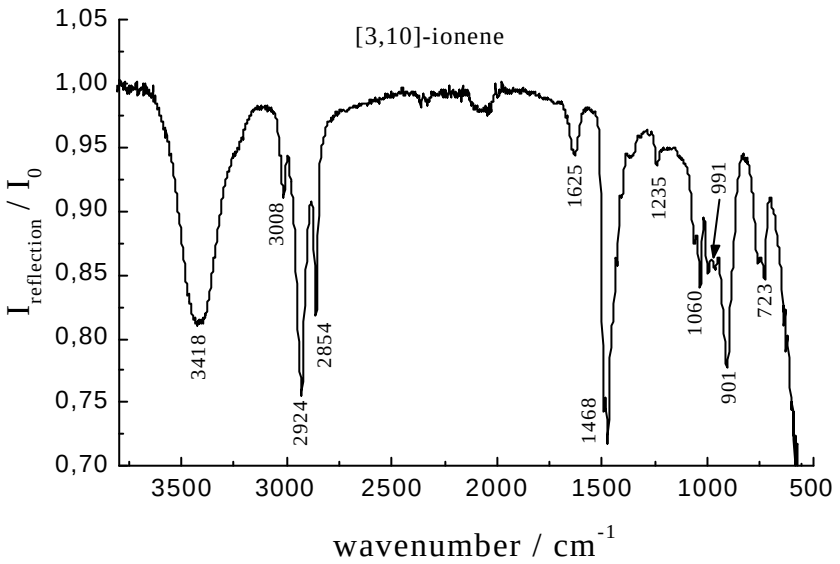

Figure 3.54 ATR-IR spectrum of [3,10]-ionene

3.5.1.1 The stability of [3,10]-ionene

The differential scanning calorimetry (DSC) curve indicated an absorption peak at about 50 °C, and the enthalpy was only about –1.57 J/g. After cooling the sample to room temperature and repeating the above process there was no absorption peak any more, i.e. after heating the sample the absorption peak had disappeared, maybe there was a low-molecular-weight compound in [3,10]-ionene. When the sample was heated, the low-molecular-weight compound was vaporized from [3,10]-ionene.

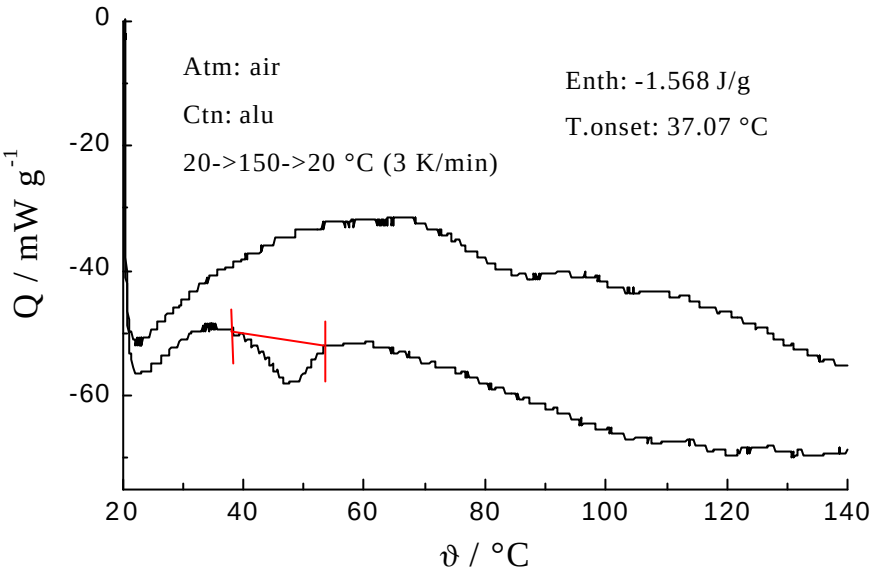

Figure 3.55 DSC of [3,10]-ionene

As the TG diagram (Fig. 3.56) displays, there was an endothermic peak from 50 °C to 100 °C in DTA curve, and in the second stage of TG diagram from 50 °C to 100 °C the weight loss was about 1.99 %. In agreement with the DSC curve (fig. 3.55), the features in this temperature range should be caused by the evaporation of methanol, which was left from the preparation at room temperature. The removal of methanol over phosphorous pentoxide in vacuum was incomplete.

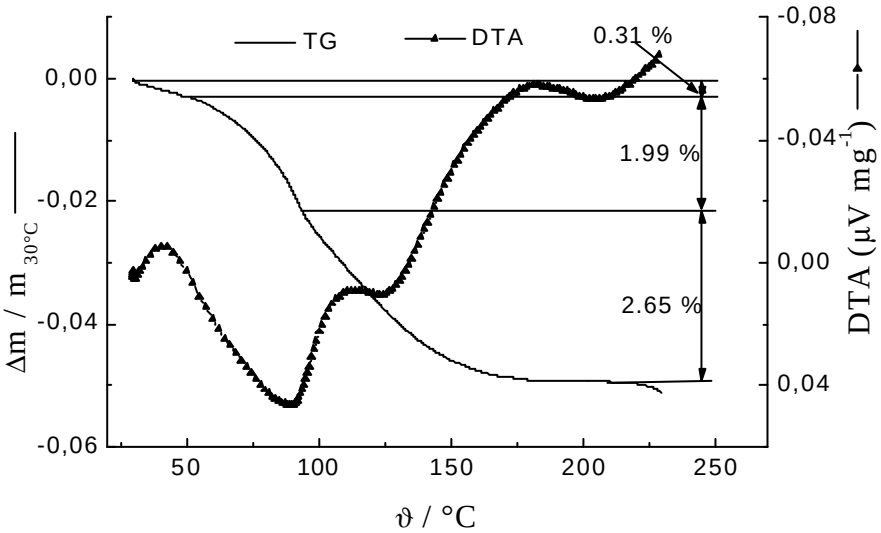

Figure 3.56 Thermogravimetric analysis of [3,10]-ionene; heating rate 5 K/min.

The sample from Fig. 3.55 was analysed by ATR-IR spectroscopy. The comparison between [3,10]-ionene and heated [3,10]-ionene reveals only small changes: the absorption peak at 1028 cm^{-1} diminished as did the OH-band at 3418 cm^{-1}. As these bands were caused by methanol [3,10]-ionene proved stable up to 150 °C, consistent with the TG diagram (Fig. 3.56).

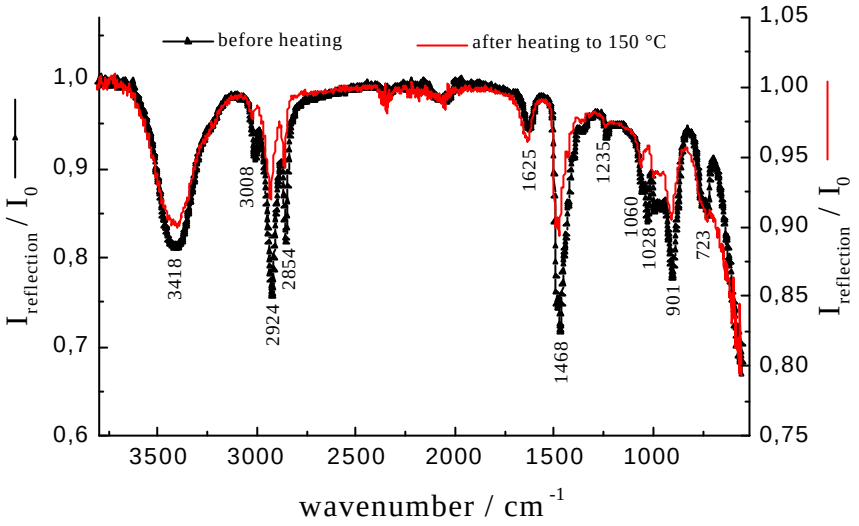

Figure 3.57 ATR-IR spectra of [3,10]-ionene before and after heating

3.5.2 [3,10]-ionene decyl sulfate stoichiometric complex

The stoichiometric complex structure of [3,10]-ionene decyl sulfate is displayed below.

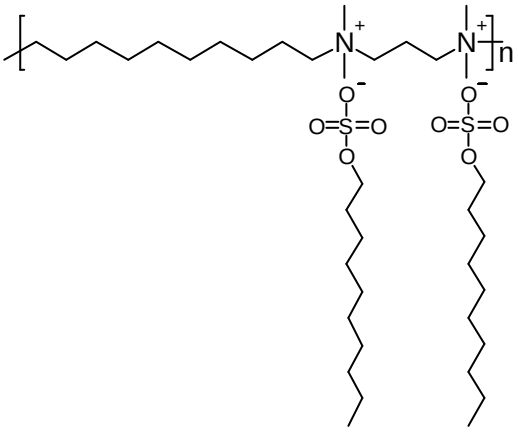

structure of [3,10]-ionene decyl sulfate complexes

The NMR spectra of the [3,10]-ionene decyl sulfate stoichiometric complex in DMSO consisted of two parts, one was [3,10]-ionene, and another was decyl sulfate.

^{1}H-NMR of [3,10]-ionene decyl sulfate stoichiometric complex (*d*/ppm at 500 MHz in DMSO): 0.85 (t, 3 H, -CH_3 in decyl sulfate), 1.24-1.28 (br, 26 H including (14 H, ($\gamma, \delta, \varepsilon, \zeta, \eta, \theta, \iota$)-$CH_2$ in decyl sulfate) and (12 H, ($\gamma, \delta, \varepsilon$)-$CH_2$-decano- in [3,10]-ionene)), 1.46 (br, 2 H, β-CH_2 in decyl sulfate) 1.67 (br, 4H, β-CH_2 –decano- in [3,10]-ionene), 2.14 (br, 2 H, β-CH_2-propano- in [3,10]-ionene), 3.04 (br, 12 H, $(CH_3)_2N^+$), 3.25-3.32 (br, α-CH_2 and H_2O), 3.68 (t, 2 H, α-CH_2 in decyl sulfate).

wavenumber(cm^{-1})	assignment
3475	H-bridge, O-H stretching
3033	chelate H-bridge, O-H stretching
2922	antisymmetric CH_2 stretching
2853	symmetric CH_2 stretching
1466	C-H torsional vibration in the $–CH_2N^+$ moiety
1210	asymmetric (OSO_3^-) stretching
1058	symmetric (OSO_3^-) stretching
981	symmetric (N-CH_3) stretching
622	asymmetric (OSO_3^-) bending
579	symmetric (OSO_3^-) bending

Table 3.13 The wavenumbers and band assignments of [3,10]-ionene decyl sulfate stoichiometric complex

Fig. 3.58 displayed the ATR-IR spectrum of the [3,10]-ionene decyl sulfate stoichiometric complex. The strong asymmetric (OSO_3^-) stretching bands at 1210 cm^{-1} and the C-H torsional vibration in the $–CH_2N^+$ moiety at 1466 cm^{-1} were the characteristic absorption peaks of the [3,10]-ionene decyl sulfate stoichiometric complex. In Table 3.13 the wavenumber and band assignments of the [3,10]-ionene decyl sulfate stoichiometric complex are listed.

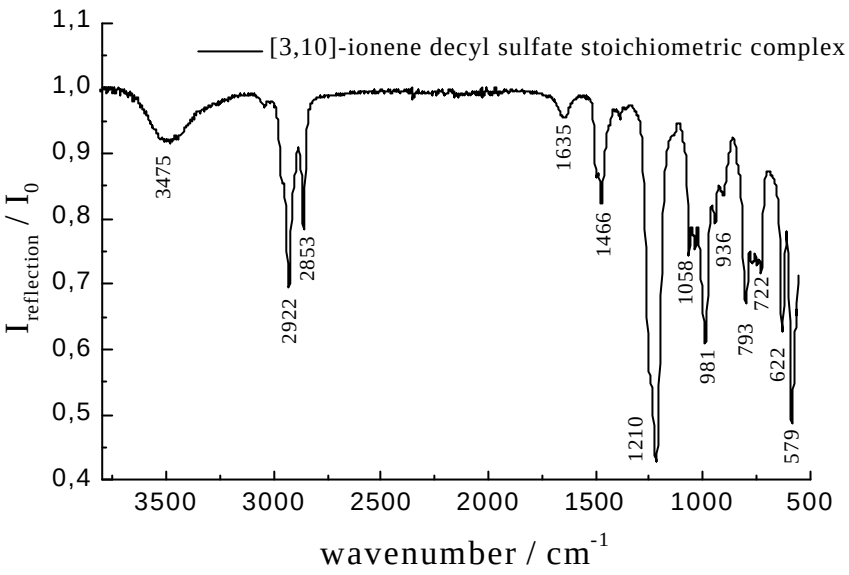

Figure 3.58 ATR-IR spectra of [3,10]-ionene decyl sulfate stoichiometric complex

3.5.2.1 The stability of [3,10]-ionene decyl sulfate stoichiometric complex

The ATR-IR spectrum before and after heating the [3,10]-ionene decyl sulfate stoichiometric complex to 150 °C kept almost unchanged (Fig. 3.59). This indicated that the functional groups of the [3,10]-ionene decyl sulfate stoichiometric complex didn't change during heating, i.e. the stoichiometric complex was stable under these conditions.

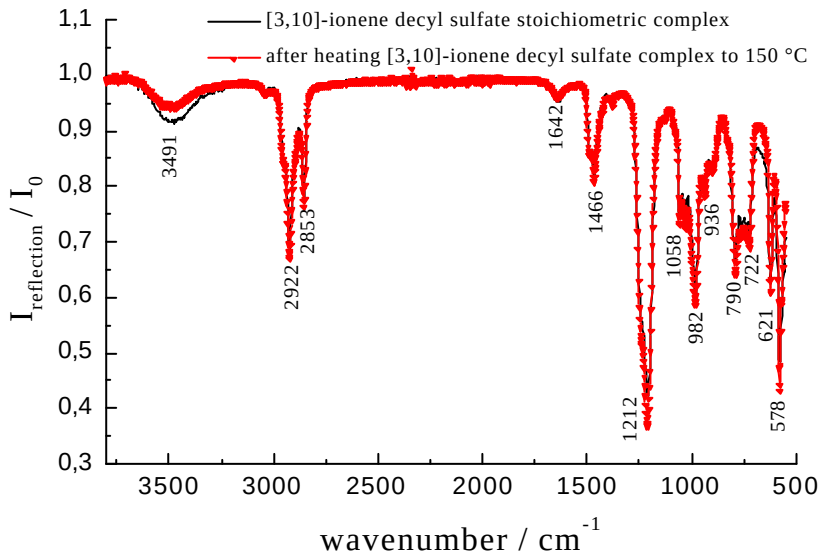

Figure 3.59 ATR-IR spectra of the [3,10]-ionene decyl sulfate stoichiometric complex before and after heating

The spectra also reveal that the stoichiometric complex contains some water (peak at 3491 cm^{-1}), which the sample probably has taken up after exposure to air for taking the spectrum. Before heating there was a stronger intensity of O-H stretching band, which indicated that some water was vaporized from the complex after heating sample to 150 °C.

Differential scanning calorimetry (DSC) supported the assignment of the absorption peak to the loss of water. As expected, there was an absorption peak at about 100 °C in the DSC diagram (Fig. 3.60). It was a weak peak and its enthalpy was only about 3 J g^{-1}. In the second run of the DSC curve this peak had vanished, in keeping with water being removed from complex.

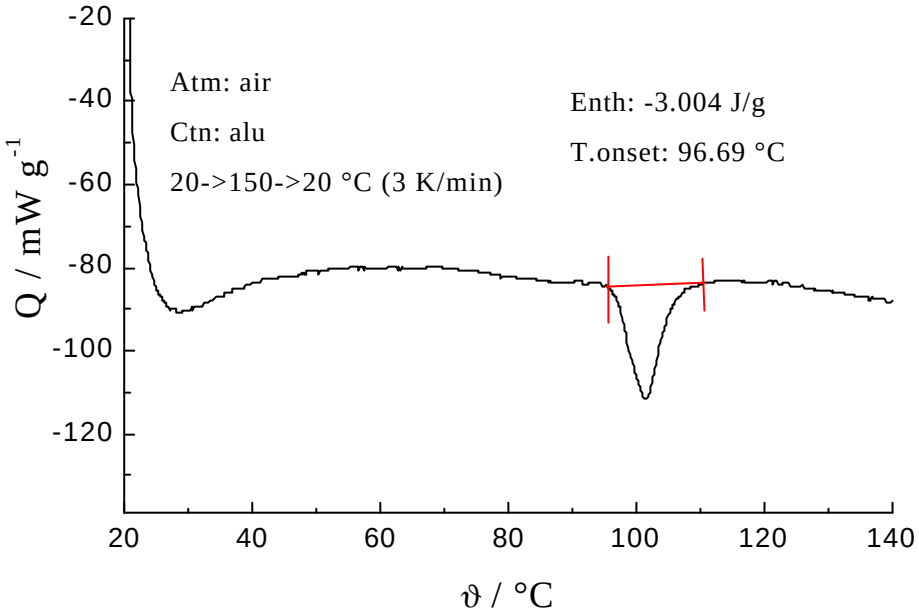

Figure 3.60 DSC of [3,10]-ionene decyl sulfate stoichiometric complex

A thermogravimetric analysis (TG) also confirmed assignment of the absorption peak to the loss of water. In the TG diagram (Fig. 3.58) the second stage from 55 °C to 118 °C reveals a weight loss of about 1.52 %, which was caused by water evaporation from the stoichoimetric complex. There was an endothermic peak at about 90 °C in the DTA curve, which was consistent with the existence of an endothermic peak in the DSC diagram. The fragment peaks (Fig. 3.62) at m/z = 18 and m/z =17 were found at about 91 °C, clearly indicating water as the fragment evaporating from the stoichiometric complex.

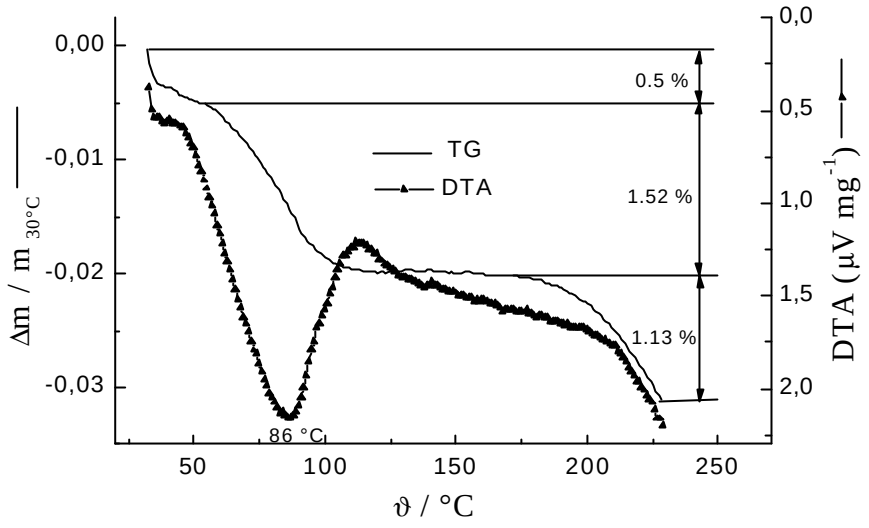

Figure 3.61 Thermogravimetric analysis of [3,10]-ionene decyl sulfate stoichiometric complexes; heating rate 5 K/min.

At temperatures above 175 °C the third stage of weight loss started, the fragment peaks (Fig. 3.62) at m/z = 29 were found from about 200 °C, and the intensity increase with increasing temperature, indicating thermal degradation. According to the mass fragments the [3,10]-ionene decyl sulfate stoichiometric complex decomposed into CH_3N (m/z =29) ions.

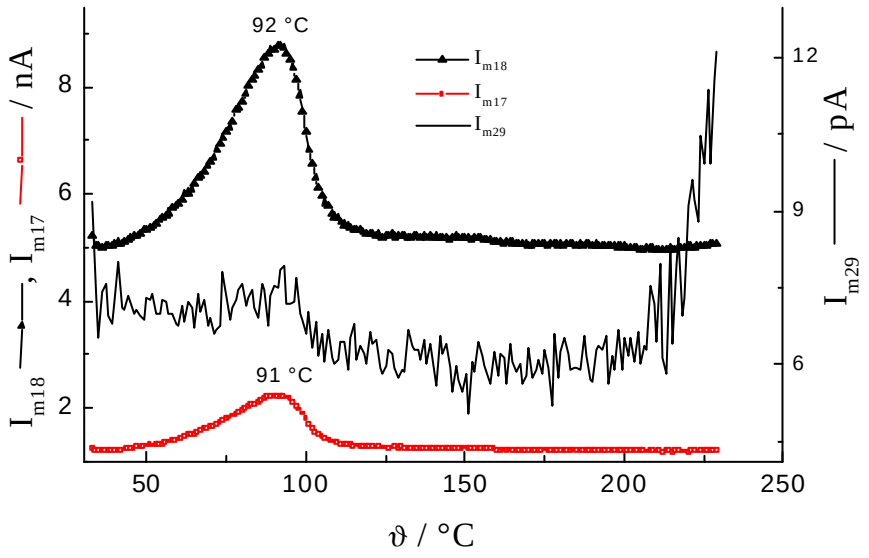

Figure 3.62 Fragments produced in thermogravimetric analysis of [3,10]-ionene decyl sulfate stoichiometric complexes; heating rate 5 K/min

The weight loss according to water was about 1.52 %. From this value we calculate that every ion pair unit of the [3,10]-ionene decyl sulfate stoichiometric complex absorbs only about 0.3 water molecules, when the complex was in equilibrium with ambient air. The samples were optically isotropic when prepared at ambient conditions, the [3,10]-ionene decyl sulfate stoichiometric complex was stable below 170 °C, but it can easily absorb water in air and when it was heated water was also easily lost.

3.5.2.2 Isotropic-mesogenic properties of the [3,10]-ionene decyl sulfate stoichiometric complex

The [3,10]-ionene decyl sulfate stoichiometric complex easily absorbs water when it was exposed to increased relative humidity. While the optical properties did not change at relative humidities up to 60 %, at 65 % the film changed from optically isotropic to optically anisotropic. A polarizing microscope confirmed the existence of optically anisotropy. It will be shown below that a mesogenic phase was formed thereby.

The DSC curve for a sample equilibrated at 58 % relative humidity (Fig. 3.63, curve for a(H_2O) = 0.58) exhibited an emission peak at about 100 °C, which moved to 82 °C at 65 % relative humidity, i.e. after transition to the anisotropic mesogenic phase. This indicates slightly different lyotropic structures of the various samples.

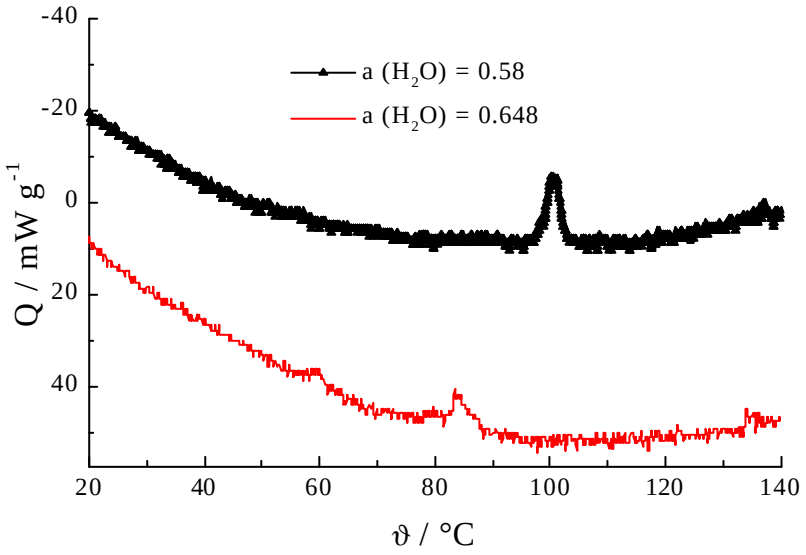

Figure 3.63 DSC-curve of [3,10]-ionene stoichometrically complexed with decyl sulfate for two samples equilibrated at constant relative humidities: 58 % and 64.8 %; heating rate 1 K/min.

The transition point from optically isotropic to optically anisotropic was also nicely reflected, when the enthalpy and the temperature of the maximum of the emission peak measured by DSC were plotted as a function of the relative humidity (Fig. 3.64). Both variables exhibited a quite sharp minimum at the relative humidity, at which the sample switches to anisotropic.

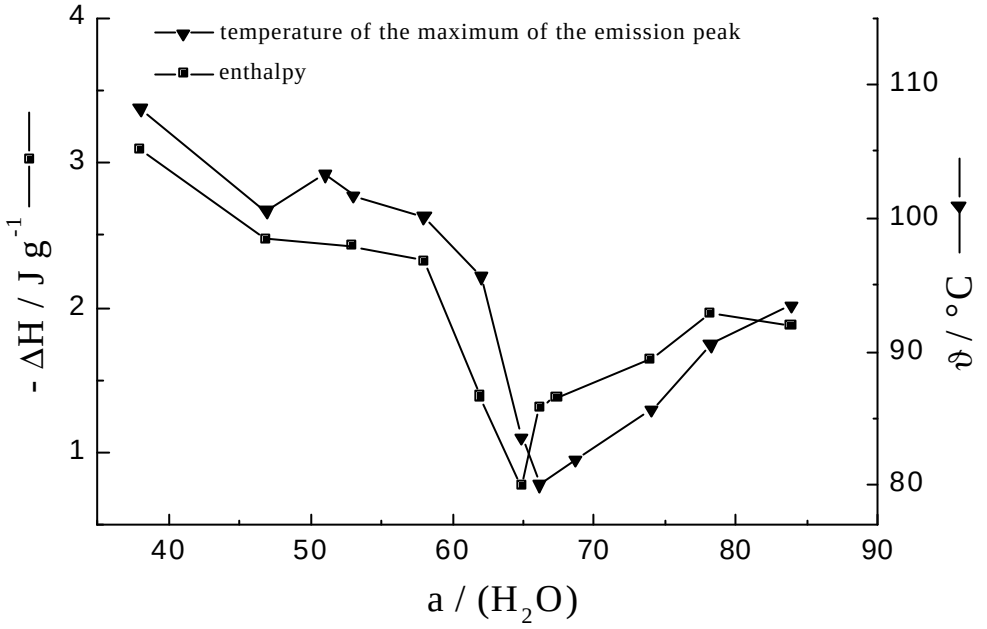

Figure 3.64 Enthalpy and temperature of the maximum of the exothermic peak of [3,10]-ionene decyl sulfate stoichiometric complexes measured by DSC; heating rate 1 K/min.

From Figure 3.65 it follows that the take up of water was proportional to the activity of water in the gas phase. At the transition point (ca. $a(H_2O) = 0.65$) for the changing from optically isotropic to optically anisotropic every ion pair of [3,10]-ionene decyl sulfate stoichiometric complex absorbed about 2 water molecules.

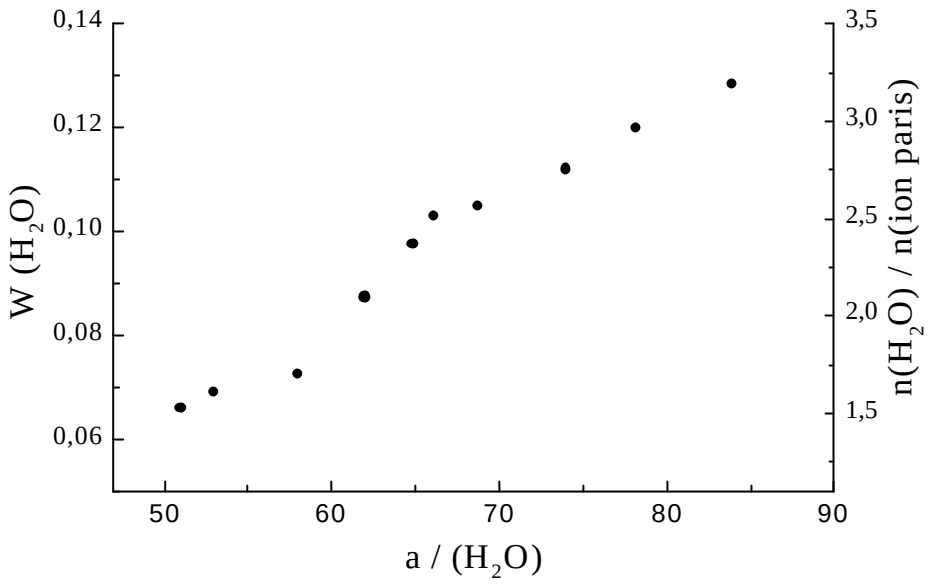

Figure 3.65 Swelling (mass fraction *w* of water) of [3,10]-ionene decyl sulfate stoichiometric complexes and number of water molecules per ion pair unit ($n(H_2O)$) as a function of the relative humidity ($a(H_2O)$) applied to the dry sample at room temperature.

Figure 3.66 shows the texture of the anisotropic mesogenic phase of the stoichiometric complex after cooling (at about 86.5 ± 1.5 °C) from the isotropic phase as it appeared on the polarizing microscope. The texture indicates a hexagonal mesogenic structure.

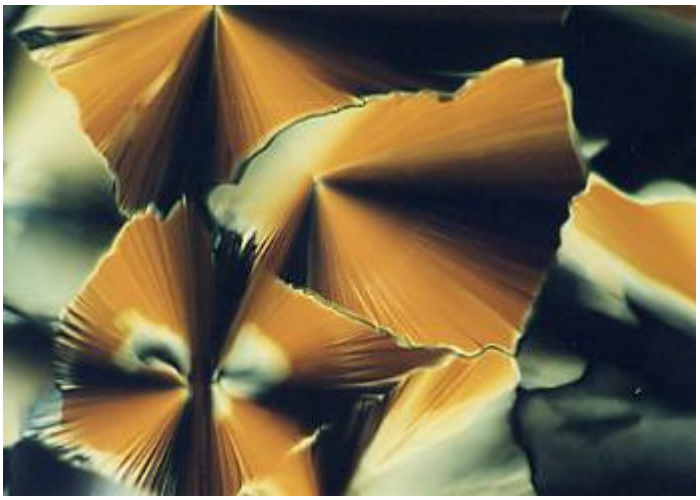

Figure 3.66 Texture of the anisotropic mesogenic phase in [3,10]-ionene decyl sulfate stoichiometric complexes obtained from a polarizing microscope. Magnification 100X, sample prepared at $a(H_2O) = 0.75$.

3.5.3 [3,10]-Ionene dodecyl sulfate stoichiometric complex

The stoichiometric complex structure of [3,10]-ionene dodecyl sulfate is shown below.

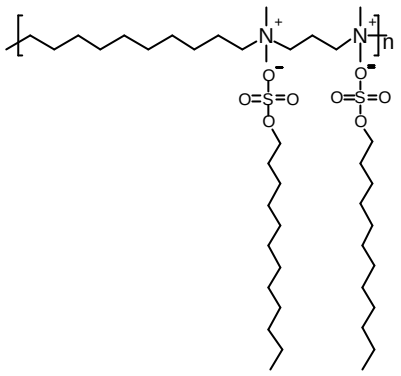

structure of [3,10]-ionene dodecyl sulfate complexes

The NMR spectra of [3,10]-ionene dodecyl sulfate stoichiometric complex in DMSO were consisted of two parts, one was [3,10]-ionene, and another was dodecyl sulfate.

^{1}H-NMR of [5,10]-ionene dodecyl sulfate stoichiometric complex (d/ppm at 500 MHz in DMSO): 0.85 (t, 3 H, -CH_3 in dodecyl sulfate), 1.24-1.28 (br, 30 H including (18 H, ($\gamma, \delta, \varepsilon, \zeta, \eta, \theta, \iota, \kappa, \lambda$)-$CH_2$ in dodecyl sulfate) and (12 H, ($\gamma, \delta, \varepsilon$)-$CH_2$-decano- in [3,10]-ionene)), 1.47 (br, 2 H, β-CH_2 in dodecyl sulfate) 1.67 (br, 4H, β-CH_2 –decano- in [3,10]-ionene), 2.1 (br, 2 H, β-CH_2-propano- in [3,10]-ionene), 3.04 (br, 12 H, $(CH_3)_2N^+$), 3.27-3.32 (br, α-CH_2 and H_2O), 3.68 (t, 2 H, α-CH_2 in dodecyl sulfate).

wavenumber(cm^{-1})	assignment
3494	H-bridge, O-H stretching
3037	chelate H-bridge, O-H stretching
2921	antisymmetric CH_2 stretching
2853	symmetric CH_2 stretching
1466	C-H torsional vibration in the $–CH_2N^+$ moiety
1373	CH_3 bending of dodeyl sulfate
1212	asymmetric (OSO_3^-) stretching
1058	symmetric (OSO_3^-) stretching
989	symmetric (N-CH_3) stretching
623	asymmetric (OSO_3^-) bending
578	symmetric (OSO_3^-) bending

Table 3.14 The wavenumber and IR band assignments of the [3,10]-ionene dodecyl sulfate stoichiometric complex

Fig. 3.67 displays the ATR-IR spectrum of the [3,10]-ionene dodecyl sulfate stoichiometric complex. The strong asymmetric (OSO_3^-) stretching bands at 1212 cm^{-1} and the C-H torsional vibration in the $–CH_2N^+$ moiety at 1466 cm^{-1} were characteristic absorption peaks of the complex. Table 3.14 lists the wavenumbers and band assignments.

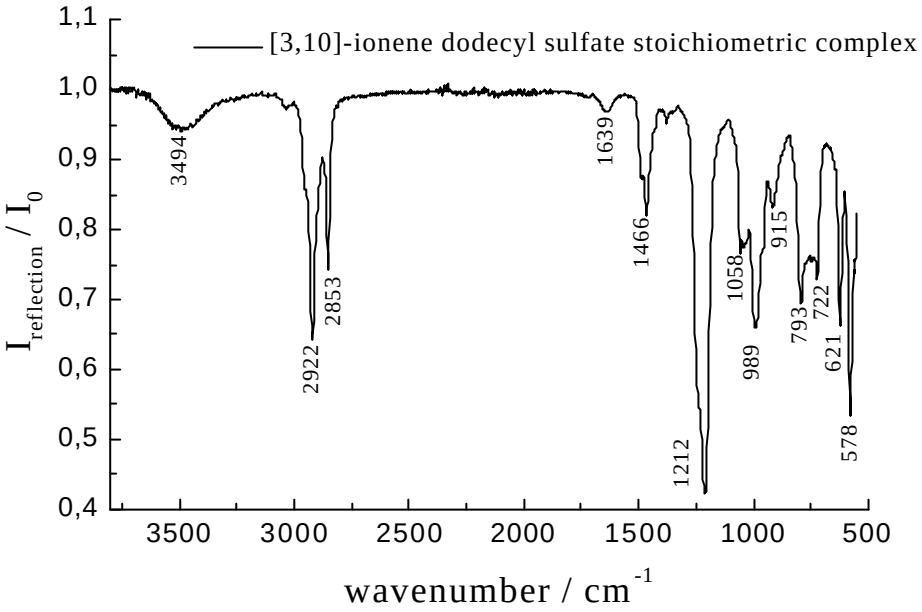

Figure 3.67 ATR-IR spectrum of the [3,10]-ionene dodecyl sulfate stoichiometric complex

3.5.3.1 The stability of [3,10]-ionene dodecyl sulfate stoichiometric complex

The ATR-IR spectrum before and after heating the [3,10]-ionene dodecyl sulfate stoichiometric complex to 150 °C was almost constant (Fig. 3.68). This determined that the functional groups of [3,10]-ionene dodecyl sulfate stoichiometric complexes didn't change during heating, i.e. the complex was stable under these conditions. The spectra also reveal that the stoichiometric complex contains some water (or another compound with an OH-group; peak at 3494 cm^{-1}). In contrast to the [3,10]-ionene decyl sulfate stoichiometric complex band intensity here kept constant before and after heating. This showed that was difficult to remove the water from the [3,10]-ionene dodecyl sulfate stoichiometric complex even at 150 °C.

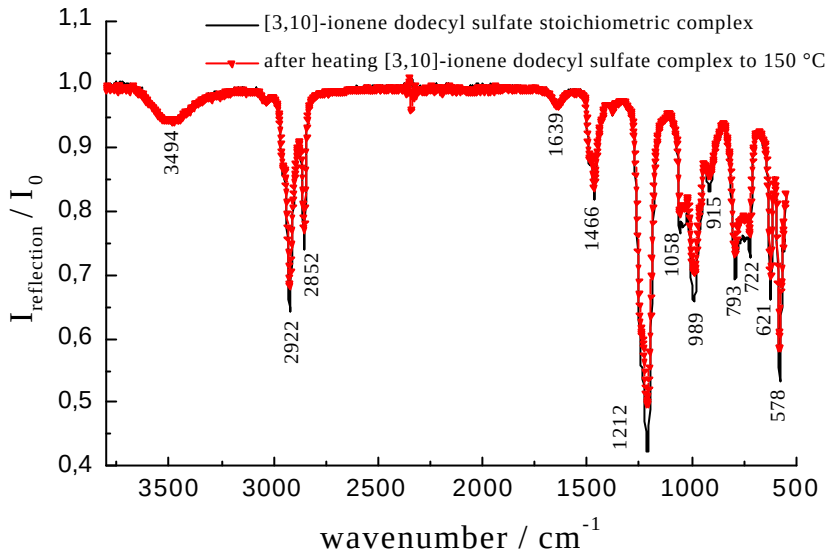

Figure 3.68 ATR-IR spectra of the [3,10]-ionene dodecyl sulfate stoichiometric complex before and after heating

Compared to the previously described systems, it was somewhat strange that there was no clearly visible absorption peak from 20 °C to 150 °C in the DSC diagram (Fig. 3.69). From the ATR-IR spectra of [3,10]-ionene dodecyl sulfate stoichiometric complex we know the complexes contained water, and this is apparently not removed upon heating.

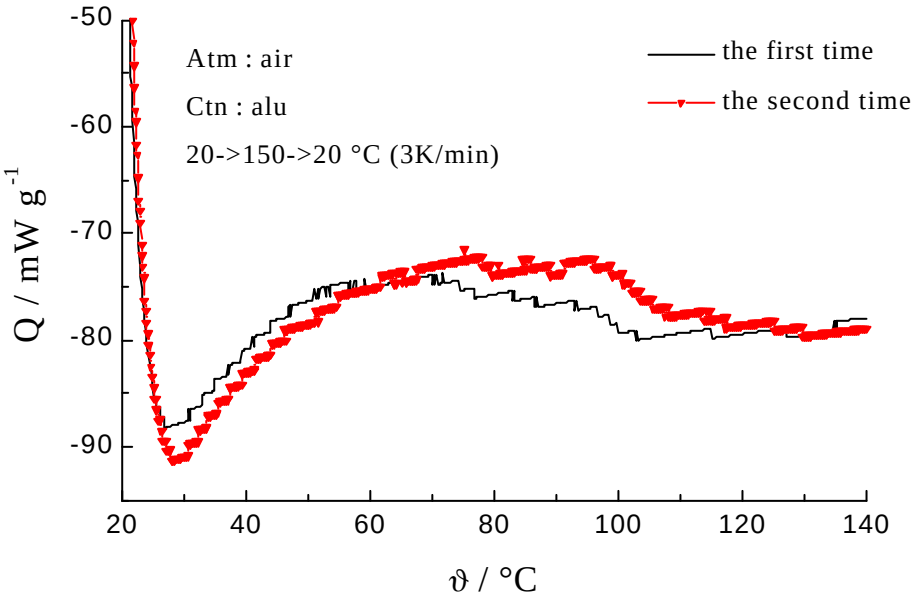

Figure 3.69 DSC of the [3,10]-ionene dodecyl sulfate stoichiometric complex

In the DSC diagram, too, a peak attributable to the evaporation of water from the complexes was not found. The binding between the [3,10]-ionene dodecyl sulfate stoichiometric complex and water therefore might be stronger than in the other complexes.

But a thermogravimetric analysis (TG) confirmed the loss of water. In the TG diagram (Fig. 3.70) the second stage from 38 °C to 95 °C reveals a weight loss of about 1.66 % which was consistent to an absorption peak at 82 °C in the DTA diagram and was caused by water evaporation from the stoichoimetric complex, as revealed by the fragment peaks (Fig. 3.71) at m/z = 18 and m/z =17, which were found at about 91 °C. The quite large temperature interval within which the evaporation proceeds may have prevented the clear-cut appearance of the respective peak in the DSC diagram (Fig. 3.69).

The third stage from 96 °C to 185 °C, in DTA curve this stage had two absorption peaks respectively at 119 °C and 162 °C. In the DSC diagram, however, there was no corresponding peak between 20 °C and 150 °C. But there is a difference between the [3,10]-ionene dodecyl and the [3,10]-ionene decyl sulfate stoichiometric complex: the [3,10]-ionene dodecyl sulfate stoichiometric complex is more stable than the [3,10]-ionene decyl sulfate stoichiometric complex, as even at 230 °C the thermal degradation does not happen.

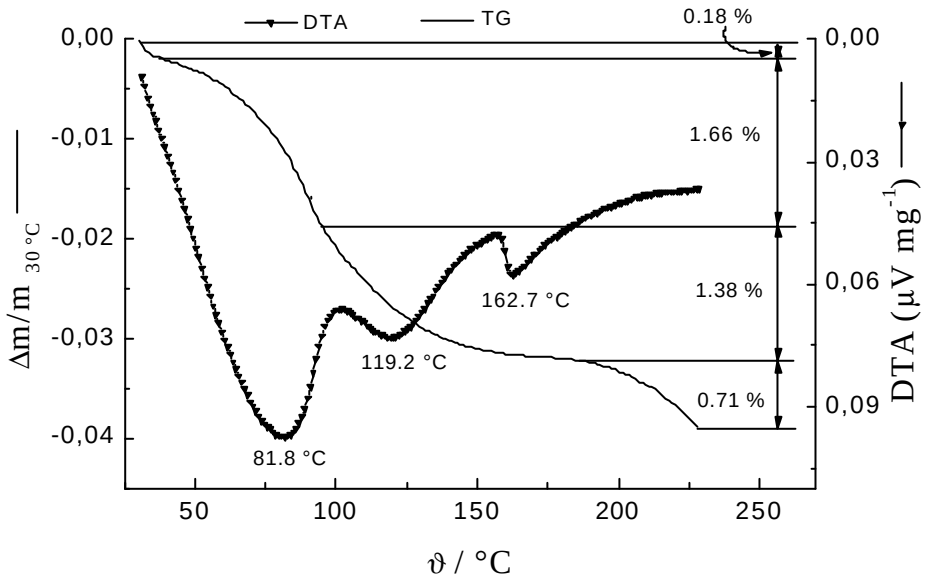

Figure 3.70 Thermogravimetric analysis of [3,10]-ionene dodecyl sulfate stoichiometric complexes; heating rate 5 K/min.

The weight loss according to water was about 1.66 %. From this value we calculate that every ion pair unit of the [3,10]-ionene dodecyl sulfate stoichiometric complex absorbs only about

0.32 water molecules, when the complex was in equilibrium with ambient air. The samples were optically isotropic when prepared at ambient conditions. So the [3,10]-ionene dodecyl sulfate stoichiometric complex was stable below 170 °C, but it can absorb water in air.

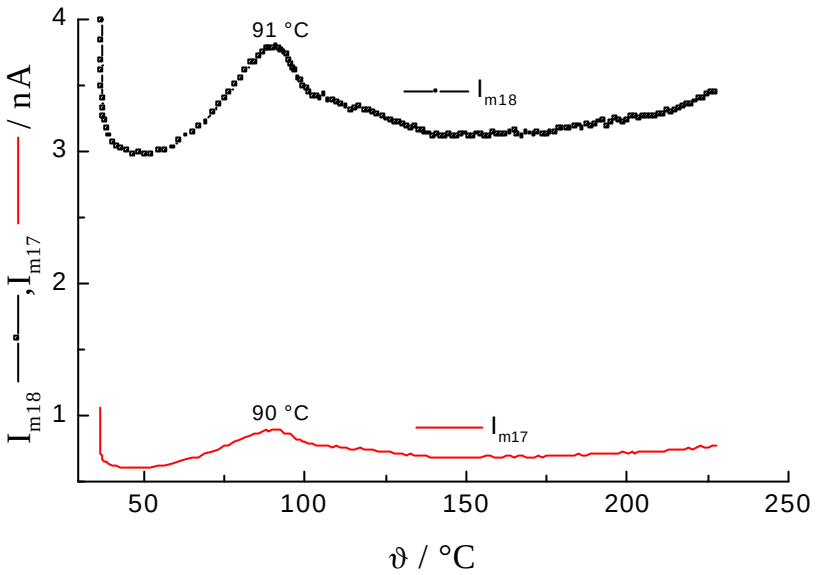

Figure 3.71 Fragments produced in the thermogravimetric analysis of [3,10]-ionene dodecyl sulfate stoichiometric complexes; heating rate 5 K/min

3.5.3.2 Isotropic-mesogenic properties of the [3,10]-ionene dodecyl sulfate stoichiometric complex

The [3,10]-ionene dodecyl sulfate stoichiometric complexes easily absorbed water when they were exposed to increased relative humidity. But the optical properties did not change at relative humidities up to 56 %. At 58 % the film changed from optically isotropic to optically anisotropic. A polarizing microscope confirmed the existence of optical anisotropy. We will show below that a mesogenic phase was formed thereby.

The DSC curve for a sample equilibrated at 53 % relative humidity (Fig. 3.72, curve for a(H_2O) = 0.53) exhibited an emission peak at about 150 °C. If we again assign this peak to the reaction enthalpy of the hydrolysis of the alkyl sulfate, the high temperature means that water is not available for the reaction at lower temperatures, in keeping with a missing endothermic peak for the evaporation of water.

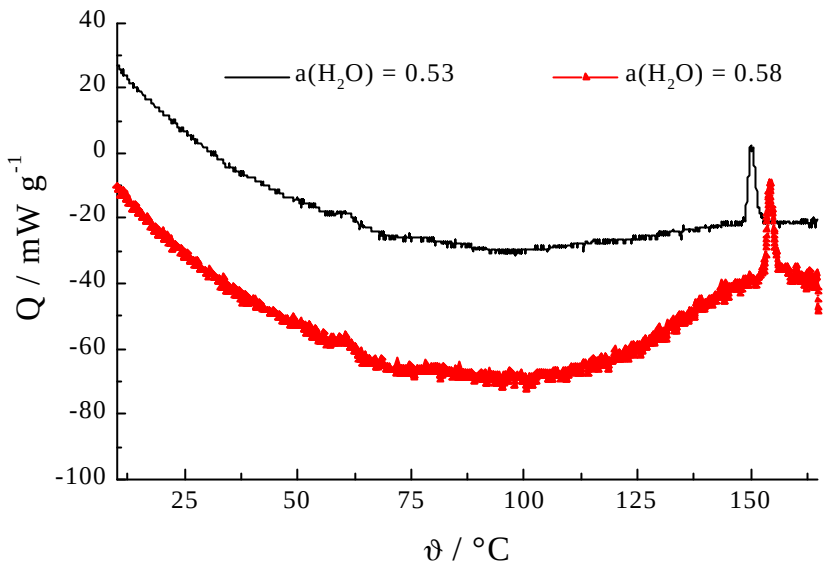

Figure 3.72 DSC-curve of [3,10]-ionene stoichometrically complexed with dodecyl sulfate for two samples equilibrated at constant relative humidities: 53 % and 58 %; heating rate 1 K/min.

In this case the plot of enthalpy (or temperature of the maximum of the emission peak) vs. relative humidity cannot be used to indicate the isotropic-anisotropic phase transition, as only broad maximum were obtained in the transition region (Fig. 3.73).

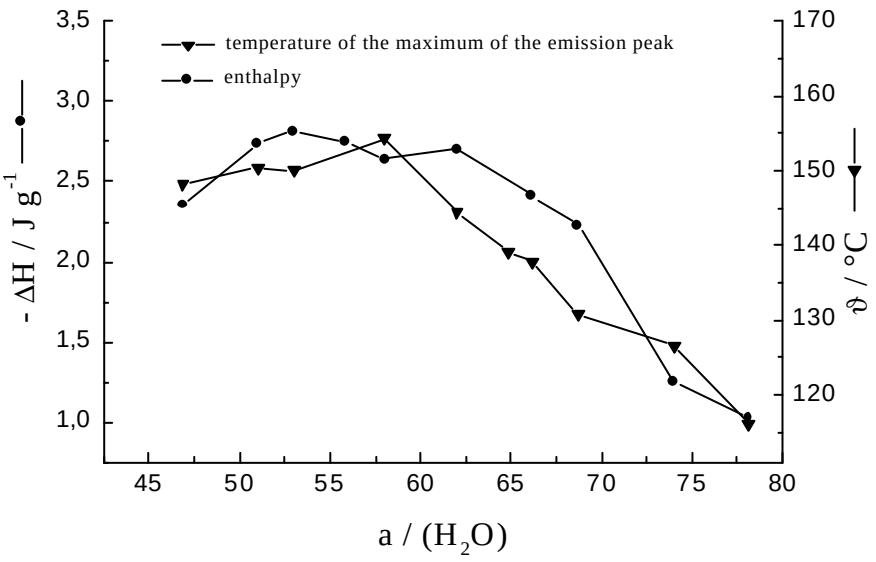

Figure 3.73 Enthalpy and temperature of the maximum of the exothermic peak of [3,10]-ionene dodecyl sulfate stoichiometric complexes measured by DSC; heating rate 1 K/min.

From Figure 3.74 it follows that the take up of water was proportional to the fraction of water in the gas phase. At the transition point changing from optically isotropic to optically anisotropic every ion pair of [3,10]-ionene dodecyl sulfate stoichiometric complex absorbed about 1.5 water molecules.

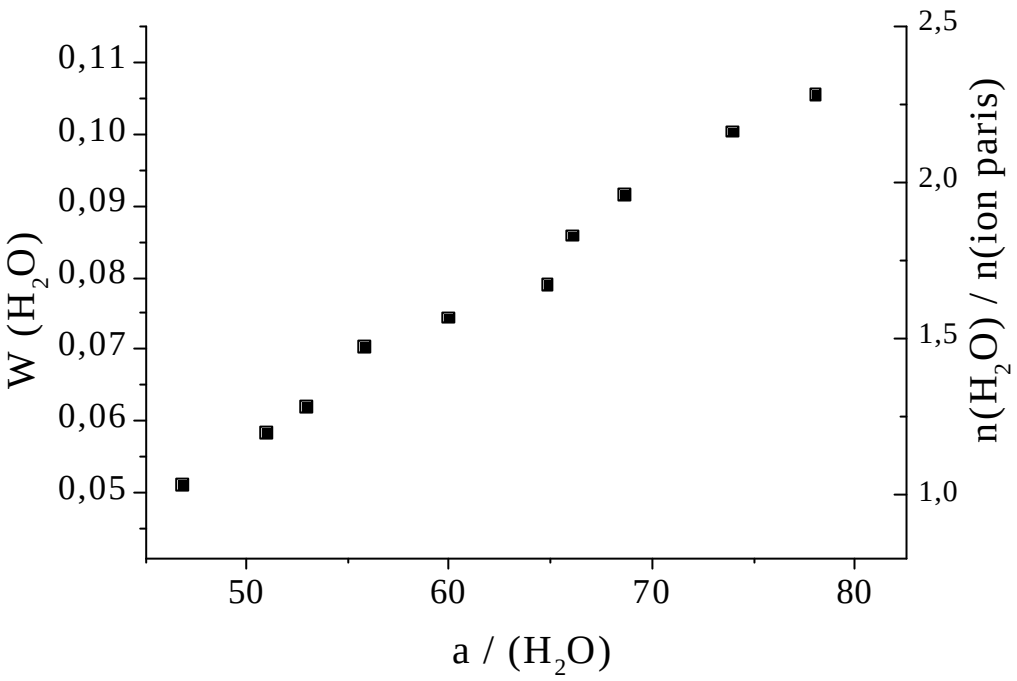

Figure 3.74 Swelling (mass fraction *w* of water) of [3,10]-ionene dodecyl sulfate stoichiometric complexes and number of water molecules per ion pair unit ($n(H_2O)$) as a function of the relative humidity ($a(H_2O)$) applied to the dry sample at room temperature.

Figure 3.75 shows the texture of the anisotropic mesogenic phase of the stoichiometric complex after cooling (at about 131 ± 1 °C) from the isotropic phase as it appeared on the polarizing microscope. As in the other systems the picture shows a fan texture, which typically indicates a hexagonal mesogenic structure.

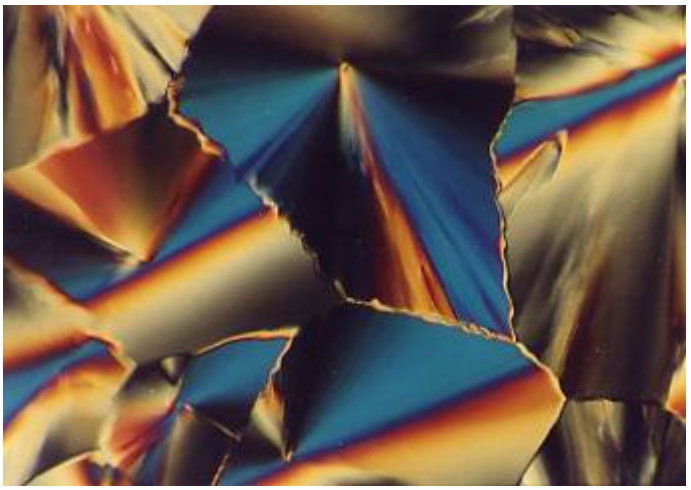

Figure 3.75 Texture of the anisotropic mesogenic phase in [3,10]-ionene dodecyl sulfate stoichiometric complexes obtained from a polarizing microscope. Magnification 100X, sample prepared at a(H_2O) = 0.69.

4 Discussion

4.1 Solution behavior

4.1.1 Viscosities

From inspection of Figures 3.1 and 3.2 it follows that normal polyelectrolyte behaviour was observed for [3,22]-ionene and [3,12]-ionene in methanol: as the concentration of the ionene decreased in salt-free solution, the charges on the backbone become less shielded by the counterions, leading to an increase in intramolecular repulsion. This causes the polymer to expand, resulting in a dramatic rise in reduced viscosity as shown in Figure 3.1, but when a simple salt as NaBr was added to the polyelectrolyte solution, some of the mobile electrolyte diffuses into the polyion coil [85]. The electrostatic screening of the charged segments by the electrolyte resulted in a marked reduction in the repulsive potential between segments. The polyion contracted and caused a corresponding decrease in the viscosity of the solution, so the ionene in simple salt solution behaved like a nonionic solute.

The intrinsic viscosity [η] (or the coefficient A in the Fuoss equation) can be taken as a relative measure of molecular weights. The [η] value for [3,22]-ionene exceeds that for [3,12]-ionene by a factor of 3. The evaluation of light scattering experiments however leads to 8366 g/mol for [3,22]- and 1900 g/mol for [3,12]-ionene (Tab. 3.2), i.e. the molecular weights differ by a factor of more than 4. So there is only a rough agreement between the two methods.

4.1.2 Fluorescence of 1-anilinonaphthalene-8-sulfate (ANS) in methanol environments

It is known [104,105] that the fluorescence maximum of ANS is sensitive to the polarity of the immediate surrounding of the ANS probe molecule. When the probe enters a region of different polarity, the wavelength at which a maximum in emission intensity occurs will shift [106], i.e., the maximum decreases from 515 nm in H_2O to 473 in methanol, to 460 nm in octanol, and eventually to 430 nm in hexane. The results for increasing sodium dodecyl sulfate concentration in methanol suggest that in the absence of ionene there is no marked effect of SDS, which indicates that micelles are not formed in methanol under the conditions investigated. Solutions of the ionenes in methanol provide an environment more polar than methanol. This can be interpreted in terms of ANS anions strongly bound to the cationic units

of the ionenes. This situation is gradually changed while SDS is added, whose dodecyl sulfate anions obviously bind more strongly to the cationic units than the ANS ions, which are consequently replaced and find themselves in a methanol environment. Therefore the maximum emission wavelength decreases until the stoichiometric point is reached and levels off thereafter at approximately the methanol value 473 nm (Fig. 3.5 to 3.7). These experiments clearly monitor and prove the ionene-surfactant complex formation.

For sodium decyl sulfate differing features were observed. The fact that the stoichiometric point is not indicated suggests that decyl sulfate binds less strongly to the ionenes, so that the complexes in methanol solution are not completely formed. On the other hand, the decrease of the fluorescence maximum below the methanol value (473 nm) indicates that ANS induces the formation of micelles of sodium dodecyl sulfate, which shield ANS from methanol (Fig. 3.8 and 3.9).

4.2 Ionene

Four ionenes were synthesized, of which [3,22]-ionene had a comparatively high molecular weight (about 8500 g/mol), while the other three ionenes had low molecular weights only about 2000 g/mol.

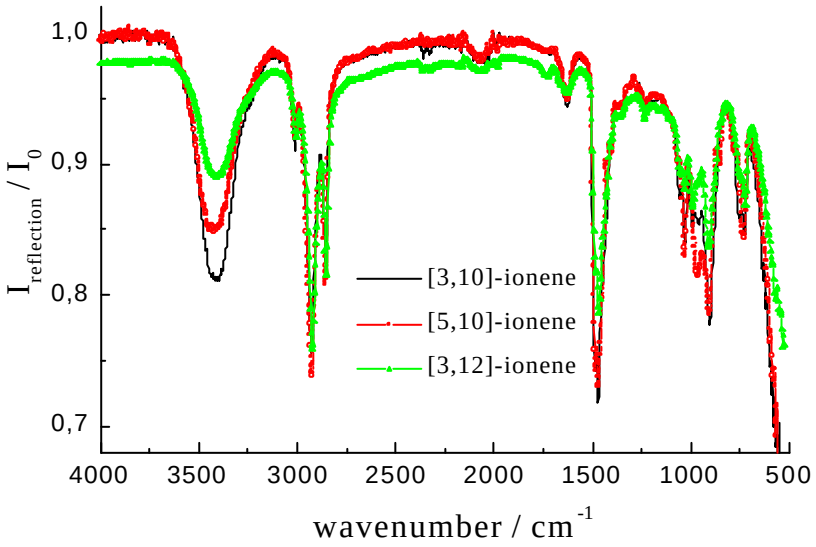

Figure 4.1 ATR-IR spectra of ionenes

All ionenes have similar functional groups, so they also have the widely agreeing IR-spectra, which are compared in Fig. 4.1. Only the O-H stretching intensity exhibits some difference.

But this band was caused by low-molecule-weight impurities (water or methanol), as ionene does not contain O-H groups.

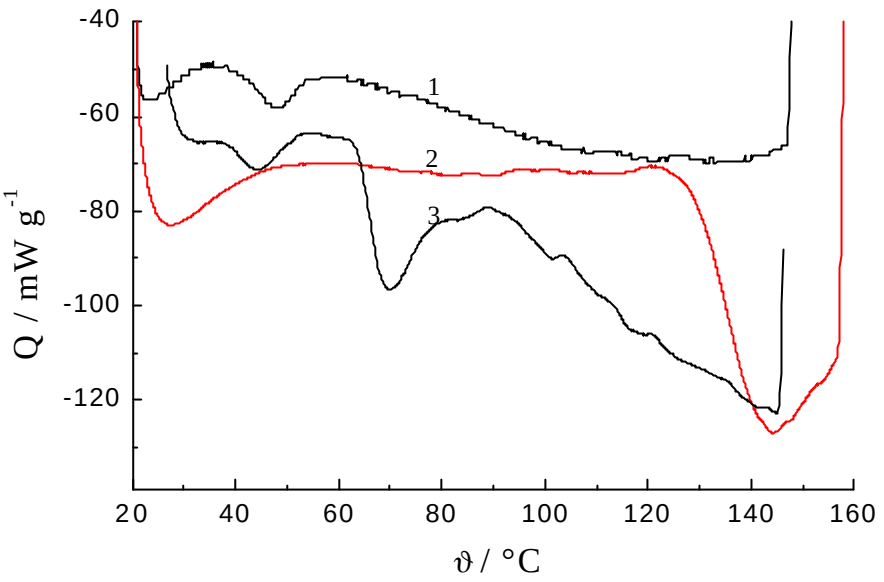

Figure 4.2 DSC of ionenes 1: [3,10]-ionene (3 K/min); 2: [5,10]-ionene (3 K/min); 3: [3,12]-ionene (5 K/min)

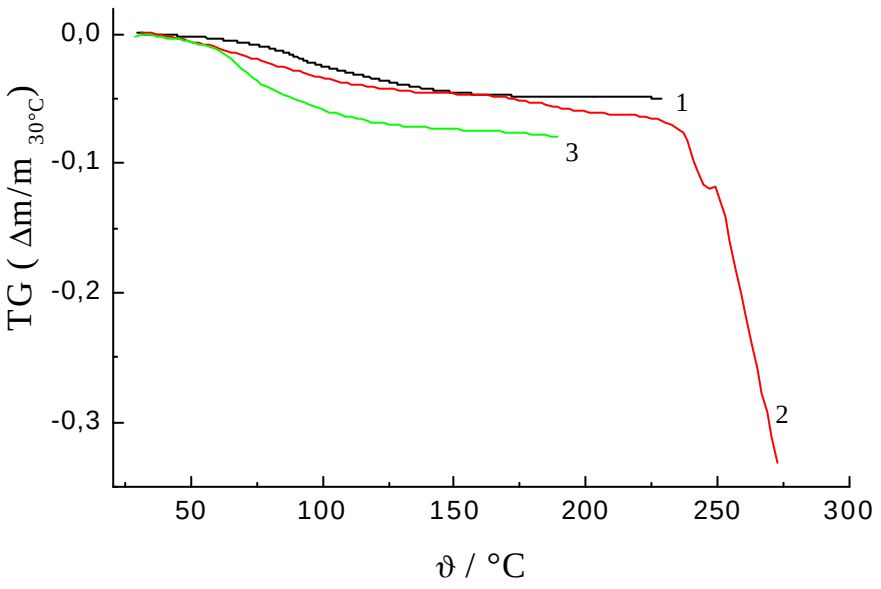

Figure 4.3 Thermogravmetric analysis of ionenes; 1: [3,10]-ionene; 2: [5,10]-ionene; 3: [3,12]-ionene; heating rate 5 K/min.

ATR-IR spectra, DSC and TG diagrams indicated that [3,12]- and [3,10]-ionenes always contained some methanol, which was used as solvent during the synthesis, and which was difficult to remove completely at room temperature over phosphorous pentoxide in vacuum. [5,10]-ionene, in contrast, easily absorbed water (Fig. 4.2, 3.33). Up to 170 °C [3,12], [3,10] and [5,10]-ionenes were stable in nitrogen atmosphere, the weight losses were due to the evaporation of methanol or water and not to the decomposition of ionene. For [5,10]-ionene the thermal degradation happened at higher temperature, above 223 °C it quickly decomposed (Fig. 4.3).

4.3 Ionene alkyl sulfate stoichiometric complexes

Ionene alkyl sulfate stoichiometric complexes have identical functional groups, which are in slightly differing molecular surroundings. So they also have very similar ATR-IR spectra, which are displayed in Fig. 4.4. All stoichiometric complexes contained water, but the content varied. At ambient conditions, every ion pair unit of the [3,12]-ionene dodecyl sulfate stoichiometric complex absorbs 0.9 water molecules, which reduces to 0,03 water molecules in the case of the [5,10]-ionene decyl sulfate complex.

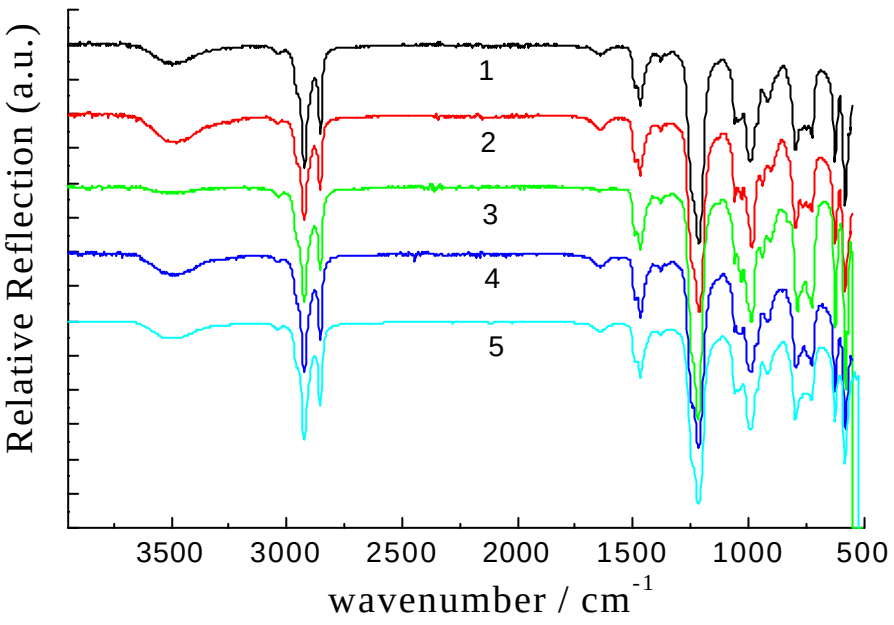

Figure 4.4 ATR-IR spectra of ionene alkyl sulfate stoichiomtric complexes. 1: [3,10]-ionene dedyl sulfate; 2: [3,10]-ionene dodecyl sulfate; 3: [5,10]-ionene dedyl sulfate; 4: [5,10]-ionene dodecyl sulfate; 5: [3,12]-ionene dodecyl sulfate

The capability of the complexes to absorb water was indicated by ATR-IR spectra as well as by DSC and TG diagrams. DSC curves of [3,12]-ionene dodecyl sulfate, [5,10]-ionene dodecyl sulfate and [3,10]-ionene decyl sulfate complexes show an unequivocal absorption peak at about 100 °C (Fig 4.5), which was caused by water vaporizing from the stoichiometric complex. In DSC diagrams of the [3,10]-ionene dodecyl sulfate stoichiometric complex there was no absorption peak, indicating a high binding energy between ion pairs and water, which precludes the evaporation of water below 150 °C.

For the [5,10]-ionene decyl sulfate stoichiometric complex the typical water evaporation peak is also missing. Instead, at low temperature (60 °C) there was an endothermic peak, and at high temperature (130 °C) an exothermic peak, and the TG-MS (Fig. 3.49, 4.5) clearly proved that below 160 °C no water escaped from complex. But in the DTA curve there was a weak peak at about 100 °C, the weight loss was only about 0.13 %, so this amount is negligible. So there was also a strong force between the [5,10]-ionene decyl sulfate stoichiometric complex and water, only at high temperature (> 150 °C) the strong force can be weakened, and then water easily escaped.

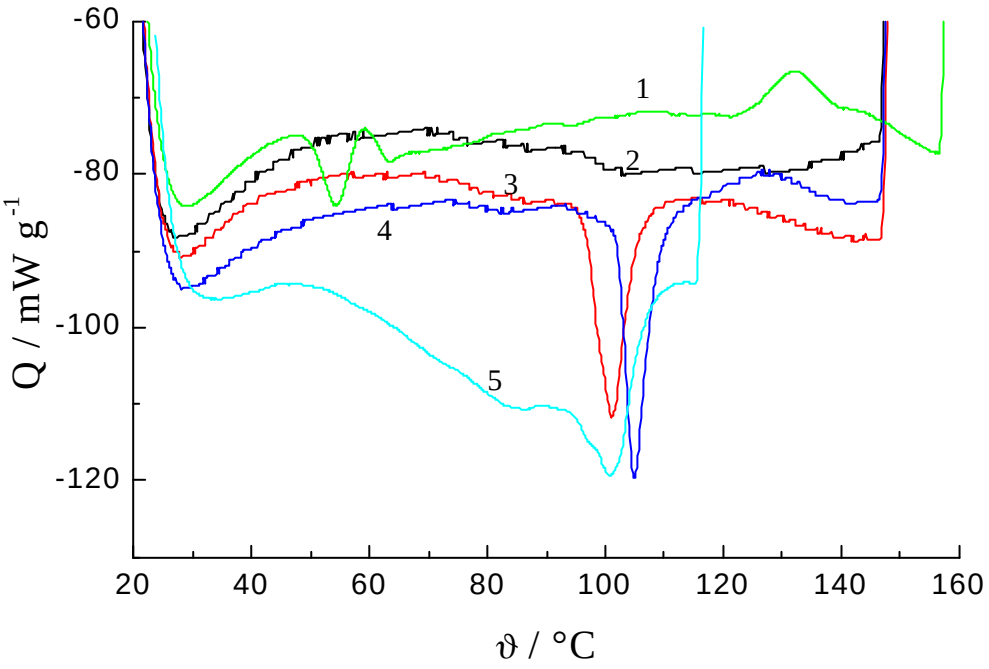

Figure 4.5 DSC of ionene alkyl sulfate stoichiometric complexes. 1: [5,10]-ionene decyl sulfate (3 K/min); 2: [3,10]-ionene dodecyl sulfate (3 K/min); 3: [3,10]-ionene decyl sulfate (3 K/min) 4: [5,10]-ionene dodecyl sulfate (3 K/min) 5: [3,12]-ionene dodecyl sulfate (5 K/min)

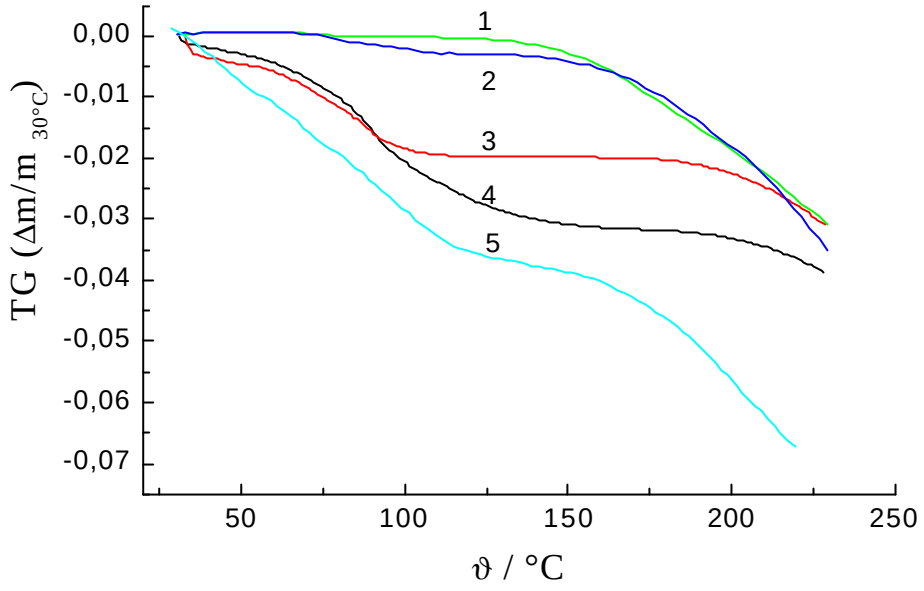

Figure 4.6 Thermogravimetric analysis of ionene alkyl sulfate stoichiometric complexes. 1: [5,10]-ionene decyl sulfate; 2: [5,10]-ionene dodecyl sulfate; 3: [3,10]-ionene dedyl sulfate 4: [3,10]-ionene dodecyl sulfate 5: [3,12]-ionene dodecyl sulfate; heating rate 5 K/min.

Ionene alkyl sulfate stoichiometric complexes had the same stability as ionenes at ambient humidity. [3,12], [5,10], and [3,10]-ionenes were stable below 170 °C, and [3,12], [5,10] and [3,10]-ionene alkyl sulfate stoichiometric complexes were also stable below 170 °C; [5,10]-ionene thermally decomposed above 170 °C, and [5,10]-ionene alkyl sulfate stoichiometric complexes also become unstable at high temperature; the decomposition of the ionene moiety in the complexes was indicated by the mass fragments CH_3 (m/z =15) and CH_3N^+(m/z =29). The ionenes in the [3,10]-ionene decyl sulfate stoichiometric complex decomposed into CH_3N^+(m/z =29) ion above 200 °C.

From curves 1 and 2 in Fig. 4.6 similar processes can be concluded: the [5,10]-ionene alkyl sulfate stoichiometric complexes contained less water than other ionene alkyl sulfate stoichiometric complexes, and therefore below 170 °C the weight loss was also negligible. The [3,12]-ionene dodecyl sulfate stoichiometric complex contained more water than the other complexes, so below 170 °C the weight loss was the largest.

The apparent discrepancy between the stability of the stoichiometric complex from [3,12]-ionene and dodecyl sulfate against temperature at ambient humidity (Fig. 3.17) and the instability upon periodically heating the hydrated sample to >80 °C has to be rationalized. A likely cause is the instability of dodecyl sulfate in the presence of water at high temperature,

which leads to hydrolysis yielding dodecyl alcohol and sulfuric acid. Initially small amounts of dodecyl alcohol may stabilize the anisotropic phase [107]. Further progress of hydrolysis increases the lack of dodecyl sulfate resulting in a complete breakdown of the structure of the complex and melting. That dodecyl alcohol is formed indeed, was proved by ^{1}H-NMR (Fig. 3.28) and ATR-IR spectra (Fig. 3.29), cf. [108]. Further the emission peaks in the DSC diagrams at elevated humidity (attributed to the hydrolysis reaction) are in keeping.

The hysteresis of transition temperatures observed in heating and cooling cycles (Fig. 3.26) indicates either a hindered transition or a transition of second order. When the long equilibration time revealed by Fig. 3.21 is considered, the former explanation is more likely.

Lyotropic phase transitions in water swollen solid polyelectrolyte-surfactant complexes triggered solely by a temperature change are rarely described. It is a unique feature in the use of ionene as a backbone that the electrostatic forces and hydrophobic effects (governing the lyotropic properties) can be balanced without the addition of inorganic salt by varying the number of CH_2-groups between the cationic sites and in the alkyl sulfate. As a consequence no binding strength of ion pairs has to be sacrificed to allow a phase transition at suitable temperatures.

Lyotropic phase transitions induced by an increase of humidity, i.e. the solvent is offered from the gas phase, is a new feature discovered in our group [94].

Ionene alkyl sulfate stoichiometric complexes take up water at ambient humidity. The complexes nevertheless still display the isotropic phase; this would change to anisotrpic when the complexes were exposed to sufficiently high humidity. The results have shown, that this phenomenon is connected with the position and the enthalpy of an exothermic peak arising in the DSC curves when these are measured at elevated relative humidity. Fig. 4.7 and Fig. 4.8 comprise the DSC diagrams before and after the humidity induced transition form the isotropic to the anisotropic phase.

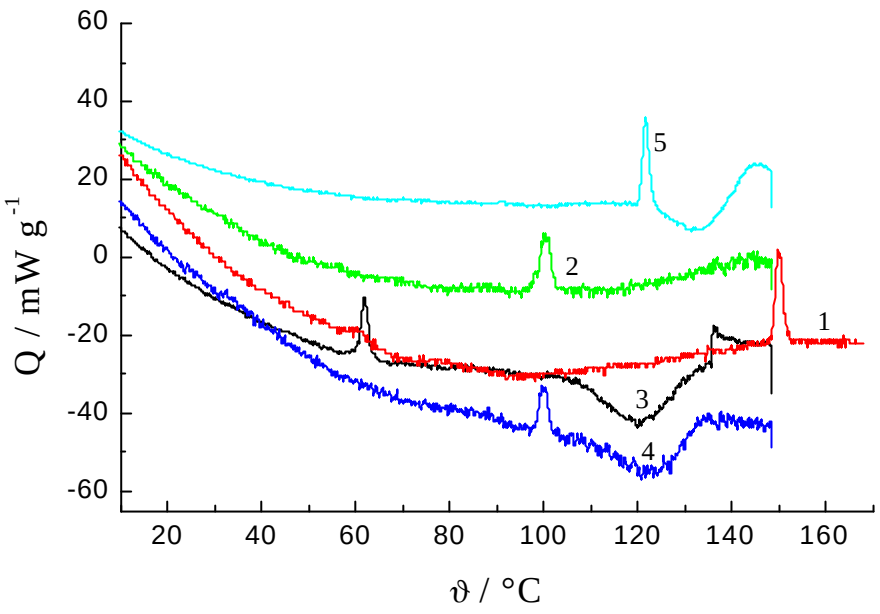

Figure 4.7 DSC-curve of ionene stoichometrically complexed with alkyl sulfate for samples equilibrated at constant relative humidities: 1) 53 % [3,10]-ionene dodecyl sulfate; 2) 58 % [3,10]-ionene decyl sulfate; 3) 58 % [5,10]-ionene decyl sulfate; 4) 67.4 % [5,10]-ionene dodecyl sulfate; 5) 88.1 % [3,12]-ionene dodecyl sulfate; heating rate 1 K/min. All the stoichiometric complexes showed optical isotropy.

In Fig. 4.7 and 4.8 the DSC diagrams of samples at constant relative humidities shortly below (Fig. 4.7) and shortly above (Fig. 4.8) the humidity induced phase transition from isotropic to anisotropic are comprised. Inspection of the figures reveal that for identical ionenes complexed with varying alkyl sulfates similar endothermic (absorption) peaks were found: [3,12]-ionene alkyl sulfate stoichiometric complexes show similar endothermic peaks at 132-135 °C before and after the transition; [5,10]-ionene alkyl sulfate stoichiometric complexes behave analogously in exhibiting endothermic peaks at 120-122 °C. But [3,10]-ionene alkyl sulfate stoichiometric complexes have not these endothermic peaks between 0 °C and 170 °C, which indicates that below 170 °C no water was vaporized from these complexes. For all stoichiometric complexes below and above the humidity induced transition there are exothermic peaks, which are missing in the DSC curves of samples at ambient humidity. These peaks were assigned to the chemical reaction of alkyl sulfate with water. The alkyl sulfate was hydrolysed to form alkyl alcohol. As the exothermic peaks appear at distinct

temperatures we can conclude that the ionenes have a specific influence on the stability of alkyl sulfates in the stoichiometric complexes.

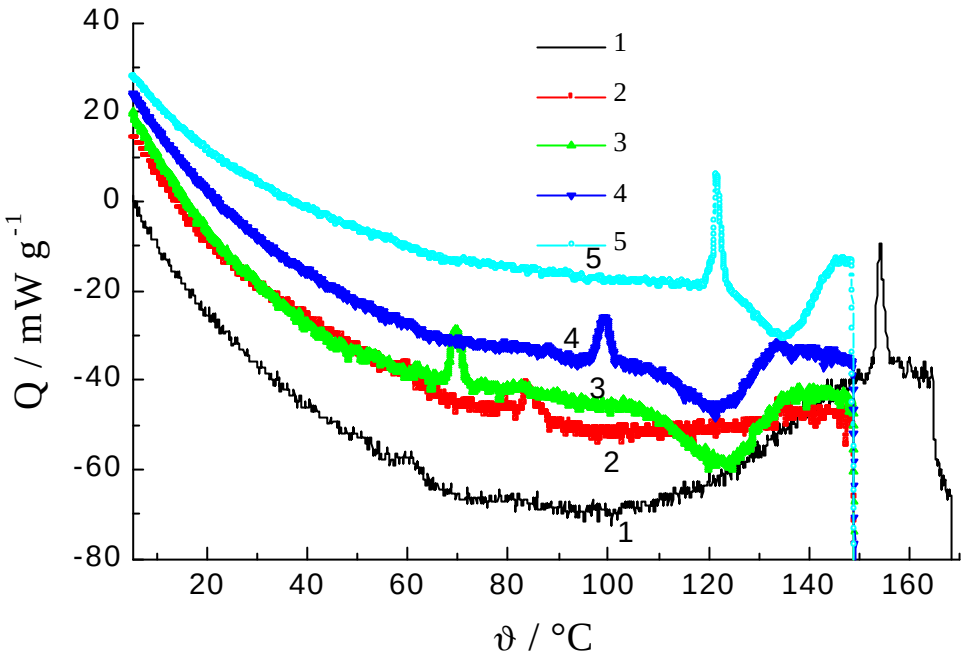

Figure 4.8 DSC-curve of ionene stoichometrically complexed with alkyl sulfate for two samples equilibrated at constant relative humidities: 1) 58 % [3,10]-ionene dodecyl sulfate; 2) 64.8 % [3,10]-ionene decyl sulfate; 3) 62 % [5,10]-ionene decyl sulfate; 4) 69 % [5,10]-ionene dodecyl sulfate; 5) 91.4 % [3,12]-ionene dodecyl sulfate; heating rate 1 K/min. All the complexes showed optical anisotropy at room temperature.

As the formation of alkyl alcohol from alkyl sulfate has been proven for the [3,12]-ionene dodecyl sulfate complex, we can with high probability attribute the exothermic peak to the reaction enthalpy of the hydrolysis of alkyl sulfates. This reaction requires comparatively free water (and a sufficient temperature). Obviously, the availability of water in the complex varies during the transformation isotropic-anisotropic. Therefore the emission peaks shift accordingly in most cases and can be used to indicate the humidity induced transition point (Fig. 3.41 and related). At the humidity induced transition point the respective values changed very quickly (Fig. 3.22, 3.41, 3.51, 3.64, 3.73), but the curve forms were different.

	n(C-atoms/unit)	Transition humidity $a(H_2O)$	Transition temperature* T/°C	$n(H_2O)$ / n(ion pairs)
312C12	27	0.914	102	4
510C10	25	0.69	62	2.38
510C12	27	0.62	97	2
310C10	23	0.648	80	2
310C12	25	0.58	154	1.5

* Sample prepared at the relative humidity given in the $a(H_2O)$ column

Table 4.1 The properties at the transition point for ionene alkyl sulfate stoichiometric complex. 312C12: [3,12]-ionene dodecyl sulfate stoichiometric complex; 510C10: [5,10]-ionene decyl sulfate stoichiometric complex; 510C12: [5,10]-ionene dodecyl sulfate stoichiometric complex; 310C10: [3,10]-ionene decyl sulfate stoichiometric complex; 310C12: [3,10]-ionene dodecyl sulfate stoichiometric complex; $n(H_2O)$/n(ion pairs): number of water molecules per ion pair unit.

Inspection of the table reveals that transition humidities ($a(H_2O)$) do not correlate with the total number of C-atoms per ionic unit (chain segments + surfactant) nor with the lengths of the ionene chain segments of surfactant chains. On the other hand the number of water molecules needed for the humidity induced phase transition fairly correlates with the relative humiditiy at the phase transition point. This correlation meets the intuition. The transition temperature column clearly reveals that dodecyl sulfate complexes need higher temperatures for the thermal transition to the isotropic phase as compared to the decyl sulfate complexes. This can be rationalized in terms of a more stable hexagonal order in the surfactants with the longer alkyl chain.

All ionene alkyl sulfate stoichiometric complexes (except [3,22]-ionene complexes) showed phase transitions hexagonal-isotropic upon heating, provided that there was sufficient humidity present to allow the formation of the hexagonal phase [110]. Phase transitions in [3,12]-ionene dodecyl sulfate stoichiometric complexes can be induced in a thermotropic way (Fig. 3.26) or in a lyotropic way (Fig. 3.21), if we accept the take up of water through the gas phase as a lyotropic process. If the stability problem (hydrolysis of alkyl sulfates) can be overcome, the systems may be readily applied to develop hygrometers. In this respect, surfactants which are stable against water may be more promising complex partners.

Complexes of [3,22]-ionene were not suitable for the purpose of the thesis as the complexes with alkyl sulfates did not form transparent films. The reason might be a too large distance between the ionic units leading to a behavior much like non-polyelectrolytes, in which the long CH_2-segments form crystalline domains. A less likely reason is that the comparatively high molecular weight achieved in the preparation of this ionene precludes the formation of transparent films (8000 g/mol as compared to 2000 g/mol).

5 Conclusion

1. The ionenes investigated behaved as polyelectrolytes in methanol in the absence of added simple electrolytes and like a nonionic polymer in methanol in the presence of added electrolytes, because some of the mobile electrolyte diffused into ionene, and the electrostatic screening of the charged segments by the electrolyte resulted in a marked reduction in the repulsive potential between segments. Differences in the molecular weights of the ionenes were reflected by the respective intrinsic viscosities [η].
2. The apparent hydrodynamic radius; R_H^{app} of [3,12] and [5,10]-ionene (in the absence of salt) did not change significantly within the concentration range 10-40 g l^{-1}; but for their alkyl sulfate stoichiometric complexes, apparent hydrodynamic radius; R_H^{app} changed significantly within the concentration range 10-40 g l^{-1}; [3,12]-ionene dodecyl sulfate stoichiometric complexes (in the absence of salt) in methanol had a lower apparent hydrodynamic radius (R_H^{app}) than [3,12]-ionene dodecyl sulfate stoichiometric complexes in the presence of simple salt.
3. Fluorescence experiments with the spectroscopic probe 1-anilinonaphthalene-8-sulfate (ANS) in methanol environments confirms the ionene-surfactant complex formation between ionene and SDS, but for sodium decyl sulfate the complexes in methanol solution are not completely formed.
4. [3,12], [3,10]-ionenes always contained some methanol, while [5,10]-ionene easily absorbed water. From 20 °C to 170 °C [3,12]-, [3,10]-, and [5,10]-ionenes were stable in nitrogen atmosphere, but for [5,10]-ionene above 170 °C thermal degradation happened. Ionene in ionene alkyl sulfate stoichiometric complexes probably decomposed into CH_3 (m/z =15) ion and CH_3N(m/z =29) ion.
5. All ionene alkyl sulfate stoichiometric complexes easily absorbed water when they were exposed to air. Below 170 °C the weight loss in TG experiments was mainly caused by the evaporation of water from ionene alkyl sulfate stoichiometric complexes.
6. The sort of ionene used influences the stability of ionene alkyl sulfate stoichiometric complexes in a specific way.
7. The stoichiometric complexes of ionene alkyl sulfate display mesogenicity, i.e. lyotropic and thermotropic phase transitions from the optically anisotropic to the optically isotropic phase (and vice versa) can be induced. They were all sensitive to

both humidity and temperature. In principle, the effects can be applied to measure humidity.

8. [3,12]-, [5,10]-, and [3,10]-ionene alkyl sulfate stoichiometric complexes exhibit hexagonal structures in the optical anisotropic phase.

6 Literature

1. Jönsson, Bo., et al. ; *Surfactants and Polymers in Aqueous Solution* (1998); John Wiley & Sons.
2. *Interactions of Surfactants with Polymers and Proteins*; CRC Press. Boca Raton, FL 1993.
3. T. Wolff, B. Klaussner; *Adv. Colloid Interface Sci.*; 59 (1995) 31-94
4. D. F. Evans; H. Wennerström; The Colloidal Domain where Physics, Chemistry, Biology, and Technology Meet; VCH Publishers Inc.; 1994; 14-15.
5. George E. Kimball, Melvin Cutler, Harold Samelson; *J. Phys. Chem*.; 1952; 56(1); 57-60.
6. G. Petzold, H.-M. Buchhammer and K. Lunkwitz; *Colloids Surf. A Physicochem. Eng. Aspects;* 119 (1996), p. 87
7. Wågberg and R. Hägglund; *Langmuir;* 17 (2001); p. 1096
8. G. Petzold, A. Nebel, H.-M. Buchhammer and K. Lunkwitz; *Colloid Polym. Sci.*; 276 (1998), p. 125.
9. M. Müller, K. Lunkwitz; *Macromol. Rapid Commun*; 22 6 (2001), p. 390.
10. Muller, M.; Kessler, B.; Lunkwitz, K.; *J. Phys. Chem. B.*; 2003; 107(32); 8189-8197.
11. B. Magny, I. Iliopoulos, R. Zana, R. Audebert; *Langmuir*; 1994; 10(9); 3180-3187.
12. Rjumtsev, E. I.; MacKnight, W. J.; *Macromolecules*; 1996; 29(4); 1320-1325.
13. Fundin, J.; Hansson, P.; Lidegran, I.; *Macromolecules*;1997; 30(4); 1118-1126.
14. Ilekti, P.; Martin, T.; Piculell, L.; *J. Phys. Chem. B.* ;1999; 103(45); 9831-9840
15. Liu, J.; Takisawa, N.; Sakamoto, K.; *J. Phys. Chem. B.* ;1997; 101(38); 7520-7523
16. Carnali, J. O.; *Langmuir;* 1993, *9*, 2933.
17. Kogej, K.; Evmenenko, G.; Reynaers, H.; *Langmuir*;2001; 17(11); 3175-3184
18. Zhou, S.; Burger, C.; Yeh, F.; Chu, B.; *Macromolecules*;1998; 31(23); 8157-8163
19. Khandurina, Yu. V.; Dembo, A. T.; Rogacheva, V. B.; Zezin, A. B.; Kabanov, V. A. *Polym*. *Sci*. 1994, *36*, 189.
20. Liao, X.; Higgins, D. A.; *Langmuir*; 2001; 17(20); 6051-6055.
21. Faul, C.; Antonietti, M.; Hentze, H.-P.; *Langmuir;*2001; *17*(6); 2031-2035.
22. Ganeva, D.; Faul, C. F. J.; Sanderson, R. D.; *Macromolecules;*2003; *36*(8); 2862-2866.
23. Ganeva, D.; Antonietti, M.; Sanderson, R.; *Langmuir;*2003; *19*(16); 6561-6565.
24. C. K. Ober and G. wegner; *Advanced Materials;* 9 (1997) 1; 17-31.

25. Thunemann, A. F.; Nuyken, O.; Voit, B.; *Macromolecules;*1999; *32*(22); 7414-7421.
26. Antonietti, M.; Neese, M. *Langmuir;* 1996, *12*, 4436.
27. MacKnight, W. J.; Ponomarenko, E. A.; Tirrell, D. A.; *Acc. Chem. Res.*; 1998; 31(12); 781-788.
28. Antonietti, M.; Conrad, J.; Thunemann, A. *Macromolecules;* 1994, *27*, 6007.
29. Antonietti, M.; Kaul, A.; Thunemann, A. *Langmuir;* 1995, *11*, 2633.
30. Antonietti, M.; Maskos, M. *Macromolecules* 1996, 29, 4199.
31. Okuzaki, H.; Osada, Y. *Macromolecules* 1995, 28, 380.
32. Thunemann, A. F.; Ruppelt, D.; *Langmuir;*2000; *16*(7); 3221-3226.
33. Zhou, S.; Yeh, F.; Burger, C.; Chu, B.; *J. Phys. Chem. B.;*1999; *103*(12); 2107-2112.
34. Zhou, S.; Hu, H.; Burger, C.; Chu, B.; *Macromolecules;*2001; *34*(6); 1772-1778.
35. Bronich, T. K.; Popov, A. M.; Kabanov, A. V.; *Langmuir;* 2000; *16*(2); 481-489.
36. Ponomarenko, E. A.; MacKnight, W. J.; *Langmuir;* 1996; *12*(9); 2169-2172.
37. Tirrell, D. A.; MacKnight, W. J.; *macromolecules;* 1996; *29*(27); 8751-8758.
38. Bakeev, K. N.; Yang, M. S.; MacKnight, W. J.; Zezin, A. B.; Kabanov, V. A. *Macromolecules* 1994, *27*, 300.
39. Thunemann, A. F.; Ruppelt, D.; *Langmuir;* 2001; *17*(16); 5098-5102.
40. Dedinaite, A.; Claesson, P. M.; Bergstrom, M.; *Langmuir;* 2000; *16*(12); 5257-5266.
41. Behnke, M.; Tieke, B.; *Langmuir;* 2002; *18*(10); 3815-3821.
42. Thunemann, A. F.; Schnoller, U.; Nuyken, O.; Voit, B.; *Macromolecules;*1999; *32*(22); 7414-7421.
43. Cojocariu, G.; Natansohn, A.; *Macromolecules;*2003; *36*(7); 2404-2411.
44. Thunemann, A. F.; Lochhaas, K. H.; *Langmuir*;1999; 15(14); 4867-4874
45. Thunemann, A. F.; Ruppelt, D.; Blaul, J.; *Macromolecules;* 2000; *33*(6); 2124-2128.
46. Ponomarenko, E. A.; MacKnight, W. J.; *Macromolecules;* 1998; *31*(5); 1584-1589.
47. Antonietti, M.; Forster, S.; Zisenis, M.; Conrad, J. *Macromolecules* **1995**, *28*, 2270.
48. Ponomarenko, E. A.; MacKnight, W. J.; *Macromolecules;*1996; *29*(12); 4340-4345.
49. Zhou, S. Q.; *Adv. Mater.* 2000, *12*, 545-556
50. Thunemann, A. F.; Wendler, U.; Schnablegger, H.; *Langmuir;*2002; *18*(11); 4500-4504.
51. Wang, J.; Bard, A. J. *Anal. Chem.* 2001, *73*, 2207.
52. Liao, X.; Higgins, D. A.; *Langmuir;* 2002; *18*(16); 6259-6265.
53. Lysenko, E. A.; Kabanov, A. V.; *Macromolecules;* 1998; *31*(14); 4511-4515.
54. Lysenko, E. A.;Kabanov, A. V.; *Macromolecules*; 1998; *31*(14); 4516-4519.

55. Dreja, M.; Lennartz, W.; *Macromolecules;* 1999; *32*(10); 3528-3530.
56. Okahata, Y.; En-na, G. J. *Phys. Chem.* 1988, *92*, 4546.
57. Dautzenberg, H.; Jaeger, W.; Seidel, Ch.; Stscherbina, D.; *Polyelectrolytes-Formation, Characterization and Application*; Hanser Publishers: Munich, Germany, 1994.
58. Dominguez, V. Enkelmann, W. H. Meyer, G. Wegner; *Polymer*; 30, 2030 (1989).
59. Arh, K.; Pohar, C.; Vlachy, V.; *J. Phys. Chem. B.* ; 2002; 106(38); 9967-9973.
60. Valdir Soldi, Frank H. Quina; *J . Am. Chem. Soc.* 1988, 110, 5137-5143.
61. Zhuomei Li, Yuanzhen Zhong; *Macromolecules*; 1992; 25(1); 450-453.
62. D. Casson, A. Rembaum; *Macromolecules*; 1972; 5(1); 75-81.
63. Edward G. Knapick, Paul Ander; *Macromolecules*; 1985; 18(5); 1015-1021.
64. H. Karakane, M. Tsyumoto, in Proc. Int. Conf. Pervaporation Processes Chem. Ind., 3. Ed., by R.A. Bakish Mater. Corp., Englewood, NJ, 1988, p. 194.
65. Suzuki, Y.; Quina, F. H.; Hinze, W. L.; *Anal. Chem*. ; 2001; 73(8); 1754-1765.
66. Niyazi Bicak, Umit Tunca; *Polymer Bulletin* 43, 477-483 (2000)
67. Chen, L.; Yu, S.; Kagami, Y.; Osada, Y.; *Macromolecules*; 1998; 31(3); 787-794.
68. X, Zheng and W, Cao; *European Polymer Journal*, 2001, 37(11), 2259-2262
69. Jens Frömmel and Thomas Wolff; *J. of colloid and interface science* 201,86-92 (1998)
70. T. Wolff, B. Klaußer, G. von Bünau; *Progr Colloid Polym Sci*; 83(1990), 176-180
71. R. H. Stokes, R. A. Robinson; *Ind. Eng. Chem*.; 1949; 41(9); 2013-2013.
72. Stepanek, M.; Prochazka, K.; Tuzar, Z.; Brown, W.; *Langmuir*; 2001; 17(14); 4240-4244.
73. S. Natelson and S. Gottfried, *Org. Syntheses, Coll*. Vol. 3 381(1955)
74. H. E. Baumgarten; *Org. Synth.;* Collective Vol 5, 1973, p 533 John Wiley & Sons, Inc.
75. H. Hünig and E. Lücke, *Ber.* 92, 652 (1959)
76. Willie L. Hinze, Hong Wang; *Anal. Chem*. 1994, 66, 3449-3457
77. Valdir Soldi, Frank H. Quina; *J. Am. Chem. Soc*.; 1988; 110(15); 5137-5143.
78. Rembaum, H. Noguchi; *Macromolecules*; 1972; 5(3); 261-269.
79. Kakugo, A.; Shikinaka, K.; Osada, Y.; *Bioconjugate Chem*.; 2003; 14(6); 1185-1190.
80. Pirogov AV, Buchberger W.; *J. Chromatogr A*; 916 (1-2): 51-59 MAY 4 2001
81. Daniel, C., Harris; *Quantitative Chemical Analysis*, Third Edition, New York, 1991, 170-172, 352-354.
82. R. M. Fuoss; *J. Polym. Sci*.; 3, 603(1948)

83. Anthony J. Sonnessa, W. Cullen, P. Ander; *Macromolecules*; 1980; 13(1); 195-196.
84. Ulrich P. Strauss, Edward H. Smith; *J. Am. Chem. Soc.;* 1953
85. Ksenija Kogej and Jože Škerjanc ; *Acta Chim. Slov*. 1999, 46(4), pp. 481-492.
86. Yamazaki, S.; Muroga, Y.; Noda, I.; *Langmuir*; 1999; 15(12); 4147-4149.
87. Farida Holler, James B. Callis; *J. Phys. Chem.;* 1989; 93(5); 2053-2058.
88. Dietrich O. Hummel; Atlas der Tensidanalyse FTIR-Spektren und ihre Interpretation (1996); Carl Hanser Verlag München Wien.
89. Smith, Brian C.; Infrared spectral interpretation, a systematic approach; CRC Press; 1999
90. Hansen, Diana L.; The Sprouse collection of infrared spectra: Book III surface active agents; Sprouse Scientific Systems, inc.; 1988.
91. Peng, B.; Johannsmann, D.; Ruhe, J.; *Macromolecules*; 1999; 32(20); 6759-6766.
92. Ide, M.; Mori, T.; Ichikawa, K.; Oshiyama, H.; Mizuno, W.; *Langmuir*; 2003; 19(2); 429-435.
93. Fushimi, C.; Araki, K.; Yamaguchi, Y.; Tsutsumi, A.; *Ind. Eng. Chem. Res.;* 2003; 42(17); 3929-3936.
94. B. Klaußer, J, Frömmel, T. Wolff; *Designed Monomers and Polymer*; 2 (1999); 53-59.
95. Lee, J. L.; Pearce, E. M.; Kwei, T. K.; *Macromolecules*; 1997; 30(22); 6877-6883.
96. Tork, A.; Bazuin, C. G.; *Macromolecules*; 2001; 34(22); 7699-7706.
97. Wang, J.; Ober, C. K.; *Macromolecules*; 1997; 30(24); 7560-7567.
98. John M. Patterson, et, al; *J. Agric. Food Chem*.; 1984; 32(4); 782-784.
99. Sprouse collection of infrared spectra, book III: surface active agents; diana L. Hansen (1988); sprouse scientific systems. Inc.
100. E.Berwig, etal; *polymer Degradation and Stability*; 79(2003) 93-98
101. Thunemann, A. F.; Kubowicz, S.; Pietsch, U.; *Langmuir*; 2000; 16(23); 8562-8567.
102. Y. W. Hui, M. M. Labes; *J. Phys. Chem*.; 1987; 91(23); 6066-6069.
103. Atlas der Tensidanalyse FTIR-Spektren und ihre Interpretation (1996), Dietrich O. Hummel. Carl Hanser Verlag München Wien; P. 66.
104. H. Buschmann, T. Wolff; *Journal of Photochemistry and Photobiology A: Chemistry*; 121(1999) 99-103
105. Nomula, S.; Cooper, S. L.; *Macromolecules*; 2000; 33(17); 6402-6406.
106. Mistiniene, E.; Luksa, V.; Sereikaite, J.; Naktinis, V.; *Bioconjugate Chem*.; 2003; 14(6); 1243-1252
107. Wanless, E. J.; Davey, T. W.; Ducker, W. A.; *Langmuir*; 1997; 13(16); 4223-4228.

108. Vollhardt, D.; Brezesinski, G.; Siegel, S.; Emrich, G.; *J. Phys. Chem. B.* ; 2001; 105(48); 12061-12067.

109. Lee, J. L.; Pearce, E. M.; Kwei, T. K.; *Macromolecules;* 1997; 30(26); 8233-8244.

110. Quanwei Yu, Jens Frömmel, Thomas Wolff, et al. Colloid Polym. Sci (2004) 282: 1039-1043.

Versicherung

Hiermit versichere ich, dass ich die vorliegende Arbeit ohne unzulässige Hilfe Dritter und ohne Benutzung anderer als der angegebenen Hilfsmittel angefertigt habe, die aus fremden Quellen direkt order indirekt übernommenen Gedanken sind als solche kenntlich gemacht. Die Arbeit wurde weder im Inland noch Ausland in gleicher order ähnlicher Form einer anderen Prüfungsbehörde vorgelegt.

Erklärung

Die vorliegende Arbeit wurde unter Anleitung von Herrn Prof. Dr. T. Wolff im Zeitraum von Nov 2001bis Okt 2004 im Institut für Physikalische Chemie und Elektrochemie der Technischen Universität Dresden angefertigt. Es habe keine frühen erfolglosen Promotionsverfahren stattgefunden. Ich erkenne die Promotionsordnung der Technische Universität Dresden, der Fakultät Mathematik und Naturwissenschaften von 16.04.2003 an.

Dresden, den Okt 2004

Quanwei Yu